

SARJA - SER. D OSA - TOM. 1076

MEDICA - ODONTOLOGICA

# PET IMAGING OF OSTEOMYELITIS

Feasibility of  $^{18}\text{F}$ -FDG,  $^{68}\text{Ga}$ -chloride  
and  $^{68}\text{Ga}$ -DOTAVAP-P1 tracers  
in staphylococcal bone infections

by

Petteri Lankinen

TURUN YLIOPISTO  
UNIVERSITY OF TURKU  
Turku 2013

From the Department of Orthopaedic Surgery and Traumatology,  
Orthopaedic Research Unit, and the Department of  
Clinical Physiology and Nuclear Medicine, Turku PET Centre, Faculty of Medicine,  
University of Turku and Turku University Hospital, Finland

**Supervised by**

Professor Hannu T. Aro, MD, PhD  
Department of Orthopaedic Surgery and Traumatology  
University of Turku and Turku University Hospital  
Turku, Finland

**Reviewed by**

Professor Matti Lehto, MD, PhD  
School of Medicine  
University of Tampere  
Tampere, Finland

and

Professor Aapo Ahonen, MD, PhD  
HUS Medical Imaging Center  
Helsinki University Hospital  
Helsinki, Finland

**Dissertation opponent**

Professor Teemu Moilanen MD, PhD  
School of Medicine, University of Tampere  
Coxa, Hospital for Joint Replacement  
Tampere, Finland

The originality of this dissertation has been checked in accordance with the University of Turku quality assurance system using the Turnitin OriginalityCheck service.

ISBN 978-951-29-5428-5 (PRINT)  
ISBN 978-951-29-5429-2 (PDF)  
ISSN 0355-9483  
Painosalama Oy – Turku, Finland 2013

*to Roosa*



## TIIVISTELMÄ

Petteri Lankinen

**LUUINFEKTIOIDEN PET-KUVANTAMINEN – <sup>18</sup>F-FDG, <sup>68</sup>Ga-KLORIDI JA <sup>68</sup>Ga-DOTAVAP-P1 MERKKIAINEIDEN KÄYTTÖ STAFYLOKOKKIEN AIHEUTTAMISSA LUUINFEKTIOISSA**

TULES-toimialue, Ortopedian tutkimusyksikkö ja Kliininen fysiologia ja isotooppilääketiede, Valta-kunnallinen PET-keskus, Lääketieteellinen tiedekunta, Turun yliopisto ja Turun yliopistollinen keskussairaala

Annales Universitatis Turkuensis, Medica-Odontologica, 2013, Turku, Finland

Painosalama Oy – Turku, Finland 2013

Osteomyeliitti on luukudoksen ja luuytimen etenevä, yleisimmin *S. aureuksen* aiheuttama bakteeritulehdus, joka aiheuttaa luun tuhoutumista. Ongelma on erityisen suuri ikääntyneen väestön keskuudessa, joilla sekä tekonivelkirurgian että luunmurtumakirurgian tarve on lisääntynyt voimakkaasti, ja joilla on lisääntynyt alttius kirurgisille infektioille. Infektioyypistä riippuen tulehdus voi olla nopeasti kehittyvä tai hitaasti syntyvä, matala-asteinen ja se voi aiheuttaa implanttien irtoamisen. Tilannetta pahentaa taudinaiheuttajien antibioottiresistenssin yleistäminen.

Nykyisillä kuvantamismenetelmillä on selviä rajoituksia osteomyeliitin ja implanti-infektioiden toteamisessa. Positroniemissiotomografia (PET), jossa käytetään <sup>18</sup>F-fluorodeoksiglukoosia (<sup>18</sup>F-FDG) merkkiaineena, on todettu toimivaksi kroonisten luuinfektioiden diagnostiikassa. Menetelmä perustuu aktivoituneiden tulehdussolujen lisääntyneeseen glukoosin kulutukseen. <sup>18</sup>F-FDG kertyy myös steriilin inflammaation alueelle ja kuvaukseen liittyy vääriä positiivisia löydöksiä esimerkiksi kudoksen paranemisreaktioista johtuen. Tämän takia tarvitaan uusia infekti spesifisimpiä PET-merkkiaineita. Toisaalta on edelleen epäselvää, miksi <sup>18</sup>F-FDG PET kuvaus ei toimi odotetulla tavalla yleisimmin *S. epidermidis*-bakteerin aiheuttamien tekonivelinfektioiden diagnostiikassa.

Tässä väitöstutkimuksessa testattiin uusia PET-merkkiaineita (<sup>68</sup>Ga-kloridia ja <sup>68</sup>Ga-DOTAVAP-P1) luuinfektioiden diagnostiikassa, sekä arvioitiin PET-diagnostiikan tarkkuuteen vaikuttavia bakteriologisia tekijöitä. Kokeellisissa *S. epidermidis* ja *S. aureus* luu/implantti-infektio malleissa arvioitiin taudinaiheuttaja-patogeenin merkitystä <sup>18</sup>F-FDG kertymään. Kliinisessä retrospektiivisessä analyysissä arvioitiin positiivisen ja negatiivisen bakteeriviljelytuloksen merkitystä <sup>18</sup>F-FDG kertymään osteomyeliittipotilailla.

<sup>18</sup>F-FDG ja <sup>68</sup>Ga-kloridi merkkiaineiden kertyminen oli samankaltainen luuinfektioissa, mutta <sup>68</sup>Ga-kloridi ei kertynyt paranevan luun alueelle. Löydös viittasi siihen, että <sup>68</sup>Ga-kloridi voi olla spesifisempi merkkiaine luuinfektioiden diagnostiikassa varhaisessa postoperatiivisessa tai posttraumaattisessa vaiheessa. Kehitetty synteettinen peptidi, <sup>68</sup>Ga-DOTAVAP-P1, sitoutuu verisuonten endoteelisolujen pinnalla ilmenevään tartuntamolekyyliin (VAP-1). Sen avulla pystyttiin osoittamaan luun paranemisen käynnistymiseen liittyvä inflammaatioreaktio. <sup>68</sup>Ga-DOTAVAP-P1 kertymä todettiin myös luuinfektioissa, joten se ei ole käytettävissä inflammaation ja infektion erotusdiagnoosiin. *S. epidermidis* bakteerin aiheuttama implanti-infektio aiheutti vain vähäisen <sup>18</sup>F-FDG merkkiainekertymän osoittaen, että aiheuttajabakteerin virulenssi ja sen aiheuttaman tulehdusreaktion voimakkuus vaikuttavat PET-diagnostiikkaan. Kliinisessä tutkimuksessa ei todettu merkittävää <sup>18</sup>F-FDG kertymän eroa viljelypositiivisten ja viljelynegatiivisten osteomyeliittipotilaiden välillä. Löydös viittaa, että <sup>18</sup>F-FDG PET voi tukea histologista osteomyeliittidiagnoosia potilailla, joilla bakteeriviljelytulos jää negatiiviseksi.

**Avainsanat:** osteomyeliitti, implanti-infektio, positroniemissiotomografia (PET), <sup>18</sup>F-FDG, gallium-68, vascular adhesion protein-1 (VAP-1), <sup>68</sup>Ga-DOTAVAP-P1

## ABSTRACT

Petteri Lankinen

**PET IMAGING OF OSTEOMYELITIS – FEASIBILITY OF  $^{18}\text{F}$ -FDG,  $^{68}\text{Ga}$ -CHLORIDE AND  $^{68}\text{Ga}$ -DOTAVAP-P1 TRACERS IN STAPHYLOCOCCAL BONE INFECTIONS**

Department of Orthopaedic Surgery and Traumatology, Orthopaedic Research Unit, and Department of Clinical Physiology and Nuclear Medicine, Turku PET Centre, Faculty of Medicine, University of Turku and Turku University Hospital, Finland

Annales Universitatis Turkuensis, Medica-Odontologica, 2013, Turku, Finland

Painosalama Oy – Turku, Finland 2013

Osteomyelitis is a progressive inflammatory disease of bone and bone marrow that results in bone destruction due to an infective microorganism, most frequently *Staphylococcus aureus*. Orthopaedic concern relates to the need for reconstructive and trauma-related surgical procedures in the fast growing population of fragile, aged patients, who have an increased susceptibility to surgical site infections. Depending on the type of osteomyelitis, infection may be acute or a slowly progressing, low-grade infection. Peri-implant infections lead to implant loosening. The emerging antibiotic resistance of common pathogens further complicates the situation.

With current imaging methods, significant limitations exist in the diagnosing of osteomyelitis and implant-related infections. Positron emission tomography (PET) with a glucose analogue,  $^{18}\text{F}$ -fluorodeoxyglucose ( $^{18}\text{F}$ -FDG), seems to facilitate a more accurate diagnosis of chronic osteomyelitis. The method is based on the increased glucose consumption of activated inflammatory cells. Unfortunately,  $^{18}\text{F}$ -FDG accumulates also in sterile inflammation regions and causes false-positive findings, for example, due to post-operative healing processes. Therefore, there is a clinical need for new, more infection-specific tracers. In addition, it is still unknown why  $^{18}\text{F}$ -FDG PET imaging is less accurate in the detection of periprosthetic joint infections, most frequently due to *Staphylococcus epidermidis*.

This doctoral thesis focused on testing novel PET tracers ( $^{68}\text{Ga}$ -chloride and  $^{68}\text{Ga}$ -DOTAVAP-P1) for early detections of bone infections and evaluated the role of pathogen-related factors in the applications of  $^{18}\text{F}$ -FDG PET in the diagnostics of bone infections. For preclinical models of *S. epidermidis* and *S. aureus* bone/implant infections, the significance of the causative pathogen was studied with respect to  $^{18}\text{F}$ -FDG uptake. In a retrospective analysis of patients with confirmed bone infections, the significance of the presence or absence of positive bacterial cultures on  $^{18}\text{F}$ -FDG uptake was evaluated.

$^{18}\text{F}$ -FDG and  $^{68}\text{Ga}$ -chloride resulted in a similar uptake in *S. aureus* osteomyelitic bones. However,  $^{68}\text{Ga}$ -chloride did not show uptake in healing bones, and therefore it may be a more-specific tracer in the early post-operative or post-traumatic phase.  $^{68}\text{Ga}$ -DOTAVAP-P1, a novel synthetic peptide binding to vascular adhesion protein 1 (VAP-1), was able to detect the phase of inflammation in healing bones, but the uptake of the tracer was elevated also in osteomyelitis. Low-grade peri-implant infections due to *S. epidermidis* were characterized by a low uptake of  $^{18}\text{F}$ -FDG, which reflects the virulence of the causative pathogen and the degree of leukocyte infiltration. In the clinical study, no relationship was found between the level of  $^{18}\text{F}$ -FDG uptake and the presence of positive or negative bacterial cultures. Thus  $^{18}\text{F}$ -FDG PET may help to confirm metabolically active infection process in patients with culture-negative, histologically confirmed, low-grade osteomyelitis.

**Keywords:** osteomyelitis, implant infection, positron emission tomography (PET),  $^{18}\text{F}$ -FDG, gallium-68, vascular adhesion protein-1 (VAP-1),  $^{68}\text{Ga}$ -DOTAVAP-P1

## TABLE OF CONTENTS

TIIVISTELMÄ.....	4
ABSTRACT.....	5
TABLE OF CONTENTS.....	6
LIST OF ORIGINAL PUBLICATIONS.....	9
ABBREVIATIONS.....	10
1. INTRODUCTION.....	11
2. REVIEW OF THE LITERATURE.....	12
2.1. Bone.....	12
2.1.1. Bone healing.....	12
2.2. Osteomyelitis.....	14
2.2.1. Aetiology.....	14
2.2.2. Microbial involvement.....	16
2.2.3. Classification.....	18
2.2.4. Microbial and laboratory diagnostics.....	19
2.3. Imaging of osteomyelitis.....	20
2.3.1. Radiography.....	20
2.3.2. Computed tomography.....	20
2.3.3. Magnetic resonance imaging.....	20
2.3.4. Conventional nuclear medicine methods.....	21
2.3.5. Positron emission tomography.....	23
2.3.5.1. Scanner and basic principle.....	23
2.3.5.2. Tracers.....	24
2.3.5.2.1. <sup>18</sup> F-2-fluoro-2-deoxyglucose.....	24
2.3.5.2.2. <sup>68</sup> Gallium-chloride.....	24
2.3.5.2.3. Other tracers.....	25
2.3.5.3. <sup>18</sup> F-FDG PET.....	26
2.4. PET imaging of inflammatory reaction.....	30
2.4.1. Imaging of inflammatory conditions in the skeletal system.....	30
2.4.2. Vascular adhesion protein-1.....	32
2.5. Animal models of osteomyelitis.....	33
3. AIMS OF THE STUDY.....	35
4. MATERIALS AND METHODS.....	36
4.1. Experimental studies.....	36
4.1.1. Experimental animals.....	36
4.1.2. Anaesthesia and peri-operative care.....	36
4.1.3. Pathogens used in the induction of osteomyelitis and foreign-body infection.....	36
4.1.4. Experimental animal models and study protocols.....	36
4.1.4.1. Tibial osteomyelitis model of rat.....	36

4.1.4.2. Tibial osteomyelitis and foreign-body bone infection models of rabbit .....	37
4.2. Clinical study .....	37
4.2.1. Patients .....	37
4.3. Analysis methods .....	38
4.3.1. Experimental studies .....	38
4.3.1.1. Positron emission tomography .....	38
4.3.1.2. Ex vivo measurement of tracer accumulation .....	39
4.3.1.3. Peripheral quantitative computed tomography .....	39
4.3.1.4. Radiography .....	39
4.3.1.5. Microbiological analysis .....	40
4.3.1.6. Histology .....	41
4.3.2. Clinical study .....	42
4.3.2.1. Clinical follow-up and analyses .....	42
4.4. Statistical analyses .....	42
5. RESULTS .....	43
5.1. Comparison of <sup>18</sup> F-FDG and <sup>68</sup> Ga-chloride in the PET imaging of <i>S. aureus</i> osteomyelitis and uncomplicated bone healing in a rat model .....	43
5.1.1. Confirmation of <i>S. aureus</i> infection .....	43
5.1.2. In vivo uptake of <sup>18</sup> F-FDG and <sup>68</sup> Ga-chloride .....	43
5.1.3. Ex vivo analysis of <sup>18</sup> F-FDG and <sup>68</sup> Ga-chloride accumulation .....	43
5.2. Evaluation of <sup>68</sup> Ga-DOTAVAP-P1 for the differentiation of inflammatory and infectious bone processes in a rat model .....	44
5.2.1. Confirmation of the induction of <i>S. aureus</i> infection .....	44
5.2.2. Histological evaluation of inflammatory reaction and VAP-1 expression .....	44
5.2.3. In vivo PET uptake of <sup>68</sup> Ga-DOTAVAP-P1 .....	44
5.3. <sup>18</sup> F-FDG uptake in the differentiation of <i>S. aureus</i> and <i>S. epidermidis</i> bone infections in a rabbit model .....	45
5.3.1. Confirmation of culture-positive infection .....	45
5.3.2. Histological appearance of osteomyelitis .....	45
5.3.3. Correlation of <sup>18</sup> F-FDG PET uptake, leukocyte infiltration, and inoculated pathogen .....	45
5.4. Intensity of <sup>18</sup> F-FDG uptake in the patients with microbiologically or histologically confirmed chronic bone infections .....	46
6. DISCUSSION .....	47
6.1. PET imaging of osteomyelitis in healing bones .....	47
6.1.1. <sup>68</sup> Ga-chloride PET imaging of osteomyelitis and bone healing .....	47
6.1.2. <sup>68</sup> Ga-DOTA-VAP-P1 imaging of osteomyelitis and bone healing .....	48
6.2. Significance of causative bone pathogens and the presence of positive bacterial cultures in PET .....	49
6.2.1. <sup>18</sup> F-FDG uptake in <i>S. aureus</i> osteomyelitis and <i>S. epidermidis</i> foreign-body bone infection .....	49
6.2.2. <sup>18</sup> F-FDG uptake in culture-positive and culture-negative patients with histologically confirmed chronic osteomyelitis .....	50
6.3. Animal models .....	51
6.4. Limitations of the study .....	52
6.5. Future prospects .....	53

# / Thesis / Table of Contents

---

7. CONCLUSIONS .....	54
ACKNOWLEDGEMENTS.....	55
REFERENCES.....	56
ORIGINAL PUBLICATIONS (PAPERS I-IV) .....	67



## LIST OF ORIGINAL PUBLICATIONS

This thesis is based on the following original publications that are referred to in the text by their respective Roman numerals I–IV:

- I **Mäkinen TJ, Lankinen P, Pöyhönen T, Jalava J, Aro HT, Roivainen A.** Comparison of  $^{18}\text{F}$ -FDG and  $^{68}\text{Ga}$  PET imaging in the assessment of experimental osteomyelitis due to *Staphylococcus aureus*. *Eur J Nucl Med Mol Imaging*. 2005 Nov;32(11):1259–1268.
- II **Lankinen P, Mäkinen TJ, Pöyhönen TA, Virsu P, Salomäki S, Hakanen AJ, Jalkanen S, Aro HT, Roivainen A.**  $^{68}\text{Ga}$ -DOTAVAP-P1 PET imaging capable of demonstrating the phase of inflammation in healing bones and the progress of infection in osteomyelitic bones. *Eur J Nucl Med Mol Imaging*. 2008 Feb;35(2):352–364.
- III **Lankinen P, Lehtimäki K, Hakanen AJ, Roivainen A, Aro HT.** A comparative  $^{18}\text{F}$ -FDG PET/CT imaging of experimental *Staphylococcus aureus* osteomyelitis and *Staphylococcus epidermidis* foreign-body-associated infection in the rabbit tibia. *EJNMMI Res*. 2012;2(1):41.
- IV **Lankinen P, Seppänen M, Mattila K, Kallajoki M, Knuuti J, Aro HT.** The intensity of  $^{18}\text{F}$ -FDG PET uptake in culture-negative and culture-positive chronic osteomyelitis. (Manuscript)

The original publications are reproduced with the permission of the respective copyright holders.

## ABBREVIATIONS

ANOVA	analysis of variance
<sup>18</sup> F-FDG	<sup>18</sup> F-2-fluoro-2-deoxyglucose
<sup>67</sup> Ga-citrate	<sup>67</sup> gallium citrate
<sup>68</sup> Ga-chloride	<sup>68</sup> gallium chloride
<sup>99m</sup> Tc	<sup>99m</sup> technetium
<sup>111</sup> In	<sup>111</sup> indium
ATCC	American type culture collection
cfu	colony-forming unit
CRP	C-reactive protein
CRMO	chronic recurrent multifocal osteomyelitis
CT	computed tomography
DNA	deoxyribonucleic acid
DPD	dicarboxypropane diphosphonate
ESR	erythrocyte sedimentation rate
GLUT	glucose trans-membrane transporter
HDP	hydroxyl diphosphonate
HEDP	hydroxyethylidene diphosphonate
HMPAO	hexamethylpropyleneamine oxime
MDP	methylene diphosphonate
MRI	magnetic resonance imaging
P	probability
PCR	polymerase chain reaction
PET	positron emission tomography
PMMA	polymethyl methacrylate
PFGE	pulsed-field gel electrophoresis
pQCT	peripheral quantitative computed tomography
PVE	partial-volume effect
ROI	region of interest
SAPHO	synovitis, acne, pustulosis, hyperostosis, osteitis syndrome
SD	standard deviation
SPECT	single photon emission computed tomography
SSAO	semicarbazide-sensitive amine oxidase
SUV	standardized uptake value
VAP-1	vascular adhesion protein-1
WBC	white blood cell

## 1. INTRODUCTION

Osteomyelitis, a disease that has been known since antiquity, is characterized by progressive inflammatory destruction and the apposition of new bone due to an infective microorganism. In the pre-antibiotic era, osteomyelitis was associated with a significantly high mortality rate. Despite new potent treatment strategies and advanced surgical methods, it can still result in devastating outcomes, for example, significant morbidity, excruciating pain, chronically draining sinuses, loss of function, and even amputation or death. It is anticipated that the number of bone infections will increase as the number of reconstructive skeletal procedures performed with biomaterials grows. The increasing number of elderly patients who need surgical treatment for skeletal disorders and trauma, in addition to the alarming antibiotic resistance of common pathogens, will produce unmatched challenges in the near future.

Accurate and quick diagnosis plays a crucial role in the patient management of infectious diseases. The diagnosis and treatment of bone infections is based on a systemic approach that starts with the accurate identification of the pathogen and its sensitivity to antimicrobial treatment. Such standard diagnostic tools as magnetic resonance imaging (MRI), computed tomography (CT) and nuclear medical scans are known to have major limitations in the diagnosis of osteomyelitis.

Positron emission tomography (PET) with the radiolabelled glucose analogue  $^{18}\text{F}$ -2-fluoro-

2-deoxyglucose ( $^{18}\text{F}$ -FDG) has been shown to be a promising imaging modality in the detection of orthopaedic infections. It measures biochemical and physiological processes in vivo through the quantitative imaging of positron-emitting radiotracers injected into the human body. With PET, it is possible to determine anatomical loci in vivo and to quantitate disease activity on the basis of physiological or metabolic changes. However, the specificity of  $^{18}\text{F}$ -FDG PET is limited, because it also accumulates in sterile inflammatory regions. Due to the inflammatory phase of bone healing, after trauma or surgery, non-specific uptake may cause false-positive results. Therefore, new more-specific tracers are needed.

Osteomyelitic patients have varying clinical states because of diverse infection routes and differences in the pathomechanisms of multiple potential causative microbes.  $^{18}\text{F}$ -FDG PET seems to be reliable, but its applicability may vary in different situations. More evidence is required to expand its applicability and to identify possible limitations and factors contributing to its accuracy.

This study was initiated to test and validate novel, more-specific radiopharmaceuticals for the PET imaging of bone infections and to investigate the feasibility of using  $^{18}\text{F}$ -FDG PET in the diagnostics of experimental bone infections caused by low virulence pathogens and in the differentiation between patients with culture-positive osteomyelitis and those with culture-negative osteomyelitis.

## 2. REVIEW OF THE LITERATURE

### 2.1. Bone

Bone is metabolically a highly active tissue, it is able to adapt to changing conditions and regenerate and repair itself (Buckwalter et al. 1995 and Buckwalter 1996). Bone tissue is composed of cells embedded in a mineralized matrix. Most of bone tissue is composed of an inorganic mineral substance that accounts for 65%–70% of its dry weight, which is predominantly composed of calcium hydroxyapatite with a smaller portion of calcium phosphate (Copenhaver et al. 1978, Recker 1992). The organic matrix of fibrous protein and collagen accounts for 30%–35% of the dry weight of bone tissue (Copenhaver et al. 1978, Recker 1992). Approximately 20% of bone tissue is composed of water (Kalfas 2001). The cellular component (osteogenic precursor cells, osteoblasts, osteocytes, and haematopoietic elements of bone marrow) of bone accounts for only 2% of bone mass. Osteogenic precursor cells form the deep layer of the periosteum and the endosteum and are present on all non-resorptive surfaces. In fracture healing, osteoblasts are bone-forming cells that secrete osteoid (unmineralized organic matrix composed mainly of type-I collagen with attached glycoproteins) that is mineralized in the process. A fraction of osteoblasts converts to osteocytes, and some remain as lining cells on periosteal and endosteal surfaces as their activation nears completion. Once the matured osteoblast is trapped within the bone matrix, it is called an osteocyte. Over 90% of the cells in a mature skeleton are osteocytes. Osteoclasts are large, multinucleated cells that are responsible for bone resorption.

Microscopically, the following types of bone can be characterized: woven bone, lamellar bone, and trabecular bone. Woven bone can be considered to be immature bone, as it is composed of random collagen bundles and irregular vascular spaces lined with osteoblasts. Woven bone is found during pathological states such as osteogenesis imperfecta, hyperparathyroidism, Paget disease, and tumours, but it is also found during embryonic development and during frac-

ture healing in the formed callus (Recker 1992, Kalfas 2001). Lamellar bone, also called compact or cortical bone, forms through the remodelling of immature woven bone. Micro-structurally, cortical bone is composed of vascular channels (Haversian canals) lined with cylindrical-shaped lamellar bone, which forms the osteon or the Haversian system. The microstructure of trabecular or cancellous bones is constantly undergoing remodelling to provide maximum resistance to mechanical stress (Myers and Wilson 1997). In adults, cortical bone accounts for approximately 85% of the skeleton, while 15% is trabecular bone.

#### 2.1.1. Bone healing

Fracture repair is a unique process. Through a highly regulated, multistage sequence, bone tissue is capable, in optimal circumstances, of healing without the formation of fibrous scar, and its original structure and function are restored (Barnes et al. 1999). Four main spatial areas, including the medullary canal, the cortex, the periosteal layer and the surrounding soft tissues, all contribute to the process (Einhorn 2005). Classically, two histological paths of fracture healing have been described. Primary or direct healing occurs without callus formation, and secondary or indirect healing takes place through a callus precursor phase (Greenbaum and Kanat 1993, Einhorn 1998). However, the outcome of different healing types seems to be highly uniform (Aro and Chao 1993).

In primary bone healing, a direct attempt occurs to re-establish the pre-existing anatomy between the two fragments. Direct bone healing occurs only when the fracture is anatomically reduced by rigid fixation with decreased interfragmentary strain (Klein et al. 2003, Claes et al. 2012). New Haversian systems are established through the formed haematoma by remodelling units called “cutting cones” (Russell 1992). Osteoprogenitor cells arising from endothelial cells and perivascular mesenchymal cells differentiate to osteoblasts initiating the healing sequence.

Most fractures heal through secondary or indirect healing as a combination of intramembranous and endochondral ossification (Dimitriou et al. 2005). In contrast to primary healing, motion enhances the process, and rigid fixation inhibits it. In intramembranous ossification bone tissue is formed directly, without a cartilage phase, from osteoprogenitor cells and undifferentiated mesenchymal cells originating from the periosteum. This process leads to callus formation and is referred to histologically as the “hard callus” (Bielby et al. 2007). In the endochondral healing process, bone forms through a cartilage phase in the “soft callus”, as it does in the growth plate (Bolander 1992, Bielby et al. 2007). The secondary bone healing of fractures can be described as the following five consecutive processes: 1) the immediate response to trauma, 2) intramembranous bone formation, 3) chondrogenesis, 4) endochondral bone formation, and, finally, 5) bone remodelling (Barnes et al. 1999) (Figure 1). The induction of the separate

stages is regulated spatially and temporally by a complex array of routes signalled by cytokines and growth factors (Kon et al. 2001, Liebermann et al. 2002) (Figure 1). The initial inflammatory response after bone-involved trauma lasts approximately 48 hours. In the inflammation phase, haematoma is formed, and inflammatory cells (macrophages, monocytes, lymphocytes and polymorphonuclear leukocytes) infiltrate the site, guided by prostaglandins, the result being the migration of mesenchymal cells, the ingrowth of vasculature, and the formation of granulation tissue (Hulth 1989, Stanford and Keller 1991). As the initial inflammation subsides, dead bone is replaced by cartilage-like tissue over a period of 7 days. Three to four weeks after the initial trauma, the formed fibrocartilage begins to calcify from each side towards the centre of the fracture. In the sixth week the healing bone begins to remodel from fibrous bone towards the original affected bone, the period lasting from two months up to two years.

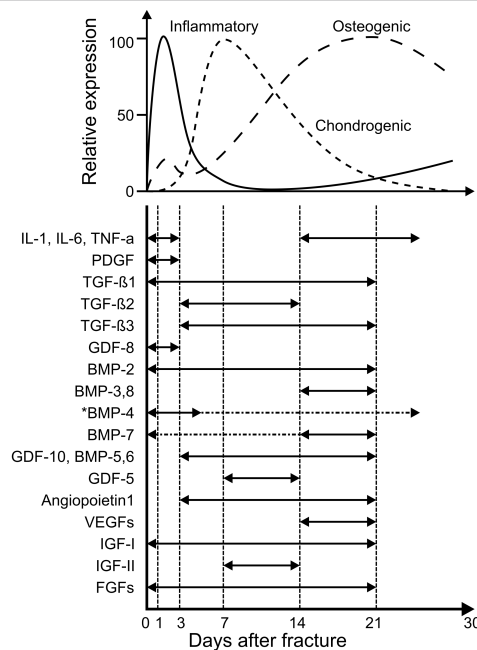


**Figure 1.** Schematic illustration of bone healing cascade and associated temporal expression of cytokines and growth factors. Modified from Cho et al. (2002) and Dimitriou et al. (2005). (Pro-inflammatory cytokines: IL-1 and -6 = Interleukin-1 and -6, TNF- $\alpha$  = tumour necrosis factor- $\alpha$ . Growth and differentiation factors: PDGF = platelet derived growth factor; TGF- $\beta$ 1, - $\beta$ 2, - $\beta$ 3 = transforming growth factor- $\beta$ 1, - $\beta$ 2, - $\beta$ 3; GDF-5, -8, -10 = growth differentiation factor-5, -8, -10; BMP-2, -3, -4, -5, -6, -7, -8 = bone morphogenic protein-2, -3, -4, -5, -6, -7, -8; GDF-5, -10 = growth and differentiation factor-5, -10; IGF-I, -II = insulin-like growth factor-I, -II; FGFs = fibroblast growth factors. Angiogenic factors: VEGFs = vascular-endothelial growth factors; angiopoietin).

## 2.2. Osteomyelitis

Osteomyelitis is characterized by progressive inflammatory destruction and the apposition of new bone that results from infective microorganisms (Lazzarini et al. 2004, Brady et al. 2006). In the pre-antibiotic era osteomyelitis was associated with a high mortality rate. Even now, despite new, potent, antimicrobial treatment methods and good surgical methods, it can lead to devastating results.

Normal bone is highly resistant to infection (Andriole et al. 1973). However, infection can occur after exposure to a massive amount of a microbial inoculum, with bone and adjacent soft-tissue trauma or in the presence of foreign bodies (Table 1) (Wald 1985). The pivotal point of the pathogenesis is for the microbe to gain entry into the host and, secondly, to be able to colonize bone. Surrounding tissues are damaged as phagocytes attempt to destroy invading pathogens and, in the process, generate toxic oxygen radicals and proteolytic enzymes that contribute to the necrosis of tissue, the breakdown of bone, and the removal of calcium. In addition, several bacterial components act as bone-modulating factors (Nair et al. 1996). As infection progresses, pus spreads into vascular channels and raises the intraosseous pressure. This process causes deficient blood flow. Zones of ischaemic necrosis, called sequestra, are formed. Sequestra can act as foreign bodies and result in biofilm formation on their surface and, therefore, harbour treatment-resistant bacteria (Gristina et al. 1990). Bone tissue highly resists swelling due to infection and the formation of pus. Pus may eventually reach the surface of bone and form subperiosteal abscesses. Later the abscesses can burst into soft tissues. Simultaneously, as the breakdown of bone occurs, bone apposition appears in the form of periosteal apposition and new bone formation. During infection, growth factors and cytokines that normally control osteoblasts and osteoclast function show altered local concentrations (Klosterhalfen et al. 1996, Manolagas 2000). The main histological findings of acute osteomyelitis are the appearance of microorganisms, the infiltration of neutrophils, and congested or thrombosed blood ves-

sels (Lew and Waldvogel 1997). Chronic osteomyelitis can be distinguished as the presence of necrotic bone with no living osteocytes present (Lew and Waldvogel 1997).

### 2.2.1. Aetiology

From a clinical viewpoint, the distinction of three aetiological types of osteomyelitis is practical: haematogenous osteomyelitis, osteomyelitis due to a contiguous source (post-traumatic and post-operative), and osteomyelitis due to vascular insufficiency. In 1970, Waldvogel et al. (1970a) reported that 19% of osteomyelitis cases were haematogenous, 34% were associated with vascular insufficiency, and 47% were due to a contiguous focus of infection. The clinical picture of osteomyelitis is evolving. In 2003, Tice et al. published a study of 454 osteomyelitic patients, 6% of whom had haematogenous osteomyelitis, 2% had osteomyelitis in association with vascular insufficiency, 90% experienced osteomyelitis caused by a contiguous focus of infection, and 2% were classified as having osteomyelitis due to other causes.

In haematogenous osteomyelitis, pathogens reach the bone through the bloodstream, the bacteria originating from septic foci elsewhere in the body. Haematogenous osteomyelitis is classically described as a disease of children, as it usually involves rapidly growing bone and it characteristically affects the metaphysis of long bones, especially in the femur and tibia. Brodie's abscess is a rare subacute or chronic manifestation of osteomyelitis characterized by a localized intraosseous pyogenic abscess surrounded by dense fibrous tissue and bone sclerosis, and it is generally caused by *Staphylococcus aureus* (Brodie 1832, Strobel et al. 2006). Typically Brodie's abscess is reported to affect young males with unfused epiphyseal plates predominantly in the tibia and less frequently in the femur (Henderson and Simon 1924, Grey et al. 1998). A rare type of haematogenous osteomyelitis is vertebral infection, a disease that mainly affects people over 50 years of age. Vertebral infection accounts for 2%–4% of all osteomyelitis cases (Jevtic 2004). Clinical signs of haematogenous osteomyelitis

are typically chills, fever and malaise, local pain, and swelling. Cultures made from blood specimens from children are positive from 50% to 60% of the patients (Kaplan 2005). With regard to vertebral infections, blood cultures often offer no explanation for the symptoms, and CT-guided needle biopsy with multiple specimens for microbiological and pathological examinations is advised (Lew and Waldvogel 1997, Heyer et al. 2012, Sehn and Gilula 2012). Infection causatives differ according to the age of the patient. For approximately 50% of vertebral osteomyelitis cases, the source of haematogenous spread can be identified as the urinary tract or skin, and approximately 33% are associated with endocarditis (Zimmerli 2010). *S. aureus* is the commonest cause of haematogenous osteomyelitis in neonates, but it is also found later in life (Table 1). People who use illegal drugs are in danger of getting fungal-caused osteomyelitis, as a complication of catheter-related fungemia when used drugs are contaminated with *Candida* species and cause prolonged neutropenia (Sapico and Montgomerie 1980, Lew and Waldvogel 1997, Ruotsalainen and Valtonen 2001).

Osteomyelitis due to vascular insufficiency or diabetes is found predominantly in the feet (Lipsky et al. 2012). Localized pressure or minor trauma in patients with neuropathy and microvascular disease may result in a vast spectrum of foot infections, ranging from superficial cellulitis to chronic osteomyelitis. Osteomyelitis complicates up to one third of diabetic foot infections, is often due to direct contamination from a soft-tissue lesion, and represents a clinical challenge (Marcus et al. 1996). The infection typically starts in previously injured skin in a patient with claudication. Clinically, the patient can exhibit excruciating pain or no pain at all, depending on the advancement of the neuropathy. When there is no neuropathy, and, if the bone destruction has been acute, patients suffer from severe pain. In evaluations of peripheral diabetic infections the following crucial contributing factors must be addressed: the metabolic consequences of diabetes, bone and soft-tissue ischaemia, and peripheral neuropathy, including motor, sensory, and autonomic components

(Waldvogel et al. 1970c). The commonest single causative pathogen is *S. aureus*, but frequently the infection is caused by many different pathogens, such as  $\beta$ -haemolytic streptococcus, anaerobic bacteria, and gram-negative rods (Lipsky 1997) (Table 1).

Osteomyelitis due to spread from a contiguous focus is associated with trauma or bone reconstructive surgery, as bacteria gain access to bone through direct inoculation. The incidence of osteomyelitis after open fractures has been reported to range from 0% to 16%, depending on the class and treatment received (Gustilo et al. 1976, Kaim et al. 2002), but complication rates of up to even 50% (Gustilo-Anderson type III) have also been reported (Weitz-Marshall and Bosse 2002). Infections involving foreign bodies, such as prostheses, are increasing because the number of arthroplasties performed every year is increasing worldwide. The rate of infections associated with joint arthroplasty is reported to be approximately from 0.6% to 2% (Matthews et al. 2009). Typical symptoms of acute infection are pain, loss of function, wound infection associated with swelling and erythema, joint effusion, and mild or no fever. Patients with chronic prosthesis infection generally show fewer systemic signs, but they frequently exhibit increasing pain, signs of mechanical dysfunction, and, occasionally, sinus formation and drainage. Chronic prosthesis infections due to low virulence microbes may appear as latent infection and show symptoms long after onset. Osteomyelitis secondary to a contiguous focus of infection is often characterized by polymicrobial infection (Mader et al. 1999).

Osteomyelitis may appear as part of the SAPHO syndrome. The acronym SAPHO is composed of simultaneous denominations: inflammatory synovitis, acne, palmoplantar pustulosis, hyperostosis, and osteitis (Kahn and Chamot 1992). Osteoarticular lesions in association with the SAPHO syndrome may be presented as multifocal osteomyelitis, and its pathogenesis is reported to be linked with spondyloarthropathies and plain psoriasis (Kahn and Chamot 1992, Takeuchi et al. 2007).

**Table 1.** Microorganisms typically isolated in association with clinical predisposing factors

Typical clinical association	Microorganism
Frequent microorganism in any type of osteomyelitis	<i>S. aureus</i> (susceptible or resistant to meticillin)
Foreign-body-associated infection	Coagulase-negative staphylococci or <i>Propionibacterium</i> spp.
Prosthetic joint infection	Coagulase-negative staphylococci, <i>S. aureus</i> , polymicrobial <i>Streptococcus</i> spp, gram-negative aerobic bacilli
Common in nosocomial infections	<i>Enterobacteriaceae</i> , <i>Pseudomonas aeruginosa</i> , <i>Candida</i> spp.
Post-traumatic infection	<i>S. aureus</i> , polymicrobial gram-negative aerobic bacilli, anaerobes
Vertebral osteomyelitis	<i>S. aureus</i> , gram-negative aerobic bacilli, <i>Streptococcus</i> spp, <i>Mycobacterium tuberculosis</i>
Associated with bites and decubitus ulcers	Streptococci and/or anaerobic bacteria
Diabetic foot infection	<i>S. aureus</i> , <i>Streptococcus</i> spp, <i>Enterococcus</i> spp, coagulase-negative staphylococci, gram-negative aerobic bacilli, anaerobes
Human or animal bites	<i>Pasteurella multocida</i> or <i>Eikenella corrodens</i>
Sickle-cell disease	<i>Salmonella</i> spp or <i>Streptococcus pneumoniae</i>
HIV infection	<i>Bartonella henselae</i> or <i>Bartonella quintana</i>
Immunodeficient patients	<i>Aspergillus</i> spp, <i>Candida albicans</i> , or <i>Mycobacteria</i> spp.
Populations in which tuberculosis is prevalent	<i>Mycobacterium tuberculosis</i>
Populations in which these pathogens are endemic	<i>Brucella</i> spp, <i>Coxiella burnetii</i> , geographic area-specific fungi (coccidioidomycosis, blastomycosis, histoplasmosis)

Modified from Lew and Waldvogel 2004.

### 2.2.2. Microbial involvement

The microbe causing osteomyelitis depends on both the host factors and the aetiology of the infection, as virtually any organism has the potential to cause osteomyelitis. The most frequent causative microbes of any type of osteomyelitis are staphylococci (Table 2). For paediatric patients, the possibility of non-bacterial osteomyelitis has also been introduced (Borzutzky et al. 2012). In chronic recurrent multifocal osteomyelitis (CRMO) of children, bacterial cultures may frequently or at least variably remain negative (Golla et al. 2002, Jurik 2004).

Staphylococci are gram-positive cocci that can be divided into two groups on the basis of their ability to produce the blood clotting-enzyme coagulase. *S. aureus* and *Staphylococcus epidermidis* represent the most commonly found coagulase-positive and coagulase-negative staphylococcal

species, respectively (Queck and Otto 2008). *S. aureus* is a well-established pathogen. On the contrary, *S. epidermidis* represents opportunistic microorganisms, and it has emerged as the leading nosocomial pathogen of implant-related bone infections and other hospital-acquired infections (von Eiff et al. 2002, Lew and Waldvogel 2004). The primary reasons for the increasing rate of *S. epidermidis* infections are the spreading of antibiotic resistance and the frequent use of implants and other medical devices. The rate of methicillin resistance among clinical *S. epidermidis* isolates is approaching 90%, which is much higher than the rate of its pathogenic counterpart *S. aureus* (from 46% to 53%) (NNIS 2004, Rosenthal et al. 2012). As acute and subacute haematogenous osteomyelitis in children is becoming rarer, also the microbial involvement is evolving (Craig et al. 1992, Blyth et al. 2001). From 1970 to 1990, the



prevalence of *S. aureus* infections has decreased from 50% to 31% (Craigien et al. 1992).

Due to different pathogenetic mechanisms and virulence factors, clinical manifestations of *S. aureus* and *S. epidermidis* infections markedly differ. The former usually occur as classical pyogenic infections and involve several virulence factors, such as toxins and degenerative exo-enzymes that cause tissue invasion by progressive inflammatory destruction and the new apposition of bone (Cunningham et al. 1996, Lew and

Waldvogel 1997), whereas the clinical picture of a typical foreign-body-related *S. epidermidis* infection is usually indolent without fulminant signs of infection (von Eiff et al. 2002).

Virulence factors are less aggressive with *S. epidermidis* and are mainly involved in the evasion of the immune response. In addition, the facilitation of robust attachment to implant surfaces with subsequent biofilm formation is an important phenotypic feature of *S. epidermidis* (Zimmerli et al. 2004, Otto 2008). Within protecting biofilm

<b>Table 2. Prevalence of microbiological findings in osteomyelitis</b>	
<b>Common (&gt;50% of cases)</b>	
	<i>S. aureus</i>
	<i>S. epidermidis</i> and other coagulase-negative staphylococci
<b>Occasionally encountered (&gt;25% of cases)</b>	
	Streptococci
	Enterococci
	<i>Pseudomonas</i> spp.
	<i>Enterobacter</i> spp.
	<i>Proteus</i> spp.
	<i>Escherichia coli</i>
	<i>Serratia</i> spp.
	Anaerobes ( <i>Peptostreptococcus</i> spp, <i>Clostridium</i> spp, <i>Bacterioides fragilis</i> group)
<b>Rarely encountered (&lt;5% of cases)</b>	
	<i>Mycobacterium tuberculosis</i>
	<i>Mycobacterium avium</i> complex
	Rapidly growing mycobacteria
	Dimorphic fungi
	<i>Candida</i> spp.
	<i>Aspergillus</i> spp.
	<i>Mycoplasma</i> spp.
	<i>Tropheryma whippei</i>
	<i>Brucella</i> spp.
	<i>Salmonella</i> spp.
	<i>Actinomyces</i>

Modified from Mandell et al. 2009.

against host-defence mechanisms, *S. epidermidis* strains show decreased metabolic activity (Resch et al. 2005) and a marked reduction in glucose uptake (Sousa et al. 2008). Both *S. aureus* and *S. epidermidis* have been shown to evade host defences through the mechanism of internalization within peri-implant non-phagocytic cells and also osteoblasts (Hudson et al. 1995, Broekhuizen et al. 2007, Khalil et al. 2007, Rohde et al. 2007).

**2.2.3. Classification**

There is no universally accepted method for classifying osteomyelitis, as multiple means have been used to characterize infectious states. Historically, osteomyelitis has been described by the duration of infection as acute, subacute and chronic. Osteomyelitis can also be classified on the basis of the aetiology of the infection, on the extent of the infection, and on the physiological conditions of the host. Two main classification systems for osteomyelitis have been introduced, the Waldvogel classification system and the Cierny-Mader staging system.

Acute osteomyelitis, frequently of a haematogenous origin, is considered to be a newly recognized bone infection. Patients typically have symptoms lasting from a few days to a week after the onset of the infection. The disease is predomi-

nantly found in childhood, as it usually involves rapidly growing bone and characteristically affects the metaphysis of long bones. The subacute and chronic bone infection states occur typically in adults and are frequently due to a penetrating trauma, an open fracture, or as a result of surgical procedures. Chronic osteomyelitis is commonly a continuation of an acute infection, but can occasionally be defined as chronic from the onset. Chronic osteomyelitis has somewhat arbitrarily been defined as a persistent microbial infection that evolves over a period of a month or up to years, and it is histologically characterized as involving low-grade inflammation, sequestra, and fistulous tracts (Lew and Waldvogel 2004).

The Waldvogel classification system (1970a-c) (Table 3) characterizes osteomyelitis primarily on basis of the source of the disease as haematogenous, osteomyelitis due to a contiguous focus, and osteomyelitis associated with vascular insufficiency. The duration of the infective process is also assessed. However, the classification system does not include the direct penetration of microorganisms into bone, for example, in association with penetrating trauma or surgery (Lazzarini et al. 2004). As the classification is based only on the aetiology of the disease, it is of limited value in clinical practice.

**Table 3.** Waldvogel classification of osteomyelitis

Haematogenous osteomyelitis
Osteomyelitis secondary to contiguous foci of infection
No generalized vascular disease
Generalized vascular disease
Chronic osteomyelitis

Waldvogel et al. 1970a-c.

The Cierny-Mader staging system (1985) (Table 4) includes an evaluation of the spread of infection into four anatomic stages, and it also evaluates changes in the physiology of the host (Cierny et al. 1985). The aetiology or chronicity of the infection is not assessed. In clinical practice, the staging system is applicable to the planning of treatment and to the forming

of the prognosis. Cierny-Mader stage 1 osteomyelitis can typically be treated with antimicrobial therapy alone, but stage 3 often requires combined antimicrobial therapy and surgical debridement with reconstructive procedures. It allows changes in the disease state to be evaluated dynamically, for example, in response to treatment.

<b>Table 4. Cierny-Mader staging system of osteomyelitis</b>	
<b>Anatomic type</b>	
Stage 1: Medullary osteomyelitis	
Stage 2: Superficial osteomyelitis	
Stage 3: Localized osteomyelitis	
Stage 4: Diffuse osteomyelitis	
<b>Physiological class</b>	
A Host: Healthy	
B Host:	
Bs: Systemic compromise	
Bl: Local compromise	
Bls: Local and systemic compromise	
C Host: Treatment worse than the disease	
<b>Systemic or local factors affecting immune surveillance, metabolism and local vascularity</b>	
<b>Systemic compromise (Bs)</b>	<b>Local compromise (Bl)</b>
Malnutrition, renal or hepatic failure, diabetes mellitus, chronic hypoxia, malignancy, old age, immunosuppression	Chronic lymphoedema, major vessel compromise, small vessel disease, vasculitis, venous stasis, extensive scarring, radiation fibrosis, neuropathy, tobacco abuse

Modified from Cierny et al. 1985.

### 2.2.4. Microbial and laboratory diagnostics

Laboratory tests can be helpful in detecting and monitoring the response to treatment, but they lack sensitivity and specificity, especially in the evaluation of low-grade infections (Berbari et al. 2010). Monitoring white blood cells (WBCs), erythrocyte sedimentation rate (ESR), and C-reactive protein (CRP) may provide valuable information. The WBC count can be elevated in acute osteomyelitis, but it can remain normal in chronic cases. The ESR value is typically elevated in both the acute and chronic states, and a decreasing value can be associated with a favourable response during treatment (Schulak et al. 1982). CRP has been reported to be more sensitive than ESR, but even a normal CRP value does not exclude the diagnosis of osteomyelitis (Perry 1996). For children with acute osteomyelitis, the CRP level has been found to predict the effectiveness of treatment and recovery from osteomyelitis bet-

ter than the ESR and WBC values (Unkila-Kallio et al. 1994, Pääkkönen et al. 2010).

Acquiring a precise bacteriological verification of the infecting organism from affected bone tissue or foreign-body is of fundamental importance. However, from 15% to 47% of osteomyelitis cases are reported to remain culture negative (Dich et al. 1975, Craigen et al. 1992, Floyed and Steele 2003). Wu et al. (2007) reported a low rate of positive culture results (14 of 41) for histologically confirmed cases of osteomyelitis obtained from imaging-guided bone biopsies. In studies of vertebral osteomyelitis, the negative culture rate in image-guided biopsy has been reported to vary from 68% to 70% (Heyer et al. 2012, Sehn and Gilula 2012). The factors that predict positive or negative culture results are not thoroughly known (Wu et al. 2007, Calhoun et al. 2009). Information achieved from swabs of ulcers or fistulae are commonly misleading. Only from 17.4% to 22% of sinus tract cultures have been

reported to confirm the osteomyelitis-causative bacteria (Mackowiak et al. 1978, Senneville et al. 2006). As standard, conventional microbiological methods are used in the diagnosis of osteomyelitis. Adherent bacteria (in biofilms found on surfaces of bone sequestra, infected orthopaedic implants, and methyl methacrylate, and peri-implant tissues of foreign substances) are difficult to eradicate, but they are also difficult to detect with normal microbiological methods (Gristina et al. 1985). It has been reported that some prosthetic joint infections have been classified as

aseptic loosening, but a thorough examination of retrieved tissue can reveal *S. epidermidis* infection (Broekhuizen et al. 2008). Ultrasonication of retrieved implant material or a bone tissue sample has been reported to increase the rate of positive cultures (Tunney et al. 1998). To detect low-virulent, slow-growing bacteria requires culturing for a long period. Culture-independent molecular techniques, such as polymerase chain reaction (PCR), are expected to improve the diagnostics of these infections (Fenollar et al. 2006, Fihman et al. 2007, Calhoun et al. 2009).

### 2.3. Imaging of osteomyelitis

The diagnosis of osteomyelitis is made on the basis of clinical, laboratory, and imaging results. The various important imaging methods are not competitive, but instead are complementary to each other.

#### 2.3.1. Radiography

Conventional radiographs are widely used in clinical work, for both diagnosis and follow-up. It is estimated that diagnostic anatomical changes in bone lag up to 2 weeks in the evolution of infection. Indeed, it has been proposed that from 50% to 75% of the bone matrix must be destroyed before infection can be diagnosed by conventional radiography (Butt 1973). The earliest visible changes are soft-tissue swelling and destroyed fascial planes, followed by periosteal elevation and demineralization (Butalia et al. 2008, Pineda et al. 2009). For chronic osteomyelitis, radiographic findings include disturbed bone architecture, bone sclerosis interspersed with radiolucencies, periosteal elevation, and draining sinuses (Lopes et al. 1997). In a meta-analysis of the use of radiography in the diagnosis of diabetic foot osteomyelitis, the sensitivity was 54%, and the specificity was 68% (Dinh et al. 2008).

#### 2.3.2. Computed tomography

Computed tomography (CT) is a useful tool for evaluating structural bone changes, and it is especially advantageous in the imaging of the spine, the pelvis, and the sternum. It provides valuable information on cortical bone destruction, peri-

osteal proliferation, and also, to some extent, on soft tissue changes. CT is able to visualize cortical destruction, periosteal elevation, and soft-tissue extension when no abnormalities are yet visible in plain radiographs (Wing et al. 1985, Pineda et al. 2009). It is a more sensitive method for visualizing bony destruction, gas in the bone, and bony sequestration than MRI is (Gold et al. 1991). Seltzer (1984) reported that CT plays an important role in the planning of both medical and surgical treatment. The major pitfall of CT imaging is the substantial loss of resolution due to beam-hardening artefacts in the proximity of metallic foreign bodies. Only a few reports have been published on the evaluation of CT accuracy in the evaluation of osteomyelitis (Termaat et al. 2005). Whalen et al. (1991) reported a sensitivity of 67% and a specificity of 50% in the diagnosis of vertebral osteomyelitis.

#### 2.3.3. Magnetic resonance imaging

Magnetic resonance imaging (MRI) is the currently preferred imaging method for evaluating previously normal bone, both for peripheral and central skeleton. MRI offers excellent soft-tissue to bone-marrow contrast resolution, and its multi-planar capability allows detailed anatomical evaluation in the assessment of the extent of infection (Zalavras et al. 2009). The initial visible osteomyelitic findings are due to changes in the amount of bone marrow fat, as the fat is replaced with water secondary to oedema, exudates, hyperaemia, and ischaemia. This state of disease

process is detected as a low signal intensity in T1-weighted MRI images and as a high signal intensity in T2-weighted images (Pineda et al. 2009). Sequestras appear as hypointense in T1-weighted and T2-weighted MRIs and do not exhibit gadolinium contrast enhancement. The characteristics of the MRI signal are non-specific, and several other bone involving conditions, such as tumours, neuropathic joints, and healing fractures, can also increase the water content of bone marrow. Post-operative scarring and oedema occur up to 12–13 months post-operatively, and it may be impossible to distinguish infection from bone remodelling, lesion hyperaemia, and oedema (Ma et al. 1997, Kaim et al. 2000, Ledermann et al. 2000). As a morphological cross-sectional imaging modality, MRI lacks the needed specificity but, in comparison, offers good sensitivity (Stumpe et al. 2000). The evaluation of secondary MRI osteomyelitis signs, such as cortical interruption, cutaneous ulcer, and sinus tract, have increased the diagnostic confidence in the assessment of diabetic foot (Morrison et al. 1998). The use of gadolinium enhancement is somewhat controversial, as it is also non-specific and may lead to misinterpretation (Ledermann et al. 2000). Major pitfalls of MRI in the evaluation of osteomyelitis are the limited use of whole-body imaging, the decrease in the yield of the MRI in the presence of metallic artefacts, such as fracture fixation devices and endoprostheses, the possibility that such artefacts may even make the MRI non-diagnostic, and the weakness in separating infection from trauma or fibrosis (Sammak et al. 1999, Chacko et al. 2003). In a comprehensive meta-analysis of diagnostic imaging methods involving chronic osteomyelitis by Termaat et al. (2005), MRI showed a sensitivity of 84% and a specificity of 60%. Kapoor et al. (2007) conducted a meta-analysis on the diagnosis of foot osteomyelitis and reported a sensitivity of 90% and a specificity of 82.5% for MRI.

### 2.3.4. Conventional nuclear medicine methods

Radionuclide studies are frequently used to evaluate musculoskeletal infections, as they are able to show abnormal tracer accumulation long before

anatomical changes occur. Similarly as for PET instrumentation, integrated single proton emission computed tomography (SPECT)/CT devices are currently in clinical use as the standard. In addition, conventional SPECT cameras have been developed, and indeed NanoSPECT cameras for research on experimental animals can produce images with a resolution of 1.2 mm (Cheng et al. 2010). Research on novel tracers is still being carried out for conventional scintigraphy, and the number of publications is greater than for PET (Larikka et al. 2002a and 2002b, Patel et al. 2009, van der Bruggen et al. 2010). The scintigraphic methods currently used to evaluate infection and inflammatory process include  $^{67}\text{Ga}$ -citrate scanning,  $^{99\text{m}}\text{Tc}$ -three-phase bone scanning,  $^{99\text{m}}\text{Tc}$ - or  $^{111}\text{In}$ -HMPAO-labelled leukocytes,  $^{99\text{m}}\text{Tc}$ -labelled nanocolloids or human non-specific immunoglobulin, and  $^{99\text{m}}\text{Tc}$ -labelled monoclonal anti-granulocyte antibodies.

$^{67}\text{Ga}$ -citrate, used since the 1970s, was the first scintigraphic marker used to detect infections. Like its positron-emitting isotope, it accumulates in the infectious site, due to the *in vivo* labelling of serum proteins, leukocytic lysosomes, and endoplasmic reticulum, along with increased vascular permeability and direct bacterial uptake (Hoffer 1980). Non-specific physiological uptake occurs in the liver, spleen, gastrointestinal tract, salivary and lacrimal glands, breasts, and external genitalia, as well as in the bone and haematopoietic bone marrow. Typically gallium imaging is performed 24 (18–72) hours after tracer injection. Delayed images are acquired at 48–72 hours to eliminate confusion with any bowel uptake (van der Bruggen et al. 2010). Due to its unfavourable characteristics, gallium scanning has been less frequently applied and has been replaced by other modalities. For  $^{67}\text{Ga}$ -citrate scintigraphy, a specificity of 61%–67% and a sensitivity of 25%–80% have been reported (Schauwecker et al. 1984, Al-Sheikh et al. 1985, Gratz et al. 2002). Gallium scintigraphy has also been used in conjunction with  $^{99\text{m}}\text{Tc}$ -MDP bone scanning. However, it has shown poor accuracy (only 70%) and is reported to be especially unreliable for patients with other lesions, such as bone involving surgery at the site of suspected osteomyelitis (Merkel et al. 1985).

Bone scanning has an important role in the diagnosis of osteomyelitis in the peripheral skeleton because of its ability to detect infection 24–48 hours after the onset. Due to its wide availability, the ease of the imaging procedure, and its low cost, bone scintigraphy with  $^{99m}\text{Tc}$ -labelled disphosphonates (e.g., MDP, DPD, HEDP) is widely used for the evaluation of skeletal processes (Davis and Jones 1976, Pauwels et al. 1983). The method is based on tracer accumulation through increased osteoblastic activity and skeletal vascularity (Genant et al. 1974). Imaging is conventionally performed 2–6 hours after the tracer administration. In addition to delayed images, a three-phase bone scan has been used to evaluate the process (Schauwecker 1992). Immediately after the tracer inoculation, the first phase involves assessing the blood flow to the suspected area. Within the first 5 minutes, the second phase visualizes the blood pool. These two early phases evaluate the degree of inflammation and hyperaemia. The third phase represents the tracer adsorption to bone tissue, presumably for the most part, to the mineral substance of bone. In the presence of osteomyelitis, a hot region can be detected in all three phases, in the first phase because of the commonly marked increase in blood flow to the infectious site. Arthritis, healing fractures, and previously treated osteomyelitis may cause a minor abnormality in the first two phases, but significant uptake is exhibited in the delayed bone images only (Sammak et al. 1999). Bone-scan findings are non-specific, but the method has been reported to be sensitive. Frequent false-positive results are found in relation to post-traumatic and post-operative situations, and the evaluation of chronic bone infection is troublesome. As with other scintigraphic methods, due to the low spatial resolution, differentiating between bone and soft-tissue involvement may be challenging. The meta-analyses of Termaat et al. (2005) and Prandini et al. (2006) reported a specificity of 25% and 75.2% and a sensitivity of 61% and 85.4%, respectively, for bone scintigraphy.

For peripheral skeleton, the currently preferred method is labelled WBC scintigraphy, especially when metallic foreign-bodies are present or after the occurrence of previous bone pathology or surgery (Kaim et al. 2002, Pakos et al.

2007). A variety of in vitro and in vivo leukocyte-labelling techniques with both  $^{111}\text{In}$  and  $^{99m}\text{Tc}$  has been published, including the use of HMPAO-labelled granulocytes and labelled anti-granulocyte antibodies (Becker et al. 1994). The most used method is  $^{111}\text{In}$ -oxine- or  $^{99m}\text{Tc}$ -HMPAO-labelled WBCs. For the preparation of the radiopharmaceutical, approximately 40–50 ml of the patient's blood is required for the ex vivo radiolabelling of the cells, which are subsequently re-injected into the patient. The process of preparing the tracer requires 2–3 hours. Leukocyte scintigraphy is based on the increased accumulation of WBCs, predominantly granulocytes, in the infectious site. Depending on the tracer, images are obtained 3–4 hours after the inoculation, and delayed images are obtained 18 to 24 hours after the trace administration. For the central skeleton, WBC scintigraphy is of limited value because of the normal margination of leukocytes and granulocytes in haematopoietic bone marrow that results in lower specificity (Gemmel et al. 2006, Kumar et al. 2008). Similarly, when the suspected infection site is in the marrow-containing part of the skeleton, such as the spine, the knees, or the hip, an additional bone-marrow scan is advised. It has also been reported that WBC scintigraphy is more applicable in the diagnosis of acute osteomyelitis. Chronic and low-grade infections are characterized by the predominance of macrophage involvement and may exhibit diminished granulocyte infiltration, the result being poor accuracy in WBC scintigraphy (Glithero et al. 1993, Prandini et al. 2006). On-going antimicrobial therapy may increase the number of cold lesions and also lower the sensitivity of a technique significantly (Whalen et al. 1991). Several bone-involving conditions (bone metastases, fractures, surgical defects, and irritation) have been reported to cause false-positive results (Sammak et al. 1999). The main drawbacks associated with the use of labelled leukocytes are the length of time needed for the labelling procedure, the need for specialized equipment, and the need to handle possibly contaminated blood products. One meta-analysis (Termaat et al. 2005) reported that the sensitivity for the peripheral skeleton was 84% and that, for the central skeleton, it was 21%. The

specificity for the peripheral skeleton was 80%, as compared with 60% for the central skeleton.

A combination of three-phase bone scintigraphy or  $^{99m}\text{Tc}$ -sulphur bone-marrow imaging with WBC or nanocolloid scintigraphy has been reported to be a more accurate method than the use of individual scintigraphic studies (Kaim et al. 2000, Love and Palestro 2004). Combined leukocyte and three-phase bone imaging especially performed 24 hours after tracer inoculation has been shown to increase sensitivity and specificity in the evaluation of infected joint prostheses (Larikka et al. 2001a and 2001b). However, variable rates of sensitivity (67%–88%) and specificity (78%–95%) have been reported (Wukich et al. 1987, Johnson et al. 1988, Palestro et al. 1991). Labelled leukocyte scintigraphy combined with  $^{99m}\text{Tc}$ -sulphur bone marrow imaging has been reported to be the radionuclide study of choice in the evaluation of periprosthetic infections and in differentiating between possible other causes of failure (Palestro et al. 1990 and 1991, Love and Palestro 2004). Osteomyelitis results in increased leukocyte accumulation but is associated with a suppressed uptake of sulphur colloid (Love et al. 2009). Combined leukocyte and marrow imaging has been reported to have a sensitivity of 92%–100% and a specificity of 87%–100% in the diagnosis of periprosthetic infections (Mulamba et al. 1983, Palestro et al. 1990, Love et al. 2004). However, Joseph et al. (2001) and Pill et al. (2006) reported significantly lower rates for sensitivity (46% and 50%, respectively) in the diagnosis of prosthetic joint infection. Love et al. (2004) reported that combined leukocyte and bone-marrow imaging was a more accurate method than coincidence detection-based  $^{18}\text{F}$ -FDG in the evaluation of painful lower-extremity prostheses. Despite promising results, for both of these combined methods, the most significant limitation is the ability to differentiate aseptic loosening from the infectious process.

### 2.3.5. Positron emission tomography

Positron emission tomography (PET) is an imaging modality that measures biochemical and physiological processes in vivo through the quantitative imaging of positron emitting radiotracers injected into the human body (DeGrado

et al. 1994). With PET imaging, it is possible to determine both the anatomical location and the degree of disease activity, based on physiological or metabolic changes (Zhuang and Alavi 2002).

#### 2.3.5.1. Scanner and basic principle

The patient is administered a suitable positron emitting radiopharmaceutical (e.g.,  $^{18}\text{F}$ ,  $^{11}\text{C}$ ,  $^{13}\text{N}$ ,  $^{15}\text{O}$ ,  $^{68}\text{Ga}$ ). Neutron-deficient nuclei gain stability through the transmutation from a proton (p) into a neutron (n), emitting a positron ( $e^+$ ) and an electron neutrino ( $\nu$ ) ( $p \rightarrow n + e^+ + \nu$ ) (Martinez et al. 2008). Interaction between the positron and the electron results in annihilation, creating two (511 keV) photons/gamma rays in opposite directions. A PET scanner is composed of a ring of proton detectors around the imaged subject (Figure 2). The detectors recognize two high-energy (511 keV) gamma particles emitted by the injected radionuclide and record information from the protons arriving at the detector in 180°-opposed directions in coincidence (DeGrado et al. 1994). The photon-emitting origin is calculated from the gathered data, and the image is reconstructed by processing the distribution of the detections using mathematical models. The amount of emitting substance in a lesion can be quantified (The 2004). By nature, PET images are not qualitatively influenced by metallic foreign bodies. They can have a resolution of  $\pm 5$  mm, as, in comparison, conventional SPECT instrumentation is able to produce images with a resolution of 10–15 mm (De Winter et al. 2002). The basic principle for the interpretation of PET images involves comparing the uptake values of contralateral sides. The scan is interpreted as positive when the uptake in the suspected site is greater than in corresponding healthy tissue (De Winter et al. 2002). Typically, whole-body PET imaging can be performed 40–60 minutes after tracer administration. Currently, the most novel PET cameras are combined PET/CT devices. Dual-modality PET/CT instrumentation provides tools to acquire more precise anatomical and physiological data that foremost improves specificity but also sensitivity (Kostakoglu et al. 2004, von Schulthess et al. 2006, Strobel and Stumpe 2007). The integration of CT to PET renders the conventional attenuation correction made

with a rotating radioactive source obsolete, as the data can be derived from the CT data, resulting in a 25%–30% faster imaging time as compared with that of conventional PET instrumentation (von Schulthess et al. 2006). Despite the benefits of combined instrumentation, when CT is used for attenuation correction, it causes signal artefacts in the proximity of metallic foreign bodies.

### 2.3.5.2. Tracers

#### 2.3.5.2.1. $^{18}\text{F}$ -2-fluoro-2-deoxyglucose

$^{18}\text{F}$ -2-fluoro-2-deoxyglucose ( $^{18}\text{F}$ -FDG) is currently the most widely used PET tracer. The injected tracer is a fluorinated glucose analogue; its accumulation reflects glucose metabolism. It is synthesized by substituting glucose molecules of the 2-hydroxyl group with the radioactive  $^{18}\text{F}$ -fluoride.  $^{18}\text{F}$ -fluoride is a positron-emitting substance that is manufactured with a cyclotron (Hamacher et al. 1986). The physical half-life of  $^{18}\text{F}$ -fluoride is 110 minutes.  $^{18}\text{F}$ -FDG is taken into cells by glucose transmembrane transporter (GLUT) and becomes phosphorylated in a manner similar to that of glucose by glucose 6-hexokinase (Pauwels et al. 2000). The activity of both GLUT molecules and glucose 6-hexokinase is increased in inflammatory cells at infectious and inflammatory sites. Normal glucose continues to be processed by the glycolytic pathway to produce energy. The deoxy- substitution prevents further metabolism, and it remains trapped inside the cell (Ak et al. 2000, De Winter et al. 2002). When  $^{18}\text{F}$ -FDG is used, elevated blood sugar concentrations,

especially those over 11 mol/l, may cause false-negative findings (Diederichs et al. 1998). A significant benefit of FDG is that it does not show significant physiological uptake in bone marrow, the liver, or the renal cortex (Sugawara et al. 1999).

$^{18}\text{F}$ -FDG uptake is elevated in such activated inflammatory cells as lymphocytes, granulocytes, and macrophages during their metabolic burst, because of the increased glucose use as an energy source (Kubota et al. 1992, Sugawara et al. 1999). The  $^{18}\text{F}$ -FDG uptake in inflammatory cells is often lower than in malignant cells, but, when activated, inflammatory cells exhibit a dramatic increase in tracer uptake (Heelan et al. 1998). In vitro studies performed by Lehmann et al. (2001) showed that activated neutrophils had a 209% higher  $^{18}\text{F}$ -FDG uptake than unstimulated cells.

#### 2.3.5.2.2. $^{68}\text{Ga}$ -chloride

$^{68}\text{Ga}$  is a positron-emitting transition metal that is suitable for PET imaging both when unconjugated and when used as a radioactive label for oligonucleotides or peptides (Roivainen et al. 2004 and 2012, Kumar and Boddeti 2013). Gallium in the form of  $^{67}\text{Ga}$ -citrate has been used in scintigraphy for decades for the evaluation of infectious processes. The two isotopes have several important differences. For example, the half-life of  $^{68}\text{Ga}$  (68 minutes) is much shorter than that of  $^{67}\text{Ga}$  (78 hours), enabling the use of higher doses, and the time needed to accumulate for  $^{68}\text{Ga}$  is relatively short (60 minutes). In addition, PET instrumenta-

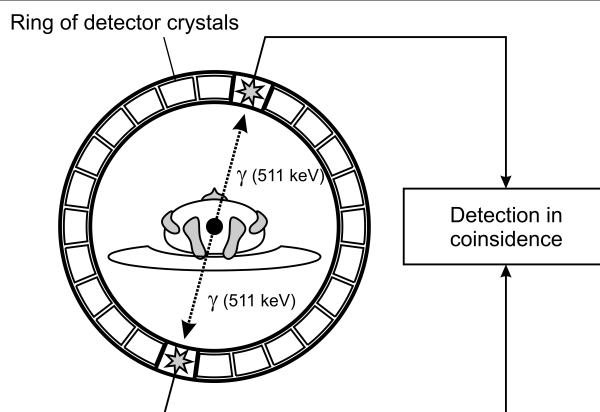


**Figure 2.** Schematic presentation of composition of PET scanner and the principle of detection of two gamma-rays arriving in coincidence on two 180°-opposed detectors. Modified from De Winter et al. 2002.



tion offers superior spatial resolution and sensitivity.  $^{68}\text{Ga}$ -chloride can be eluted using a  $^{68}\text{Ge}/^{68}\text{Ga}$  generator that eliminates the need for an onsite cyclotron (Ehrhardt and Welch 1978). Different isotopes differ only in their physical properties, but their chemical and physiological behaviour is comparable. The accumulation of gallium in inflammatory or infectious sites is partly due to the increased capillary permeability associated with inflammatory reactions; Ga exits the vascular network and is trapped in the extravascular compartment (El-Maghraby et al. 2006). As an iron analogue, it binds to circulating transferrin and, via transferrin receptors, accesses cells and evolves to a highly stable state (Chianelli et al. 1997). Gallium is able to bind to activated lactoferrin in neutrophils and to bacterial siderophores (Roivainen et al. 2012), and also uptake in macrophages has been demonstrated (Swartzendruber et al. 1971, Bernstein 1998). In addition, a direct bacterial uptake pattern has been reported (Menon et al. 1978).

Only a few  $^{68}\text{Ga}$ -labelled radiopharmaceuticals are in everyday use, but their applications are under extensive research (Roivainen et al. 2012). Recently, Nanni et al. (2010) published promising results on the evaluation of bone infections

with  $^{68}\text{Ga}$ -citrate PET/CT. It has been shown that the image qualities of  $^{68}\text{Ga}$ -tracers ( $\beta^+$  decay 90%,  $E_{\beta^+ \text{max}}$  2.91 MeV,  $T_{1/2}$  68 minutes) and  $^{18}\text{F}$ -tracers ( $\beta^+$  decay 97%,  $E_{\beta^+ \text{max}}$  0.64 MeV,  $T_{1/2}$  110 minutes) are almost equal (Sanchez-Crespo et al. 2004). However, even if the bio-distributions of the two tracers were equivalent, the radiation dose of the  $^{18}\text{F}$ -labelled compound would be less than that of the  $^{68}\text{Ga}$ -labelled one due to the significantly lower positron energy.

#### 2.3.5.2.3. Other tracers

Novel tracers have been studied both in patients and in experimental models with the objective of increasing the specificity of PET imaging (Table 5) (Goldsmith and Vallabhajosula 2009, Gemmel et al. 2009, Patel et al. 2009, Roivainen et al. 2012). However, thus far, only a few novel tracers have been tested in orthopaedic settings. High expectations have been set for such novel PET tracers as labelled antimicrobial peptides, especially with respect to differentiating between the infectious process and sterile inflammation (Lupetti et al. 2003). To date, none of the published novel imaging agents for infection imaging have been accepted for widespread clinical use.

**Table 5.** Experimental infection studies on novel PET tracers

Reference	Experimental model	Tracer
Fischman et al. 1991	Rabbit muscle fungal infection	$^{18}\text{F}$ -fluconazole (labelled antifungal drug)
Sugawara et al. 1999	Rat <i>Escherichia coli</i> muscle infection	$^3\text{H}$ -FDG ( $^3\text{H}$ -labelled FDG)
		$^3\text{H}$ -Thy or $^{11}\text{C}$ -Thy (labelled thymidine)
		$^3\text{H}$ -MET or $^{11}\text{C}$ -Met (labelled methionine)
		$^{125}\text{I}$ -HAS (labelled human serum albumin)
Siaens et al. 2004	Mice muscle fungal infection	$^{123}\text{I}$ -CHHiB_E144Q (labelled hydrolytic enzyme that breaks down the chitin of the cell walls of fungi)
Betgegowda et al. 2005	Mice muscle bacterial infection ( <i>S. aureus</i> , <i>Streptococcus pneumoniae</i> , <i>Enterococcus faecalis</i> , or <i>S. epidermidis</i> )	$^{125}\text{I}$ -FIAU (labelled nucleoside analogue)
Pellegrino et al. 2005	Rat muscle <i>E. coli</i> or <i>P. aeruginosa</i> infection	$^{18}\text{F}$ -FDG-WBC ( $^{18}\text{F}$ -FDG labelled white blood cells)
Salber et al. 2008	Rat muscle <i>S. aureus</i> infection	$^{18}\text{F}$ -UBI 29-41 (labelled antimicrobial peptide)
		$^{18}\text{F}$ -UBI 28-41 (labelled antimicrobial peptide)
Kumar et al. 2011	Rat <i>S. aureus</i> muscle infection	$^{68}\text{Ga}$ -apo-transferrin (labelled transferrin)
Ren et al. 2012	Rat models of aseptic loosening and septic loosening due to <i>S. aureus</i>	$^{18}\text{F}$ -PK11195 (labelled synthetic ligand binding to a peripheral benzodiazepine receptor)

Diaz et al. (2007) introduced the novel tracer  $^{124}\text{I}$ -FIAU [1-(2'-deoxy-2'-fluoro- $\beta$ -D-arabinofuranosyl)-5-iodouracil] for PET/CT imaging. It was studied in eight patients with suspected musculoskeletal infections. FIAU is a nucleoside analogue; as it is phosphorylated by thymidine kinase, it is trapped within a spectrum of bacterial cells that express the enzyme.  $^{124}\text{I}$ -FIAU was introduced as a promising agent with possibly higher specificity, as it is incorporated directly into the pathogen instead of into cells associated with the inflammatory process. The authors concluded that all of the patients with proven musculoskeletal infection could be delineated with the novel tracer.

In 2006, Dumarey et al. published their initial experience with PET/CT using  $^{18}\text{F}$ -FDG-labelled leukocytes in the imaging of infectious diseases. Altogether 8 of the 21 patients were studied due to suspected osteomyelitis, of which 2 were diagnosed as having a bone infection. The authors concluded that  $^{18}\text{F}$ -FDG-WBC PET/CT showed high sensitivity (86%), specificity (86%), and accuracy (86%) for the whole study group, with a negative predictive value of 100%. Rini et al. (2006) compared  $^{18}\text{F}$ -FDG-labelled leukocytes and  $^{111}\text{In}$ -labelled leukocytes in the detection of infection. A total of 51 patients were included, but, due to the low labelling efficiency of  $^{18}\text{F}$ -FDG leukocytes, it was not administered to 6 patients. Altogether 43 patients were imaged with both modalities. Most ( $n=38$ ) of the patients were suspected of having osteomyelitis or an orthopaedic implant infection.  $^{18}\text{F}$ -FDG-labelled leukocytes showed a sensitivity, specificity, and accuracy of 87%, 82%, and 84%, respectively. The results showed no statistical difference between the two modalities. Rini et al. (2006) believed that labelled WBCs showed promise for use as an infection-specific tracer and warranted further study.

Labelled antibiotic agents were introduced as substances that would bind specifically to bacterial cells and allow a differentiation between sterile inflammation and infection. Already in 1982, Prokesch and Hand studied antibiotic uptake into polymorphonuclear leukocytes in vitro using radiolabelled antibiotics, including  $^{14}\text{C}$ -rifampin,  $^3\text{H}$ -clindamycin,  $^3\text{H}$ -lincomycin,  $^{14}\text{C}$ -cephalexin,

$^{14}\text{C}$ -cefamandole,  $\text{N-}^{14}\text{CH}_3$ -erythromycin,  $^{14}\text{C}$ -penicillin,  $\text{G-}^3\text{H}$ -isoniazid,  $\text{G-}^3\text{H}$ -gentamicin, and  $^{14}\text{C}$ -ethambutol dihydrochloride. The most studied labelled antibiotic is  $^{18}\text{F}$ -ciprofloxacin (Brunner et al. 2004). It has been proposed that labelled ciprofloxacin would bind specifically to bacterial DNA/DNA gyrase, but instead the specific binding is masked with vast non-specific binding (Langer et al. 2005, Zijlstra et al. 2006). For infection imaging, Langer et al. (2005) studied four patients using  $^{18}\text{F}$ -ciprofloxacin both in vitro and in vivo. The patients had been diagnosed as having bacterial soft-tissue infections of the lower extremities. The soft-tissue infections resulted in a low uptake in both bacteria and granulocytes. Indeed, it has been proposed that  $^{18}\text{F}$ -ciprofloxacin is not suitable for use as an infection-specific tracer and that it requires further preclinical and clinical studies (Langer et al. 2005, Palestro et al. 2007).

#### 2.3.5.3. $^{18}\text{F}$ -FDG PET

Several studies have proven the usefulness of  $^{18}\text{F}$ -FDG PET in detecting a variety of orthopaedic infections, as most of the studies published on the use of  $^{18}\text{F}$ -FDG PET in evaluating infectious diseases involve the diagnosis of bone infections (Table 6). PET is cost effective when compared with the current standards used in most clinical settings (i.e., a combination of a three-phase bone scan, leukocyte scintigraphy, and a bone marrow scan) (Zhuang and Alavi 2002). Compared with expensive, laborious, and time-consuming leukocyte scanning, PET imaging can be performed within 1 hour after tracer administration, and therefore it allows a more rapid diagnosis.  $^{18}\text{F}$ -FDG allows superior image quality and resolution because of its more favourable tracer kinetics due to the smaller molecular size (Sugawara et al. 1999).  $^{18}\text{F}$ -FDG PET is not likely to be affected by on-going antibiotic treatment either (De Winter et al. 2001) or by the presence of metallic implants (Schiesser et al. 2003).  $^{18}\text{F}$ -FDG PET has been reported to be able to demonstrate the treatment response in osteomyelitis (Koort et al. 2005) and the success of infection prophylaxis by means of antibiotic releasing bioresorbable bone screws (Mäkinen et al. 2005). Guhlmann et al.

**Table 6.** Summary of clinical <sup>18</sup>F-FDG studies on osteomyelitis and implant infections

Reference	Number of patients/ confirmed infections	Type of suspected osteomyelitis	Pathogens involved	Sensitivity/ specificity/ accuracy
Guhlmann et al. (1998a)	31/18	Chronic	<i>S. aureus</i> n=12, <i>S. epidermidis</i> n=2, polymicrobial n=3, other n=1	100%/92%/97%
Guhlmann et al. (1998b)	51/28	Chronic	NR	97%–100%/95%–95%/96%–96%
Zhuang et al. (2000)	22/6	Chronic	NR	100%/87.5%/90.9%
Källicke et al. (2000)	15/15	Acute or chronic osteomyelitis/spondylitis	<i>S. aureus</i> n=8, <i>Mycobacterium tuberculosis</i> n=2, other n=1, not available n=4	NR
Schmitz et al. (2001)	16/12	Spondylitis	<i>S. aureus</i> n=5, <i>Mycobacterium tuberculosis</i> n=2, other n=2, no growth n=3	100%/92.3%/93.8%
Zhuang et al. (2001)	62 (74 prostheses)/11	Periprosthetic hip and knee	NR	90.5%/81.8%/NR
Van Acker et al. (2001)	21/6	Periprosthetic knee	<i>S. aureus</i> n=1, other n=2, not available n=3	100%/73%/81.0%
De Winter et al. (2001)	60/25	Chronic	NR	100%/88%/93%
Chacko et al. (2002)	32 (41 hips)/12	Periprosthetic hip	NR	91.7%/96.6%/95.1%
Gratz et al. (2002)	16/12	Spondylitis	NR	100%/87%/96%
Manthey et al. (2002)	23 (28 prostheses)/4	Periprosthetic hip and knee	NR	100%/100%/100%
Chacko et al. (2003)	56/34	Chronic		91.2%/91.3%/91.2%
	23/7	Post-traumatic		NR/NR/87%
	89/24	Orthopaedic implant	NR	91.7%–92%/NR/81%–96.2%
Schiesser et al. (2003)	22/12	Post-traumatic	NR	100%/93.3%/97%
Vanquickenborne et al. (2003)	17/8	Periprosthetic hip	NR	87.5%/77.8%/82.4%
De Winter et al. (2003)	57/15	Post-operative spine	NR	100%/81%/86%
Stumpe et al. (2004)	35/9	Periprosthetic hip	Coagulase neg. <i>staphylococcus</i> n=4, <i>S. epidermidis</i> n=2, other n=2, no growth n=1	22%–33%/81%–85%/69%–69%
Sahlmann et al. (2004)	17/17	Chronic	NR	NR
Mumme et al. (2005)	50/9	Periprosthetic hip	<i>S. epidermidis</i> n=3, <i>S. aureus</i> n=3, other n=3	91%/92%/91%
Reinartz et al. (2005)	63 (92 hips)/31	Periprosthetic hip	NR	94%/95%/95%
Keidar et al. (2005)	14/8	Diabetic foot	Polymicrobial n=1, NR n=8	NR
Pill et al. (2006)	89 (92 hips)/21	Periprosthetic hip	NR	95.2%/93%/NR
Stumpe et al. (2006)	28/3	Periprosthetic knee	<i>S. aureus</i> n=2, <i>S. epidermidis</i> n=1	NR
Hartmann et al. (2007)	33/18	Post-traumatic	<i>S. aureus</i> n=6, polymicrobial n=4, other n=1, no growth n=7	94%/87%/91%
García-Barrecheguren et al. (2007)	24/11	Periprosthetic hip	NR	64.3%/64.7%/NR
Schwegler et al. (2008)	20/7	Diabetic foot	<i>S. aureus</i> n=6, coagulase neg. <i>staphylococcus</i> n=1	29%/92%/70%
Chryssikos et al. (2008)	113 (127 hips)/33	Periprosthetic hip	NR	85%/93%/91%
Nawaz et al. (2010)	110/27	Diabetic foot	NR	81%/93%/90%
Familiari et al. (2011)	13/7	Diabetic foot	<i>S. aureus</i> n=4, <i>S. epidermidis</i> n=1, other n=1, no growth n=1	43%/67%/54%

NR = not reported

(1998b) and Källicke et al. (2000) have reported that, due to the superior resolution of  $^{18}\text{F}$ -FDG PET, osteomyelitis can be differentiated from infection in surrounding soft tissues.  $^{18}\text{F}$ -FDG PET has been shown to be applicable also for use with immune-suppressed patients, as it has been found to be able to identify infectious foci that remain undetected with other modalities (Mahfouz et al. 2005). Despite the relatively high spatial resolution, all nuclear medicine methods have the general restriction of producing only limited anatomical information. Combined PET/CT hardware has been introduced to improve the received anatomical information and to provide precise anatomical data. As a non-specific indicator of increased cellular glucose metabolism,  $^{18}\text{F}$ -FDG accumulates also in sites of sterile inflammation, for example, due to the healing process in the post-operative or post-traumatic phase, and in malignant lesions (Zhuang and Alavi 2002).

In general, studies of  $^{18}\text{F}$ -FDG PET have reported superior sensitivity and a negative predictive value for a variety of patient populations. In meta-analyses on all commonly used modalities by Termaat et al. (2005), Prandini et al. (2006) and Wang et al. (2011),  $^{18}\text{F}$ -FDG PET was reported to be the most accurate method for evaluating chronic osteomyelitis, infections of peripheral bone and prosthetic joint implants, and infections of the vertebral column.

$^{18}\text{F}$ -FDG PET has been shown to be applicable in diagnosing acute osteomyelitis in both peripheral and central skeleton (Källicke et al. 2000).  $^{18}\text{F}$ -FDG is able to show an increased accumulation as soon as activated leukocytes migrate to the infectious site. However, PET imaging seems not to be superior to other nuclear medicine modalities in the diagnosis of acute bone infections (Sugawara et al. 1999). Significantly fewer reports have been published on the use of  $^{18}\text{F}$ -FDG PET in the evaluation of acute osteomyelitis, and other than the seven patients in the study by Källicke et al. (2000), published data are limited to those from experimental animal models.

$^{18}\text{F}$ -FDG PET is highly sensitive and accurate in detecting low-grade and chronic infections because, as a small molecule,  $^{18}\text{F}$ -FDG is able to penetrate easier and faster to even poorly per-

fused lesions than other cellular tracers are, and PET has superior imaging characteristics.  $^{18}\text{F}$ -FDG PET has been shown to be applicable in the evaluation of Brodie's abscess and has also been reported to be a potential adjunct to MRI (Strobel et al. 2006, Fathinul and Nordin 2010). Reports on the use of  $^{18}\text{F}$ -FDG PET in the evaluation of osteitis associated with the SAPHO syndrome are mainly case reports (Pichler et al. 2003, Takeuchi et al. 2007). Guhlmann et al. (1998a), Zhuang et al. (2000) and De Winter et al. (2001) published a sensitivity of 100% for the detection of chronic osteomyelitis. The reported specificity was slightly lower in the study by De Winter et al. (2001) than in the study by Guhlmann et al. (1998a), probably because of differences in the patient selection criteria, as Guhlmann et al. excluded patients who had been operated on in the last two years. Osteomyelitis in the central skeleton is accurately diagnosed with  $^{18}\text{F}$ -FDG PET (Källicke et al. 2000, Schmitz et al. 2001, Gratz et al. 2002, De Winter et al. 2003, Gemmel et al. 2010).

$^{18}\text{F}$ -FDG PET has been proven to be a valuable imaging modality in the diagnosis of post-operative and post-traumatic, as well as implant-associated osteomyelitis.  $^{18}\text{F}$ -FDG PET is reported as the most sensitive method for this patient group (De Winter et al. 2003). Using  $^{18}\text{F}$ -FDG PET, De Winter et al. (2003) studied 57 patients with previous vertebral surgery. The specificity dropped (to 75%) only for the subgroup of patients who had undergone surgery within the past 6 months or for those with osteosynthesis material present (specificity 65%), but the authors concluded that the number of false-positive results, even in the early post-operative phase, remained acceptable. Due to inflammation associated with tissue healing, fractures and surgery causes increased  $^{18}\text{F}$ -FDG accumulation and, therefore, may cause false-positive interpretations of  $^{18}\text{F}$ -FDG PET (Meyer et al. 1994, Zhuang et al. 2003). Zhuang et al. (2003) assessed the period in which abnormal, increased  $^{18}\text{F}$ -FDG accumulation is noted after traumatic or surgical fractures. Altogether 37 patients with a traumatic or surgical fracture were evaluated: 14 patients had trauma or surgery within the previous 3 months, and 23 had fractures or surgical intervention more than 3 months

prior to the  $^{18}\text{F}$ -FDG PET. The authors concluded that abnormally elevated  $^{18}\text{F}$ -FDG uptake resulting from bone tissue trauma lasts only a short period. Previously, Zhuang et al. (2000) published a report on a series of 22 patients suspected of having osteomyelitis and reported two false-positive cases of increased  $^{18}\text{F}$ -FDG uptake in patients with tibial non-union and subsequent osteotomy. In the absence of malignancies or infection at the site of a fracture or surgery, increased  $^{18}\text{F}$ -FDG uptake should return to normal in less than 3 months, and, therefore, increased uptake after 3 months is probably due to osteomyelitis or another pathological process (Zhuang et al. 2003). Schiesser et al. (2003) evaluated  $^{18}\text{F}$ -FDG PET use prospectively in the diagnosis of osteomyelitis associated with metallic implants ( $n=22$ ). Of the 29 suspected infectious sites,  $^{18}\text{F}$ -FDG PET correctly identified infection in 14 sites; a true-negative result was confirmed for 14 patients. One false-positive finding was found for a patient who had undergone surgery 6 weeks prior to the imaging. However, 8 patients who had undergone surgery in the previous 6–8 weeks presented a true-negative finding in the PET scan. However, the level and duration of abnormally increased  $^{18}\text{F}$ -FDG uptake have not been fully established. Zhuang et al. (2003) have noted that time is not the only factor that affects the length of an increased  $^{18}\text{F}$ -FDG uptake normalization period. Bone scintigraphy returns to normal at different rates in different osseous structures; therefore it can be assumed that also  $^{18}\text{F}$ -FDG uptake patterns differ according to the bone involved.

Despite promising early results, findings of PET imaging for the evaluation of painful joint prostheses have varied. In light of this variation, a recent guideline of the American Academy of Orthopaedic Surgeons issued only a weak recommendation for the use of nuclear imaging, including  $^{18}\text{F}$ -FDG PET, in the diagnosis of periprosthetic implant infections (Della Valle et al. 2011). Initially, it was suggested that  $^{18}\text{F}$ -FDG PET would be able to differentiate loosening from an infected endoprosthesis with good confidence, but more recent data suggest that this may not be the case (Manthey et al. 1999, Van Acker et al. 2001, Zhuang et al. 2001, Stumpe et al. 2004).

Studies have shown that PET is more accurate in diagnosing infection in hip prostheses than in knee prostheses, but, so far, the explanation for this variation is unclear. Zhuang et al. (2001) studied the usefulness of PET imaging in the diagnosis of infection associated with knee and hip prostheses. They reported the sensitivity, specificity, and accuracy associated with knee prostheses to be 90%, 72%, and 78%, respectively, and the corresponding values for hip prostheses were 90%, 89%, and 90%, respectively. In a meta-analysis carried out by Kwee et al. (2008), the 89.8% specificity reported for hip prostheses was considered to be significantly higher than the specificity of 74.8% for knee prostheses. Definite criteria should be defined to characterize the uptake pattern in aseptic loosening and periprosthetic infection. It has been suggested that an increased  $^{18}\text{F}$ -FDG uptake marking infection must be present along the interface between the bone and the prosthesis to be considered infection (Van Acker et al. 2001, Zhuang et al. 2001 and 2002, Chacko et al. 2002, Vanquickenborne et al. 2003, Reinartz et al. 2005, Delank et al. 2006). Commonly, also in asymptomatic hips, an increased  $^{18}\text{F}$ -FDG uptake can be found around the neck section of a prosthesis and in the inter-trochanteric area of femurs, which should not be used as an indicator of infection (Zhuang et al. 2001, Chacko et al. 2002, Vanquickenborne et al. 2003, Reinartz et al. 2005, Delank et al. 2006). Similarly, for asymptomatic knee prostheses, diffuse  $^{18}\text{F}$ -FDG uptake has been found in the inter-condylar space (Van Acker et al. 2001). The cell-rich vascular peri-implant tissue between the bone and a loose prosthesis, and in the soft tissue around the neck of loose hip implants, contains more activated macrophages and proliferating cells, and this abundance can possibly explain the significant accumulation of  $^{18}\text{F}$ -FDG at sites of aseptic loosening (De Winter et al. 2001).

$^{18}\text{F}$ -FDG PET has been proven to be a valuable method for evaluating diabetic foot bone infections, but also significant limitations have been presented. From 15% to 25% of diabetic patients develop foot ulcers, and approximately from 15% to 20% of the ulcers exhibit underlying osteomyelitis (Reiber 1996, Ramsey et al. 1999, Lavery et

al. 2003 and 2006). Keidar et al. (2005) evaluated the use of  $^{18}\text{F}$ -FDG PET/CT with 14 patients with diabetic foot infections. They concluded that  $^{18}\text{F}$ -FDG PET/CT was applicable for these patients in that combined PET/CT instrumentation allowed a precise diagnosis for bone and soft-tissue infection; in addition, anatomic localization of abnormal  $^{18}\text{F}$ -FDG uptake can facilitate the necessary treatment. In comparison, Schwegler et al. (2008) and Familiari et al. (2011) reported significantly

worse results. In both of these studies, PET instrumentation without CT was used, which may have, to some extent, influenced the results. Diabetic patients exhibit insulin resistance, and this resistance may have influenced the insufficient cellular uptake of the glucose analogue  $^{18}\text{F}$ -FDG (Maor and Karnieli 1999, Schwegler et al. 2008). In addition, a long-lasting, marked, low-grade infectious process and the possible use of antimicrobial agents were considered as possible explanations.

## 2.4. PET imaging of inflammatory reaction

Inflammatory reaction is the initial response to trauma, tissue irritation, or microbial invasion. Inflammation, in association with both infectious and non-infectious processes, is characterized by an increase in glucose consumption by activated granulocytes, lymphocytes, and macrophages. In non-infectious diseases the pathological process is initiated at the molecular or chemical level and is subsequently followed by anatomical changes.  $^{18}\text{F}$ -FDG PET provides means for detecting and quantitatively evaluating inflammatory disease activity *in vivo* already in the pre-anatomical stage. Non-infectious inflammatory conditions involving the musculoskeletal system include osteoarthritis, rheumatoid arthritis, ankylosing spondylitis, seronegative arthritis, bursitis, tendinitis, synovitis, rotator cuff degeneration, polymyalgia rheumatica, myocitis, tissue healing process, and radiation necrosis (Metser and Even-Sapir 2007).

### 2.4.1. Imaging of inflammatory conditions in the skeletal system

The pathogenesis of osteoarthritis, a disease affecting the entire joint structure, is hypothesized to result from mechanical and biochemical degenerative changes associated with ageing. Its pathogenesis and progression have been proposed to be associated with the infiltration of inflammatory cells that lead to synovitis, osteoarticular inflammation, and subsequent progression of anatomical changes (Pelletier et al. 2001, Fernandes et al. 2002). Currently, the main diagnostic tools are clinical evaluation in concordance with conventional x-ray imaging. It is believed that  $^{18}\text{F}$ -FDG

PET could illustrate the initial metabolic changes in glucose utilizing chondrocytes that maintain the high concentration of glucosaminoglycan in cartilage (Carey et al. 2011). Various publications have evaluated the applicability of  $^{18}\text{F}$ -FDG PET, including information related to several affected joints. In 2001, Schulthess et al. reported that, in a retrospective analysis of data on 354 patients,  $^{18}\text{F}$ -FDG PET findings preceded the symptomatic findings of osteoarthritis. They found a strong correlation between  $^{18}\text{F}$ -FDG uptake, graded according to a visual assessment scale, and the patient's age. Degenerative osteoarticular changes are a common cause of  $^{18}\text{F}$ -FDG accumulation in the shoulder. Wandler et al. (2005) evaluated tracer uptake patterns in 24 patients to identify specific shoulder disease entities. According to the final diagnosis, based on the clinical diagnosis, 14 of 21 patients had consistent findings in the  $^{18}\text{F}$ -FDG PET imaging; the remaining 7 patients were found to be clinically normal. They were able to show 3 different  $^{18}\text{F}$ -FDG uptake patterns, each corresponding to a different disease entity (diffuse uptake around the glenohumeral joint that indicated osteoarthritis or bursitis, a greater focal tuberosity uptake that indicated rotator cuff degeneration, and local glenoid uptake that indicated clinically evident frozen shoulder). It must be noted that 5 non-symptomatic patients had positive PET findings, and 3 patients exhibited more than one uptake pattern. Rosen et al. (2006) determined the prevalence of abnormal  $^{18}\text{F}$ -FDG uptake in respect to degenerative spine diseases and correlated the results with CT findings. An increase in tracer uptake was the most

frequently noted in the lumbosacral region. The authors reported that the severity of the degenerative process, evaluated as the degree of  $^{18}\text{F}$ -FDG uptake, showed a significant, although weak, correspondence to CT findings. Importantly, with PET/CT, a differentiation of metastatic spinal lesions from degenerative processes was achieved. One common drawback of  $^{18}\text{F}$ -FDG PET osteoarthritis studies is that they constantly lack histopathological confirmation of the diagnosis. With PET, patients are subjected to greater radiation exposure than when plain radiographs are used, and this feature hinders the use of this method, especially in the follow-up of patients with chronic degenerative joint disorders.

Rheumatoid arthritis is a chronic autoimmune, joint-destroying disease characterized by progressive systemic inflammation and changes in synovial tissue (Brenner 2004). Synovial changes are characterized by massive leukocyte infiltration, proliferation, and hyper-vascularization, all resulting in pannus formation (Carey et al. 2011). Early diagnosis for inflammatory joint disorders is crucial so that appropriate therapy can be started before structural changes emerge. In addition, the follow-up of treatment response is important, as is identifying patients with an increased risk of rapid disease progression. At the molecular level, Lin et al (2007) demonstrated the applicability of  $^{18}\text{F}$ -FDG PET in the evaluation of inflammatory joint disorders in two rabbit models of acute knee inflammatory arthritis. They reported that  $^{18}\text{F}$ -FDG uptake correlated with synovial fluid tumour necrosis- $\alpha$  levels. In 2009, Matsui et al. studied the correlation between  $^{18}\text{F}$ -FDG accumulation and rheumatoid arthritis pathology in rats with collagen-induced arthritis. They concluded that, in the tested animal model,  $^{18}\text{F}$ -FDG accumulated in swollen joints and uptake increased with the progression of the arthritis. Tracer accumulation correlated more with pannus formation than with the infiltration of inflammatory cells. In a clinical study of 10 patients, of 9 of whom had an established inflammatory joint destructive process in the hip and 1 patient showed the same process in the ankle joint; all of the affected joints could be detected with  $^{18}\text{F}$ -FDG PET (Roivainen et al. 2003). It was

also reported that  $^{18}\text{F}$ -FDG SUV highly correlated with the synovial volume measured with MRI. Later, the  $^{18}\text{F}$ -FDG uptake was shown to correlate with MRI and ultrasound findings, as well as with laboratory parameters of serum inflammation (C-reactive protein and matrix metalloproteinase-3) (Beckers et al. 2004). Rheumatoid arthritis frequently affects small joints. In a study of 14 rheumatoid arthritis patients with symptoms in joints of the hand and the wrist, an increased  $^{18}\text{F}$ -FDG uptake was reported for 29% of the joints (Elzinga et al. 2007). The precise mechanism of  $^{18}\text{F}$ -FDG uptake to sites of rheumatoid inflammation has not been thoroughly depicted (Metser and Even-Sapir 2007). Indeed, in a study of 12 patients with ankylosing spondylitis, disease activity was introduced as being reflected predominantly by bone formation, imaged with  $^{18}\text{F}$ -fluoride, rather than by an inflammatory reaction imaged with  $^{18}\text{F}$ -FDG (Bruijnen et al. 2012).

It is widely known that, for orthopaedic patients, bone fracture and adjacent tissue healing is the most frequent cause of false-positive  $^{18}\text{F}$ -FDG PET findings (Rosenbaum et al. 2006, Meller et al. 2007). Whether  $^{18}\text{F}$ -FDG PET would be applicable in the evaluation of fractures has also been examined. Hsu et al. (2007) compared the characteristics of  $^{18}\text{F}$ -fluoride and  $^{18}\text{F}$ -FDG in the assessment of fracture healing in a rat femur model with weekly PET scans.  $^{18}\text{F}$ -fluoride, an indicator of osteoblastic activity, resulted in a progressively increased uptake in femurs with successful fracture unions, but only minimal uptake occurred in the animals with non-unions. This finding suggests that  $^{18}\text{F}$ -fluoride can be used as an indicator of disrupted bone healing. In contrast, there were no differences in the  $^{18}\text{F}$ -FDG uptake between the groups at any time point. Schmitz et al. (2002) evaluated  $^{18}\text{F}$ -FDG PET findings among patients (n=17) with vertebral compression fractures. They questioned whether  $^{18}\text{F}$ -FDG PET would distinguish pathological fractures from osteoporotic fractures. Four fractures were identified as being pathological, three had been caused by spondylodiscitis, and one was due to plasmacytoma.  $^{18}\text{F}$ -FDG PET resulted in one false-positive result, but all four of the pathological fracture patients exhibited significantly increased tracer ac-

cumulation. In light of this finding, Schmitz et al. concluded that  $^{18}\text{F}$ -FDG PET may have a potential role in distinguishing between pathological and osteoporotic vertebral fractures.

Bone radiation damage is reported to be a rare, but potentially critical complication of radiation therapy. Osteoradionecrosis may be a significant pitfall in the use of  $^{18}\text{F}$ -FDG PET with respect to oncological patients (Liu et al. 2004, Lee et al. 2008). The region of osteoradionecrosis exhibits radiation-induced ischaemic necrosis with subsequent inflammatory reaction resulting in an increased uptake of  $^{18}\text{F}$ -FDG (Metser and Even-Sapir 2007). Distinguishing osteoradionecrosis from tumour recurrence or residual tumour on the basis of radiographic CT or MRI changes may also be complicated. Therefore,  $^{18}\text{F}$ -FDG PET is more applicable in the follow-up of post-radiation bone changes, especially when CT/MRI findings remain indefinite (Liu et al. 2004).

#### 2.4.2. Vascular adhesion protein-1

Vascular adhesion protein-1 (VAP-1) was described by Salmi and Jalkanen in 1992. Further analysis of the molecule revealed that VAP-1 was a homodimeric, copper-containing, 170 kDa sialoglycoprotein that belongs to a specific group of semicarbazide oxidases (SSAOs) (Smith et al. 1998). VAP-1 is a dual-function membrane protein with adhesion properties and amine oxidase activity. Only a low level of VAP-1 can be detected on the normal endothelium of some vessels, as it is predominantly stored in intracellular

granules (Arvilommi et al. 1996). Under normal conditions, VAP-1 is abundantly present in pericytes, smooth muscle cells, and fat cells, but it is absent from all leucocytes and most capillaries and endothelial cells in large vessels (Salmi and Jalkanen 2001, Abella et al. 2003). Upon inflammatory challenge, its expression is induced and it is rapidly translocated to the luminal surface of endothelia (Salmi et al. 1993, Jaakkola et al. 2000). In addition, VAP-1/SSAO molecules occur in a soluble-circulating form in the blood stream.

WBC extravasation from the blood into tissues is crucial for an adequate inflammatory response. The leukocyte extravasation process is comprised of overlapping steps and is governed by several classes of adhesion molecules and chemokines (Figure 3) (Butcher and Picker 1996). A group of selectins and their ligands mediate the initial tethering and rolling phase. In the second step, chemoattractants help to form a more stable adhesion between the vessel endothelia and leukocytes. The final step of firm adhesion and diapedesis through the vascular wall is mediated by leukocyte integrins and members of the immunoglobulin superfamily.

VAP-1 plays a critical role in leukocyte trafficking by recruiting lymphocytes,  $\text{CD8}^+$  T-cytotoxic cells, and  $\text{CD16}^+$  natural killer cells in particular, from blood into lymphoid organs and into inflamed tissues (Figure 3) (Smith et al. 1998). VAP-1 has been shown to mediate leukocyte adhesion to venules in synovial tissue sections from patients with rheumatoid arthritis, in inflamma-

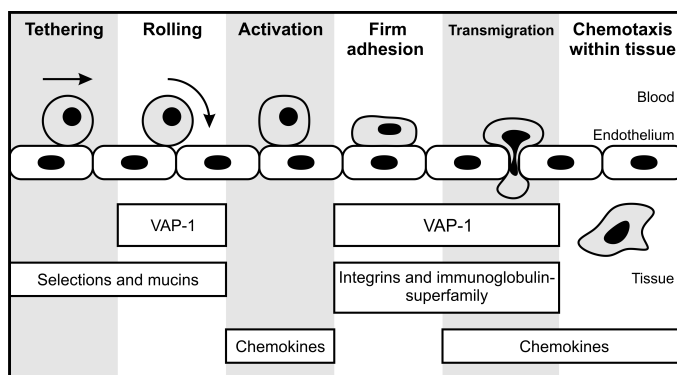


**Figure 3.** Schematic representation of leukocyte extravasation cascade and involved adhesion molecules and chemokines. Modified from Salmi and Jalkanen (2005).



tory skin diseases (e.g., psoriasis and atopic eczema), in Crohn's disease, and in ulcerative colitis (Salmi and Jalkanen 2001). In endothelial cells and adipocytes, VAP-1 can directly regulate lymphocyte rolling and stimulate glucose transport (Salmi et al. 2000, Zorzano et al. 2003, Stolen et al. 2005). In experimental acute peritoneal inflammation model blocking of VAP-1 function resulted in diminished granulocyte rolling, firm adhesion, and transmigration (Tohka et al. 2001). After the inhibition of VAP-1 activity with monoclonal antibodies, a significant decrease in inflammatory response was found in mice (Merinen et al. 2005). The enzymatic SSAO activity of VAP-1 is a key source of hydrogen peroxide generation through the deamination of methylamine and aminoacetone. Hydrogen peroxide is

a known pro-inflammatory substance, and, when locally produced, it mediates leukocyte entry into tissue (Salmi and Jalkanen 2005).

For PET imaging Ujula et al. (2009) described the synthesis and  $^{68}\text{Ga}$ -radiolabelling of linear peptide containing DOTA-chelate ( $^{68}\text{Ga}$ -DOT-AVAP-P1). Previously, the linear nine amino acid peptide was introduced to bind to a groove of a VAP-1 molecule (Yegutkin et al. 2004). Studies on VAP-1-targeting tracers in PET imaging have been published in turpentine oil-induced acute sterile inflammation, in tumour xenografts and in biodistribution studies (Autio et al. 2010 and 2011, Aalto et al. 2011). After the initial studies, VAP-1 binding radiopharmaceutical has been developed further (Silvola et al. 2010, Autio et al. 2010 and 2011).

## 2.5. Animal models of osteomyelitis

Conducting clinical studies on bone infections is difficult due to the low incidence rate, the variety of clinical presentation, the diversity of pathogens and their antimicrobial sensitivity, the variety of anatomical locations, and the differences in human host status. These difficulties have led to the development of animal models of osteomyelitis. Several animal models using different species have been described, but most studies are performed with rabbits, rats, or mice (O'Reilly and Mader 1999). The precise predictive value of the results of animal studies, as compared with those obtained with humans, still remains unclear.

The rabbit osteomyelitis model is widely used. As compared with models of other animal species, the rabbit model is effective, and the induction of infection is relatively easy. In addition, there is a low mortality rate, it also allows repeated surgical procedures, and the use of implants is possible. In 1884, Rodet performed the initial attempts to create the rabbit osteomyelitis model with the use of the intravenous "micrococcus" inoculum (Rodet 2005). Later, Lexer (1894) produced bone abscesses using intravenous *S. aureus* inoculum. Lexer concluded that acute, progressive medullary bone infection was impossible to induce through the use of an intravenous injection of pathogen alone. In 1941, Scheman et al. developed a reproducible

rabbit animal model of chronic tibial osteomyelitis using a sodium morrhuate and staphylococci injection into the metaphysis by inserting a needle into the medullary cavity percutaneously. In the experiment, some of the animals died prematurely, but most of them developed chronic, although variable, osteomyelitis. Norden (1970) and Norden and Kennedy (1971) further studied Scheman's animal model. In 1 to 3 weeks postinfection, the described model has been found to produce a diffuse acute-subacute infection, which closely mimicked human osteomyelitis (Mader and Shirliff 1999). The authors evaluated the significance of direct intramedullary bacterial inoculation with and without sodium morrhuate (Norden 1970). Sodium morrhuate is a sclerosing agent, composed of fatty acids and arachidonic acids, producing aseptic bone necrosis. Altogether 90% of the animals administered both sodium morrhuate and the staphylococcal inoculum produced microbiologically and histologically confirmed osteomyelitis at 60 or even 180 days. The rabbit model presented by Norden and Kennedy is currently the most widely used. Andriole et al. (1973 and 1974) developed a rabbit model using the insertion of a stainless steel pin. According to the Cierny-Mader classification, the model produces 1A osteomyelitis. A total of 88% of the animals given the Giorgio staphylococ-

cal inoculum after the insertion of an intramedullary pin produced culture-positive osteomyelitis with both clinical and roentgenographic findings of bone infection. The authors concluded that the model would maintain chronic bone infection for a period of 1.5 years. Currently, the Andriole model is only rarely used. Worloc et al. (1988) described an animal model that mimics post-traumatic osteomyelitis. The rabbit tibia is surgically exposed, fractured, and stabilized with a wire. Subsequently, *S. aureus* inoculum is injected into the fracture site. In addition to *S. aureus*, also other pathogens have been used in modifications of these animal models, for example, *Pseudomonas aeruginosa*, *Bacterioides* spp. (including *fragilis*, *thetaiotamicon*, *melanogenicus*) (Norden et al. 1980, Mayberry-Carson et al. 1990 and 1992, Johansson et al. 1991, Lambe et al. 1991, Petri 1991).

The most widely used rat model for osteomyelitis was originally introduced by Zak et al. (1981). Later it was described in more detail by Rissing et al. (1985a,b). Originally, the rat model was based on the Scheman et al. (1941) rabbit model. Infection was induced by the application of sodium morrhuate and *S. aureus* inoculations into the tibial metaphysis through a drilled hole. The created cortical bone defect was sealed with bone wax. The use of bone wax has been shown to have a promotional effect on the induction of experimental osteomyelitis (Nelson et al. 1990). Of 107 animals, 87 (81%) had culture-positive osteomyelitis, and the cultures remained positive for an observation period of 70 days. In a histopathological evaluation, a chronic bone infection was confirmed. Lucke et al. (2003) described a rat model of implant-related bone infection that mimicked intramedullary nailing. The infection was induced with as little as  $10^2$  cfu/10  $\mu$ l of bacterial inoculum through the use of a sterile K-wire. No additional substances, such as sclerosing agents, were needed to induce the infection.

Mice are widely used for all research purposes. Due to the vast knowledge existing on the function and regulation of the mouse immune system, a mouse model was created to study the immune response to the osteomyelitic process. Chadha et al. (1999) modified a previously described rabbit model to create a post-traumatic osteomyelitis

model for mice. A total of 27 mice were divided into two groups, a control group with a fracture without bacterial inoculum (n=7) and a group of 20 mice who received an intravenous injection of *S. aureus*, along with a created fracture of the proximal tibial growth plate. Seven days after the surgery, all of the bone cultures were positive for the mice inoculated with *S. aureus*, and, in the histological examination, osteomyelitic changes were evident. In addition, the presence of *S. aureus* was confirmed with the use of polymerase chain reaction (PCR).

Smaller animal species are unable to accommodate clinically relevant implant devices or tolerate repeated surgical procedures. In 1983, Fitzgerald published a canine model of tibial osteomyelitis. The tibial metaphysis was surgically exposed, and a 1cm cortical bone window was drilled, followed by *S. aureus* inoculum. The created defect was filled with polymethylmethacrylate (PMMA) bone cement. Later, in an important experimental study, Petty et al. (1985) evaluated and compared the incidence of infection associated with commonly used materials in orthopaedic and trauma surgery. Infection was induced in canine femur by a bacterial inoculum (*S. aureus*, *S. epidermidis* or *Escherichia coli*) and followed by the insertion of a foreign body (stainless steel, chromium cobalt, polyethylene, or PMMA). The presence of a foreign body significantly reduced the number of pathogens needed for the induction of infection. PMMA, especially when allowed to polymerize in vivo, caused osteomyelitis already with 1000 cfu of *S. aureus*.

For conventional scintigraphy, novel tracers have been studied in a number of experimental models in different animals (Patel et al. 2009). However, thus far, a significantly fewer number of experimental osteomyelitis models have been used to evaluate novel tracers for PET. Ren et al. (2012) used rat models to study  $^{11}\text{C}$ -PK11195 and  $^{18}\text{F}$ -FDG for the differentiation of septic *S. aureus* and aseptic prosthesis loosening with PET. More frequently, modifications of rabbit osteomyelitis and foreign-body infection models have been used in PET studies (Koort et al. 2004 and 2005, Jones-Jackson et al. 2005, Mäkinen et al. 2005, Brown et al. 2012).

### 3. AIMS OF THE STUDY

The present study was initiated to improve the tools for diagnosing osteomyelitis and to evaluate the accuracy of  $^{18}\text{F}$ -FDG PET under different infectious bone conditions.

The following aims are addressed in this thesis:

1. To compare  $^{18}\text{F}$ -FDG and  $^{68}\text{Ga}$ -chloride in the PET imaging of osteomyelitis and uncomplicated bone healing in a rat model.
2. To characterize the feasibility of using a new  $^{68}\text{Ga}$ -labelled synthetic peptide ( $^{68}\text{Ga}$ -DOTA-VAP-P1) targeted towards VAP-1/SSAO for PET imaging of early inflammatory and infectious processes in healing bones in a rat model.
3. To determine whether a causative bone pathogen contributes to the level of  $^{18}\text{F}$ -FDG uptake in PET imaging of *S. aureus* osteomyelitis and *S. epidermidis* biomaterial-related bone infection in a rabbit model.
4. To determine whether the level of  $^{18}\text{F}$ -FDG uptake is dependent on the virulence of the underlying pathogen and whether it differs in culture-negative and culture-positive patients of histologically and/or microbiologically proven osteomyelitis.

## 4. MATERIALS AND METHODS

### 4.1. Experimental studies

#### 4.1.1. Experimental animals

Adult male Sprague-Dawley rats (n=128) (I and II) and New Zealand white rabbits (n=22) (III) were used in the experimental studies. Before surgery, the animals were acclimated to their new environment. Throughout the experiments, the animals were allowed to move without restrictions, and their well-being was monitored daily. The Ethics Committee of the University of Turku and the Provincial State Office of Western Finland approved the study protocols. All of the experiments were carried out in the Central Animal Laboratory of the Institution, which is included in the National GLPC-Compliance Program and is managed according to the European Convention for the Protection of Vertebrate Animals Used for Experimental and Other Scientific Purposes and Statutes 1076/85 §3 and 1360/90 of the Animal Protection Law of Finland and EU Directive 86/609.

#### 4.1.2. Anaesthesia and peri-operative care

The surgical procedures were performed in a veterinary operating room with the use of standard surgical techniques under strict sterile surgical conditions. The operated hind leg was carefully shaved, disinfected, and covered with sterile sheets. The animals were anaesthetized with a mixture of fentanyl plus fluanisone (Hypnorm<sup>®</sup>) and midazolam (Midazolam Hameln). Anaesthesia was reversed by a subcutaneous injection of naloxone (Narcanti<sup>®</sup>). After the surgery, the animals were closely monitored, and standard post-operative pain medication was given. For the rats and the rabbits, buprenorphine (Temgesic<sup>®</sup>) and carprofen (Rimadyl<sup>®</sup> Vet), respectively, were administered for 3 post-operative days. All of the animals were killed with an overdose of sodium pentobarbital (Mebunat<sup>®</sup>) at stipulated intervals.

#### 4.1.3. Pathogens used in the induction of osteomyelitis and foreign-body infection

Three different staphylococcal strains were used. In studies I, II, and III *S. aureus* (strain 52/52A/80, kindly provided by Dr Jon T. Mader) was used as the pathogen. Originally, the strain was isolated from a child with osteomyelitis. The strain (52/52A/80) has been used extensively in experimental models of osteomyelitis (Rissing 1990). In study III, a foreign-body-associated infection model was created using a laboratory strain of *S. epidermidis* (ATCC 35983) and a clinical strain of *S. epidermidis* (T-54580). The T-54580 *S. epidermidis* strain was retrieved at the Turku University Hospital from a young male with a post-operative infection of a plated proximal tibial fracture. The bacterial inoculum was cultured overnight on a blood agar plate. Bacterial cells were suspended in sterile saline until the final optical density was achieved. On the basis of the optical density measured with a spectrophotometer, a suspension containing approximately  $3 \times 10^8$  cfu/ml of *S. aureus* (I, II, III) and  $10^9$  cfu/ml of *S. epidermidis* (III) was used as the inoculum. The bacterial suspension was stored at 4°C and used on the day of preparation. To confirm the actual number of bacteria in the suspension, a 10-fold dilution series was prepared, and 100 µl of each dilution was plated on blood agar plates for the calculation of the cfu/ml.

#### 4.1.4. Experimental animal models and study protocols

##### 4.1.4.1. Tibial osteomyelitis model of rat

In studies I and II, animals were divided into two groups, animals with induced osteomyelitis and control animals representing uncomplicated bone healing. In study I, comparative <sup>18</sup>F-FDG and <sup>68</sup>Ga-chloride PET imaging were performed with both tracers on consecutive days 2 weeks after the surgery. For comparative ex vivo measurements of tis-

sue radioactivity, the accumulation of  $^{18}\text{F}$ -FDG and  $^{68}\text{Ga}$ -chloride was studied in animals with induced osteomyelitis and in animals with normal bone healing at 2 weeks. In addition, comparative 120-minute dynamic  $^{18}\text{F}$ -FDG and  $^{68}\text{Ga}$ -chloride PET imaging were performed for two osteomyelitic rats.

Study II consisted of two parts. First, time series analyses of PET uptake using  $^{68}\text{Ga}$ -DOTA-VAP-P1 as a tracer were performed at 12, 24, and 36 hours and at 7, 14, and 28 days after the surgery. In the second part of the study, PET imaging was performed at 24 hours and at 7 days after the surgery on animals with induced osteomyelitis and animals with normal bone healing. In addition, 10 healthy non-operated rats were used for the harvesting of control bone samples for the histological examination.

A diffuse rat osteomyelitis model (stage IVA of the Cierny-Mader classification; osteomyelitis secondary to a contiguous focus of infection in the Waldvogel classification) was applied (Mader 1985, O'Reilly and Mader 1999). A small cortical bone defect (diameter 1.0 mm) was created in the proximal medial metaphysis of the right tibia with the use of a high-speed dental drill. Local bone marrow was removed with saline lavage. Osteomyelitis was induced by administering 0.05 ml of 5% w/v sodium morrhuate (Scleromate<sup>®</sup>). Immediately thereafter, 0.05 ml of *S. aureus* bacterial inoculum was administered into the medullary cavity. The cortical bone defect was sealed with bone wax to prevent bacterial leakage and also to provide a foreign body for infection (Nelson et al. 1990). The skin wound was cleaned with sterile saline lavage and closed in layers. In the control animals, a cortical defect of equal size was drilled, but sodium morrhuate, bacterial suspension, or bone wax were not used. Before the wound was closed, the surgical field was lavaged with sterile saline containing 150 mg of cefuroxime sodium (Zinacef).

## 4.2. Clinical study

### 4.2.1. Patients

In study IV the patient population was 40 consecutive orthopaedic patients who had  $^{18}\text{F}$ -FDG PET between May 2000 and February 2004 for an

### 4.1.4.2. Tibial osteomyelitis and foreign-body bone infection models of rabbit

In study III, the animals were randomized into three groups on the basis of the infection model and the inoculated pathogen. In group 1, a localized osteomyelitis model induced with a clinical strain of *S. aureus* was applied. In groups 2 and 3, a foreign-body-associated infection model was used, a clinical or laboratory strain of *S. epidermidis* being applied. Each animal underwent a two-stage surgery for the induction of bone infection in the medullary cavity of the proximal left tibia. In study III,  $^{18}\text{F}$ -FDG PET imaging and other analyses were performed 6 weeks after second-stage surgery.

The localized *S. aureus* osteomyelitis model (stage IIIA of the Cierny-Mader classification) was adopted from that of Koort et al. (2004), and the foreign-body-associated infection model was modified from that of Mayberry-Carson et al. (1992). With the use of an anteromedial surgical approach, a cortical bone window (6 mm × 2.7 mm) was drilled into the proximal medial metaphysis of the left tibia. Bone marrow was removed with saline lavage. A small block of bone cement was transplanted into the medullary cavity, followed by a peri-implant injection of 0.10 ml of *S. aureus* or one of the two *S. epidermidis* strains. The animals inoculated with *S. epidermidis* also received an 0.1 ml injection of aqueous sodium morrhuate (5 % wt/vol) (Scleromate<sup>®</sup>) for the induction of local bone necrosis and to promote the development of the infectious process. At 2 weeks, with the use of the previous surgical approach, the animals underwent second-look surgery for verification of the induced local infection. The bone cement block was left in place in the animals with *S. epidermidis* inoculum in order to mimic a foreign-body-associated infection, but it was removed from the *S. aureus*-inoculated animals.

evaluation of a clinically suspected bone infection. The suspicion of bone infection was based on clinical symptoms, laboratory findings, and results of conventional imaging modalities. The study cases

were retrieved from the hospital database on the basis of the reference number of the  $^{18}\text{F}$ -FDG PET imaging. The study group included 25 female and 15 male patients, with a mean age of 48.4 (SD 22.1 years; range 10–82 years). The clinical charts of the patients were retrospectively reviewed.

There was no contact with the patients, and informed consent was not obtained. The study was approved by the hospital and was conducted in accordance with the principles of Declaration of Helsinki.

Altogether 26 (65%) of the 40 patients had definite histopathological and/or microbiological diagnoses based on the examination of the samples. A total of 14 of the original 40 patients were

excluded from the current analysis: 7 cases were excluded because no histopathological or microbiological verification of the diagnosis was made; 5 cases because  $^{18}\text{F}$ -FDG PET was applied only in the evaluation of an antimicrobial treatment response; and 2 cases were excluded because the primary indication for  $^{18}\text{F}$ -FDG PET imaging was tumour imaging and not the presence of associated infection. The final diagnosis was osteomyelitis for 16 patients (62%), soft-tissue infection for 4 patients (15%), and spinal-implant infections for 2 patients (8%). In the remaining 4 cases, the final diagnoses were plasmacytoma, osteoblastoma, transient bone marrow oedema, and sternoclavicular osteoarthritis.

### 4.3. Analysis methods

A summary of the analytical methods used in each study is presented in Table 7.

#### 4.3.1. Experimental studies

##### 4.3.1.1. Positron emission tomography

PET imaging was performed using an Advance PET Scanner (General Electric Medical Systems)

in studies I, II, and IV, and in study III a Discovery PET/CT device (General Electric Medical Systems) was used.  $^{18}\text{F}$ -FDG was synthesized with an automatic apparatus by a modification of the method of Hamacher et al. (1986).  $^{68}\text{Ga}$ -chloride was eluted with 0.1 M HCl from a  $^{68}\text{Ge}/^{68}\text{Ga}$  generator (Cyclotron C) and was neutralized with 1 M NaOH before use. Linear nine amino acid

Table 7. Applied analysis methods in studies I–IV

Method	Study I	Study II	Study III	Study IV
$^{18}\text{F}$ -FDG PET	•			•
$^{68}\text{Ga}$ -chloride PET	•			
$^{68}\text{Ga}$ -DOTA-VAP-P1 PET		•		
$^{18}\text{F}$ -FDG PET/CT			•	
Ex vivo measurement of tracer accumulation	•			
pQCT	•	•	•	
Radiography	•	•	•	
Bacteriology	•	•	•	•
Histology	•	•	•	•
MRI				•
CT				•
Infection scanning				•
Bone scanning				•

peptide (GGGGKGGGG) containing DOTA-chelate was synthesized and labelled with  $^{68}\text{Ga}$  ( $^{68}\text{Ga}$ -DOTAVAP-P1) (Ujula et al. 2009). The animals fasted for 4 hours prior to the tracer injection. The tracers were injected into the rat tail vein (**I**, **II**) or into the ear vein of the rabbits (**III**). Dynamic PET imaging consisting of  $4 \times 5$  minute frames was started 40 minutes after the injection of  $^{18}\text{F}$ -FDG (**I**, **III**), 70 minutes after the injection of  $^{68}\text{Ga}$ -chloride (**I**), and 40 minutes after the injection of  $^{68}\text{Ga}$ -DOTAVAP-P1 (**II**). With the use of two rod sources containing  $^{68}\text{Ge}$ , a 5-minute transmission scan for attenuation correction was obtained after the emission imaging.

Scatter correction, random counts, and dead-time corrections were incorporated into the reconstruction algorithm. Images were reconstructed in a  $128 \times 128$  matrix. A quantitative analysis of tracer uptake was performed for the standardized circular region of interest (ROI) (diameter = 3.0 mm for the rats and radius = 3.8 mm for the rabbits) of the operated tibia and the corresponding region of the contralateral intact tibia. Tracer accumulation was reported as the SUV, which is calculated from the amount of radio activation in the ROI divided by the relative injected dose expressed per animal body weight. The SUV ratios between the operated and non-operated sides were calculated (De Winter et al. 2001).

#### 4.3.1.2. Ex vivo measurement of tracer accumulation

In study **II**, the accumulation of  $^{18}\text{F}$ -FDG and  $^{68}\text{Ga}$ -chloride was studied ex vivo for the osteomyelitic animals and for the animals with healing bone defects at 2 weeks. After the tracer accumulation (60 minutes for  $^{18}\text{F}$ -FDG, 90 minutes for  $^{68}\text{Ga}$ -chloride), an intra-cardiac blood sample was obtained, and the animals were killed.

A 15-mm-long segment of the operated proximal tibia (including the site of the bone defect) and a corresponding segment of the contralateral tibia were resected for an analysis of the tracer uptake. In addition, specimens were excised from calf muscles. The radioactivity of the blood, muscle, and bone specimens was measured with a gamma counter (1480 Wizard 3" Gamma Coun-

ter) cross-calibrated with a dose calibrator (VDC-202). The tracer accumulation was expressed as the SUV [(tissue radioactivity/tissue weight)/(total given radioactivity/rat body weight)], and the radioactivity ratios (SUV ratios) between the operated and non-operated sides were calculated. The target-to-background ratio was also calculated by dividing the SUV of the osteomyelitic or healing tibia by the SUV of the ipsilateral calf muscle.

#### 4.3.1.3. Peripheral quantitative computed tomography

After the PET imaging, each animal underwent peripheral quantitative computed tomography (pQCT) scanning (**I**, **II** and **III**). The imaging was performed with the use of a Stratec XCT Research M pQCT device (Norland Stratec Medizintechnik GmbH). The animals were placed in a holder to standardize the position of the legs. After an initial scout view, the proximal tibias at the site of the bone defect were imaged in 6 consecutive cross-sectional images. A voxel size of  $0.07 \times 0.07 \times 0.50 \text{ mm}^3$  and a slice distance of 0.5 mm were used for the rats (**I**, **II**), the corresponding distance being 0.75 mm for the rabbits (**III**). The density ( $\text{mg}/\text{cm}^3$ ) and area ( $\text{mm}^2$ ) of the trabecular and cortical bone were measured at the cross-sectional plane at the midlevel of the bone defect of the operated tibia and at the corresponding plane of the contralateral intact tibia (**I**, **II**). In study **III**, the pQCT images were analysed for the presence of osteomyelitic destruction and reactive new-bone formation.

#### 4.3.1.4. Radiography

Anterior-posterior and lateral radiographs of the operated limbs were taken on digital image plates (Fuji IP cassette) with a standard stationary X-ray unit (Philips) (**I**, **II** and **III**).

In studies **I** and **II** the radiographic presence of osteomyelitic bone changes was classified according to the Rissing osteomyelitis system (Rissing et al. 1985b) (Table 8). Two independent observers (authors PL and TJM) evaluated the radiographs with respect to four parameters (the presence of periosteal elevation, architectural distortion, widening of the bone shaft, and new bone formation),

**Table 8.** Radiographic assessment of osteomyelitic changes in rats (I, II) according to Rissing et al. (1985b)

Radiographic findings
Raised periosteum
Destruction of architecture
Widening of shaft
New bone formation
Concurrent presence of any two radiographic tests
Composite score; representing the total number of cases with each of these particular abnormalities divided by the total number tested
Percentual area of bone destruction

**Table 9.** Radiographic assessment of osteomyelitic changes in rabbits (III) according to Mader and Wilson (1983)

Grade	Radiographic findings
0	Normal
1	Elevation or disruption of periosteum or both; soft tissue swelling
2	< 10% disruption of normal bone architecture
3	10–40% disruption of normal bone architecture
4	> 40% disruption of normal bone architecture

and their consensual interpretation was used for the data analysis. The radiographic presence of destructive bone changes in the lateral view of the tibia was quantified with a computer-based image analysis system (LabVIEW 6.1). The area of bone destruction was measured and expressed as the percentage of the total area of the tibia in the lateral view. The average value of two independent observers was used in the data analysis. In study III, two independent observers (authors PL and KL) classified the radiographic bone changes according to the osteomyelitis grading system of Mader and Wilson (1983) (Table 9), and their consensual interpretation was used for the data analysis.

#### 4.3.1.5. Microbiological analysis

The bone defect area was exposed with sterile techniques to obtain bone culture specimens of bone (I, II and III) and foreign body (III). Swab cultures were taken from subfascial soft tissues. The proximal tibia was aseptically cross-sectioned with the use of a high-speed circular saw. All of the swab specimens were cul-

tured for 18 to 20 hours at 35 °C on blood agar plates. After snap-freezing in liquid nitrogen and homogenization with a mortar and pestle, all of the specimens were vortexed in saline for 5 minutes, and 10 serial 10-fold dilutions were done to determine the colony-forming units (cfu) of *S. aureus* or *S. epidermidis* per gram of bone. The dilutions were cultured for 18 to 20 hours at 35 °C on blood agar plates. The aseptically harvested bone-cement blocks were cultured on blood agar, immediately placed in BBL™ brain heart infusion broth (Becton, Dickinson and Company), and incubated up to 5 days at 35 °C. The turbidity of the broth samples was observed daily, and positive cultures were plated on blood agar plates. The plates were incubated for 18 to 20 hours at 35 °C. Negative broth samples were cultured similarly after 2 and 5 days of incubation.

The isolated pathogens were identified on the basis of morphology, the Slidex® Staph Plus latex agglutination test, and the API-Staph® identification test (bioMérieux) (van Griethuysen et al. 2001). *S. aureus* (ATCC 29213) was used as the



positive control, and *Enterococcus faecalis* (ATCC 29212) was the negative control. Pulse-field gel electrophoresis (PFGE) was used to confirm that the isolated strain of *S. aureus* was identical to the inoculated strain (52/52A/80).

#### 4.3.1.6. Histology

For the hard-tissue histopathological examination, the bone specimens were fixed in 70% ethanol, dehydrated in a graded series of ethanol, cleared in xylene, and embedded in isobornyl-methacrylate (Technovit 1200 VLC). Sections (20 µm) were prepared and stained with a modified van Gieson method (I, II and III).

For the decalcified histology, the specimens were fixed in 10% formaldehyde, decalcified, and embedded in paraffin. Sections (4 µm) were prepared and stained with haematoxylin and eosin for the evaluation of the inflammatory cell response (I, II and III).

In study II, the level of VAP-1 expression at the site of osteomyelitis or healing bone was determined from samples of decalcified, paraffin-embedded bone tissue. The staining of paraffin sections with polyclonal anti-serum, used in immunoperoxidase stainings, raised against VAP-1, was done using microwave treatment in a citrate

buffer for antigen retrieval and subsequent staining with the avidin-peroxidase method using a Vectastain kit. All of the samples were stained with rabbit anti-rat antibody, with normal rabbit serum as a negative control, and counter-stained with haematoxylin and eosin.

In studies I, II, and III, osteomyelitic changes in the periosteum, cortical bone, and medullary canal were classified according to the histopathological scoring system presented by Petty et al. (1985) (Table 10). The stage of inflammation was semi-quantitatively scored from – (score 0) to +++ (score 3), on the basis of the extent of inflammatory cell infiltrates in the bone marrow (II, III). In study II, the immunoperoxidase staining results were semi-quantitatively analysed in a blind manner using the following scoring: – (score 0), no positivity; + (score 1), faint positivity with a few positive vessels detected; +++ (score 3), strong positivity for many vessels. The rating of ++ (score 2) was given to samples falling between categories + and +++. Two independent observers (Studies I–II: authors PL and TJM; Study III authors PL and KL) classified the histological sections, and the results were presented as the average values of their interpretation.

**Table 10.** Summary of the histological classification by Petty et al. (1985) (I, II and III)

Infection Grade	Periosteal Reaction	Cortex	Medullary Canal
0	Often absent; if present, laminated and limited to 1–2 thin layers; eccentric and often related to off-centre drill defect	Haversian canals small and repair rate slow; polymorphonuclear leukocytes not in granulation tissue; occasional subperiosteal resorptive pockets, but no polymorphonuclear leukocytes	Quick repair with woven bone; inflammatory cells range from none to foci of many intact polymorphonuclear leukocytes; these leukocytes associated with macrophage clean-up; diffuse process
1	Usually laminated with 1–2 layers; often eccentric but not related to off-centre drill defect	Occasional polymorphonuclear leukocytes in Haversian canals	Subtle, diffuse increase in polymorphonuclear leukocytes; small number of microabscesses present
2	Sunburst type; often nearly circumferential; no apparent cause	Focally enlarged Haversian canals filled with granulation tissue and fragmented polymorphonuclear leukocytes; occasional microabscess	Definite diffuse increase in polymorphonuclear leukocytes with fragmented forms; several definite microabscesses
3	Florid, always sunburst type; circumferential	Subperiosteal, endosteal, and intracortical resorption associated with fragmented polymorphonuclear leukocytes; microabscesses	Vast number of microabscesses or great increase in polymorphonuclear leukocytes diffusely
4			As above, but with sinus-tract formation and soft-tissue microabscesses

### 4.3.2. Clinical study

#### 4.3.2.1. Clinical follow-up and analyses

All of the patients (n=26) underwent  $^{18}\text{F}$ -FDG PET, and correlative imaging studies were performed on the basis of the clinical assessment. All of the studies were evaluated routinely as part of clinical work. The clinical reviewers of the PET images had access to all of the patient charts, including the results of conventional imaging modalities.  $^{18}\text{F}$ -FDG PET imaging was performed in a fasted state (minimum of 6 hours) with an Advance PET scanner (General Electric Medical Systems). Dynamic acquisition was started 60 minutes after the injection of  $^{18}\text{F}$ -FDG. The mean dose of the intravenous bolus injection of  $^{18}\text{F}$ -FDG was 297 MBq (SD 71 MBq; range 160–384 MBq). MRI was performed for 20 patients, and for 9 patients CT scanning was used in routine clinical sequences. For skeletal imaging, three-phase bone scintigraphy was performed on 20 of 26 patients with  $^{99\text{m}}\text{Tc}$ -HDP or DPD. Anterior and posterior  $^{99\text{m}}\text{Tc}$ -WBC (HMPAO, Ceretec, n=12)

or  $^{99\text{m}}\text{Tc}$ -anti-granulocyte scintigraphy (LeukoScan, Immunomedics GmbHn, n=6), whole-body planar scans, or spot images were obtained 5 minutes after the injection and again 3–5 hours later.

The results of the  $^{18}\text{F}$ -FDG PET images and correlative imaging studies were retrospectively reviewed and evaluated as positive or negative for bone infection. The results obtained were reflected with the final diagnosis work, and the results were recorded as true/false positive or true/false negative. For the  $^{18}\text{F}$ -FDG PET results, a quantitative evaluation was performed. A quantitative analysis of PET tracer uptake was performed on standardized circular ROIs (diameter=1.5 cm) at the site of suspected infection with the use of transaxial slices. The tracer accumulation was reported as the average SUV (SUV mean) and the maximum SUV (SUV max), representing the highest pixel uptake in the ROI. The SUV ratios (i.e., the radioactivity ratio between the region of suspected infection and the healthy corresponding site) were also calculated.

### 4.4. Statistical analyses

The data have been given as means  $\pm$  standard deviations (SDs). The normal distribution and homogeneity of the variances were tested. A paired t-test was applied in the intra-animal comparison. An unpaired t-test was applied to study the significance of the differences between two groups. Statistical comparisons of more than two study groups were carried out with a one-way analysis of variance (ANOVA) with a Tukey's post hoc test. If the data were not normally distributed or failed to pass the test for the homo-

geneity of variance, they were analysed using the non-parametric Mann-Whitney rank sum test for the comparison of two groups or with the Kruskal-Wallis one-way ANOVA on ranks with Dunn's post hoc test for multiple groups. In addition, Fisher's exact test was used in the analysis of categorized data. The correlations between different analytical measurements were analysed using the Spearman correlation test or linear and non-linear regression models. P-values of  $<0.05$  were considered significant.

## 5. RESULTS

### 5.1. Comparison of $^{18}\text{F}$ -FDG and $^{68}\text{Ga}$ -chloride in the PET imaging of *S. aureus* osteomyelitis and uncomplicated bone healing in a rat model

#### 5.1.1. Confirmation of *S. aureus* infection

The inoculated pathogen was successfully cultured from all of the retrieved bone specimens from all of the animals with induced osteomyelitis. The isolated *S. aureus* strain was matched with the inoculated strain (52/52A/80) using PFGE. No bacteria could be cultured from the bone specimens retrieved from the control animals. The osteomyelitis group showed diffuse osteomyelitis with severe destruction of bone architecture and sequestrum in plain radiographs and pQCT imaging. The control group showed signs of uneventful healing of the cortical defect.

#### 5.1.2. In vivo uptake of $^{18}\text{F}$ -FDG and $^{68}\text{Ga}$ -chloride

PET imaging showed an increased uptake of both  $^{18}\text{F}$ -FDG (SUV ratio  $1.74 \pm 0.37$ ) and  $^{68}\text{Ga}$ -chloride (SUV ratio  $1.62 \pm 0.28$ ) in the osteomyelitic tibias as compared with the results of the contralateral intact tibias ( $P < 0.001$ ). These SUV ratios of the osteomyelitic animals differed significantly ( $P < 0.001$ ) from those of corresponding control animals with healing bone defects.

In the control animals with healing bone defects, a slightly increased uptake of  $^{18}\text{F}$ -FDG (SUV ratio  $1.16 \pm 0.06$ ), but no apparent increase in the  $^{68}\text{Ga}$ -chloride uptake (SUV ratio  $1.02 \pm 0.05$ ), was found when compared with the results of the contralateral intact tibia ( $P = 0.003$ ).

The intensity of the  $^{68}\text{Ga}$ -chloride uptake reflected pathological changes of the osteomyelitic bones as measured by pQCT (Figure 4). The uptake of  $^{18}\text{F}$ -FDG, however, did not show as close a correlation with the anatomical changes.

#### 5.1.3. Ex vivo analysis of $^{18}\text{F}$ -FDG and $^{68}\text{Ga}$ -chloride accumulation

The ex vivo measurements of retrieved tissues correlated closely with the results of the in vivo PET imaging. The SUV ratio of  $^{18}\text{F}$ -FDG was significantly ( $P = 0.003$ ) higher in the osteomyelitic group ( $1.63 \pm 0.17$ ) than in the control group ( $1.13 \pm 0.26$ ). The SUV ratio for the  $^{68}\text{Ga}$ -chloride accumulation in bone was significantly ( $P < 0.001$ ) higher in the osteomyelitis group ( $1.92 \pm 0.56$ ) than in the control group ( $0.92 \pm 0.21$ ).

In the control group, there was no statistically significant difference in the  $^{68}\text{Ga}$ -

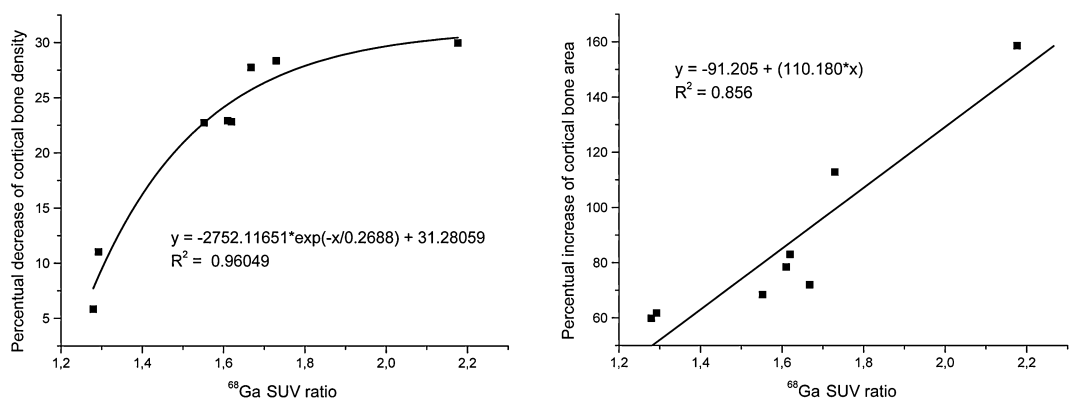


**Figure 4.** Correlation of  $^{68}\text{Ga}$ -chloride SUV ratio with the percentage change in cortical bone density (left) and area (right).

chloride uptake between the operated bone (SUV 0.28±0.10) and the contralateral bone (SUV 0.31±0.11). For the control animals, the

SUV ratio of <sup>68</sup>Ga-chloride was significantly (P=0.022) lower than the SUV ratio of <sup>18</sup>F-FDG.

## 5.2. Evaluation of <sup>68</sup>Ga-DOTAVAP-P1 for the differentiation of inflammatory and infectious bone processes in a rat model

### 5.2.1. Confirmation of the induction of *S. aureus* infection

The inoculated *S. aureus* (52/52A/80) was cultured from the homogenized bone specimens for all of the animals with induced osteomyelitis, and the isolated pathogen matched with the inoculated strain in the PFGE analysis. All of the culture specimens from the control animals with healing cortical defects were negative.

At 7 days, radiographs and pQCT imaging demonstrated moderate cortical bone destruction, circumferential periosteal reaction, reactive new bone, and sequestrum formation in the osteomyelitic tibias.

### 5.2.2. Histological evaluation of inflammatory reaction and VAP-1 expression

The inflammatory reaction in the control animals with healing cortical defects was characterized by a modest infiltration of inflammatory cells at 24 hours and 7 days (Table 11). Already at 24

hours, the osteomyelitic animals showed an increased infiltration of inflammatory cells and an occasional formation of microabscesses (Table 12).

The osteomyelitic tibias showed an increased expression of VAP-1 in blood vessel walls (Table 12). There was a significant difference in the VAP-1 expression between the osteomyelitic bones and the control healing bones at 24 hours and at 7 days (for both, P<0.0001).

### 5.2.3. In vivo PET uptake of <sup>68</sup>Ga-DOTAVAP-P1

In the time-series analysis, the uptake of <sup>68</sup>Ga-DOTAVAP-P1 occurred in both the osteomyelitic and control bones with healing defects during the first 36 hours after surgery. Thereafter, only the osteomyelitic tibias were delineated by PET.

In the pivotal series, PET imaging showed an accumulation of <sup>68</sup>Ga-DOTAVAP-P1 in both the osteomyelitic bones (SUV ratio 1.50±0.16)

**Table 11.** Mean histological score, grade of inflammatory cell influx, and grade of VAP-1 expression in the animals with healing cortical defects (mean ± SD)

	Histological score	Inflammatory cell grade	VAP-1 expression
24 hours	0.0 ± 0.0	1.25 ± 0.35	1.10 ± 0.39
7 days	0.0 ± 0.0	1.20 ± 0.42	1.00 ± 0.47
P-value	NS	NS	NS

**Table 12.** Mean histological score, grade of inflammatory cell influx, and grade of VAP-1 expression in the osteomyelitic animals (mean ± SD)

	Histological score	Inflammatory cell grade	VAP-1 expression
24 hours	0.45 ± 0.22	2.61 ± 0.49	2.39 ± 0.49
7 days	2.68 ± 0.61	2.35 ± 0.41	2.85 ± 0.34
P-value	< 0.0001	NS	0.0238

and the control bones with healing defects (SUV ratio  $1.48 \pm 0.18$ ) 24 hours after surgery. The osteomyelitic bones showed a significant increase ( $P=0.0016$ ) in the  $^{68}\text{Ga}$ -DOTAVAP-P1 uptake (SUV ratio  $1.87 \pm 0.41$ ) by 7 days. In the control animals with healing bones, representing sterile

inflammation, the region of uncomplicated defect healing showed a marked decrease ( $P=0.0008$ ) in tracer activity (SUV ratio  $1.09 \pm 0.08$ ) by 7 days, and no statistically significant difference was observed between the operated and intact contralateral tibias.

### 5.3. $^{18}\text{F}$ -FDG uptake in the differentiation of *S. aureus* and *S. epidermidis* bone infections in a rabbit model

#### 5.3.1. Confirmation of culture-positive infection

In the *S. aureus* group of animals, all of the bone cultures and those of the retrieved cement blocks were positive. In the *S. epidermidis* ATCC 35983 group of animals, the inoculum only occasionally caused culture-positive infections. The clinical *S. epidermidis* T-54580 resulted more consistently in positive bone cultures at 2 weeks. At 8 weeks, cement block cultures were positive for the inoculated *S. epidermidis* (T-54580) in 6 out of the 8 animals.

In the pQCT imaging, the animals with *S. aureus* (52/52A/80) osteomyelitis showed cortical bone destruction with a circumferential periosteal reaction, reactive endosteal new bone, and sequestrum formation. In the *S. epidermidis* (ATCC 35983) group, there were no clear osteomyelitic changes on the pQCT images, but signs of closure in the cortical defect were found. On the pQCT images, the animals with *S. epidermidis* (T-54580) inoculation showed moderate signs of local osteomyelitis, including periosteal reaction, a small amount of reactive endosteal new bone formation, and an unhealed cortical window.

#### 5.3.2. Histological appearance of osteomyelitis

The *S. aureus* group of animals showed histologically severe osteomyelitis in all of the cases, characterized by a nearly circumferential periosteal reaction, new bone formation, sequestrum formation, and infiltration of polymorphonuclear leukocytes with occasional microabscesses (Table 13). The *S. epidermidis* ATCC 35983 group of animals showed minimal histological signs of bone infection with only a limited number of inflammatory cell infiltrates, and closure of the cortical defect had occurred. The group of animals with the clinical T-54580 strain of *S. epidermidis* showed signs of chronic or subacute osteomyelitis, characterized by a periosteal reaction with periosteal sclerosis, infiltration of lymphocytes and plasma cells, and bone marrow showing signs of fibrosis.

#### 5.3.3. Correlation of $^{18}\text{F}$ -FDG PET uptake, leukocyte infiltration, and inoculated pathogen

There was a significant correlation ( $R=0.645$ ;  $P=0.0127$ ) between the semi-quantitative score of leukocyte infiltration in the medullary canal of the tibias and the mean  $^{18}\text{F}$ -FDG SUV in the ani-

**Table 13.** Mean histological scores, measured  $^{18}\text{F}$ -FDG SUV, and calculated  $^{18}\text{F}$ -FDG SUV ratios (mean  $\pm$  SD)

Inoculated microorganism	Periosteal reaction	Cortex	Leukocyte infiltration	Osteomyelitis score	$^{18}\text{F}$ -FDG SUV	$^{18}\text{F}$ -FDG SUV ratio
<i>S. aureus</i> (52/52A/80)	$2.0 \pm 0.5$	$2.1 \pm 0.3$	$2.1 \pm 0.3$	$2.1 \pm 0.2$	$1.29 \pm 0.30$	$3.75 \pm 0.80$
<i>S. epidermidis</i> (ATCC 35983)	$0.6 \pm 0.5$	$1.0 \pm 0.5$	$0.7 \pm 0.5$	$0.8 \pm 0.4$	$0.62 \pm 0.30$	$2.50 \pm 0.84$
<i>S. epidermidis</i> (T-54580)	$1.5 \pm 0.4$	$1.5 \pm 0.4$	$1.4 \pm 0.6$	$1.5 \pm 0.3$	$0.47 \pm 0.13$	$2.96 \pm 0.98$

mals with positive bacterial cultures of bone and/or retrieved cement blocks.

The PET/CT imaging showed an intense accumulation of <sup>18</sup>F-FDG in the osteomyelitic tibiae as compared with the contralateral intact bone in all of the groups. The uptake in the *S. aureus* osteomyelitic tibiae (1.29±0.30) was twofold (P<0.001) as compared with that of the two *S. epidermidis* (ATCC 35983 and T-54580) groups (0.62±0.30 and 0.47±0.13, respectively). The difference in the SUV between the two *S.*

*epidermidis* strains was not statistically significant. The SUV of the contralateral healthy tibiae of the *S. aureus* animals was significantly higher than those of the *S. epidermidis* (T-54580) animals (P<0.001), suggesting a systemic impact of staphylococcal osteomyelitis. As a result, the SUV ratios showed only a trend (P=0.053, ANOVA) between the animals with *S. aureus*, *S. epidermidis* (ATCC 35983), and *S. epidermidis* (T-54580) inoculations (3.75±0.80, 2.50±0.84, and 2.96±0.98, respectively).

### 5.4. Intensity of <sup>18</sup>F-FDG uptake in the patients with microbiologically or histologically confirmed chronic bone infections

A total of 16 patients were diagnosed as having a chronic bone infection (osteomyelitis or spondylodiscitis) verified by bacterial cultures and/or a histological analysis. For 5 of the osteomyelitis cases, *S. epidermidis* or other coagulase-negative staphylococcus was cultured, *S. aureus* in 2 cases and bacillus species in 1 case. Of the total of 16 patients, no bacteria could be detected in bone cultures from 7 patients (43.8 %), and the final diagnosis of bone infection was based on the histological examinations of bone tissue. None of the patients with negative cultures had antibiotic therapy before the sampling. For 1 patient no specimens were taken for a microbiological analysis. One of the staphylococcal infections was associated with polymicrobial infection with more than one pathogen.

In the <sup>18</sup>F-FDG PET imaging, all of the patients (n=16) with confirmed osteomyelitis were correctly interpreted as true positive. For the whole

study group (n=26) with a histopathologically or microbiologically confirmed final diagnosis, <sup>18</sup>F-FDG PET yielded three false-positive outcomes. Two false-positive results were due to periarticular soft-tissue infections, as a lack of precise anatomical information made it impossible to differentiate bone infection from surrounding soft tissue infection, and one false-positive case was due to a vertebral plasmacytoma.

In the quantitative analysis of the <sup>18</sup>F-FDG PET imaging, the SUV mean or the SUV maximum values of the culture-negative and culture-positive cases of osteomyelitis did not differ significantly (Table 14). The corresponding SUV ratios of culture-negative and culture-positive osteomyelitis did not show significant intergroup differences either (Table 14). The number of culture-positive osteomyelitis cases was too low for a statistical evaluation of the effect of the causative bone pathogen.

**Table 14.** <sup>18</sup>F-FDG uptake in osteomyelitic bones with positive or negative bone tissue cultures (mean ± SD)

	SUV Mean	Max	SUV ratio Mean	Max
Culture-positive osteomyelitis	2.18 ± 1.40	3.73 ± 1.93	4.98 ± 3.22	6.84 ± 6.20
Culture-negative osteomyelitis	2.07 ± 0.74	2.81 ± 0.96	7.65 ± 5.79	6.51 ± 5.07

## 6. DISCUSSION

It is anticipated that the overall number of surgical bone infections will increase along with the growing number of performed reconstructive orthopaedic procedures using orthopaedic fixation devices and prostheses. In addition, the rise in the number of diabetic patients, the increasing population of aged patients with a need for surgical treatment, aside from the alarming antibiotic resistance of common pathogens, are producing unmatched challenges for the near future.

Accurate and fast diagnosis plays a crucial role in establishing effective therapy for patients with orthopaedic infections. Standard diagnostic tools such as conventional radiographs, MRI, CT, and conventional nuclear medicine methods are known to have major limitations in the early diagnosis of deep bone infections. Laboratory medicine techniques determining inflammatory parameters, such as erythrocyte sedimentation rate, C-reactive protein and leukocytes, do not have sufficient sensitivity, especially in cases of

low-grade infections, and they also lack specificity.

PET has emerged from being a pure research modality into a powerful clinical tool. The currently most used method, as well as the only with clinical relevance in the evaluation of infectious processes in orthopaedics and traumatology, is  $^{18}\text{F}$ -labelled glucose analogue,  $^{18}\text{F}$ -FDG. The method is based on the intensive use of glucose by activated mononuclear cells and granulocytes. The problem is that  $^{18}\text{F}$ -FDG is not specific for infection. Aseptic inflammation, similar to infection, results in increased  $^{18}\text{F}$ -FDG uptake that mimics infection in PET, and it possibly causes false-positive results.

In the current thesis,  $^{18}\text{F}$ -FDG was used in comparison with tested novel radiopharmaceuticals in studies I–II to represent the standard clinical protocol. In studies III–IV, the applicability of  $^{18}\text{F}$ -FDG to the diagnosis of bone infections was evaluated according to different pathogen-related factors.

### 6.1. PET imaging of osteomyelitis in healing bones

Several of the signals governing the pattern of bone healing are part of the initial inflammatory process (Einhorn et al. 1995). Bone and adjacent tissue healing due to trauma or surgical intervention has been found to be the most frequent cause of false-positive findings of  $^{18}\text{F}$ -FDG PET for orthopaedic patients (Meyer et al. 1994, Fayad et al. 2003, Rosenbaum et al. 2006, Meller et al. 2007). In a limited number of experimental and clinical publications, the level and duration of increased  $^{18}\text{F}$ -FDG uptake in association with the healing process has been evaluated (Meyer et al. 1994, Zhuang et al. 2000 and 2003, De Winter et al. 2001, Koort et al. 2004 and Jones-Jackson et al. 2005).

In complicated clinical conditions, more specific tracers are needed to describe the progress of infection and uneventful fracture healing. The first phase of the current research project focused on increasing the specificity of PET imaging in the challenging early post-operative period by

developing novel tracers and on evaluating their characteristics in standardized animal models.

#### 6.1.1. $^{68}\text{Ga}$ -chloride PET imaging of osteomyelitis and bone healing

Gallium-67 citrate was the first scintigraphic marker used as an infection-specific tracer in scintigraphy. Because of such unfavourable characteristics as high radiation exposure and long examination time, it has been replaced by other modalities. The positron emitting isotope  $^{68}\text{Ga}$ -chloride can be produced without expensive cyclotrons by elution from a  $^{68}\text{Ge}/^{68}\text{Ga}$  generator with low costs. In comparison to  $^{67}\text{Ga}$ -citrate SPECT imaging,  $^{68}\text{Ga}$  PET is able to provide superior spatial resolution, higher sensitivity, a possibility of quantitative assessment, and a lower radiation dose for the patient, all of which make it a promising tracer. Currently, only a few  $^{68}\text{Ga}$ -labelled radiopharmaceuticals are in everyday use, but its applications are under extensive research

(Roivainen et al. 2012, Kumar and Boddeti 2013). The presented results were the first to describe the use of  $^{68}\text{Ga}$ -chloride as a PET tracer in the evaluation of experimental osteomyelitis.

The purpose of study I was to evaluate the uptake patterns of  $^{68}\text{Ga}$ -chloride and  $^{18}\text{F}$ -FDG in *S. aureus* osteomyelitis and uncomplicated bone healing at 2 weeks after surgery. The accumulation of  $^{68}\text{Ga}$ -chloride in the infected bone area reached a steady state approximately 70 minutes after intravenous injection to rats and therefore allowed rapid infection imaging. In PET imaging, the uptake of  $^{18}\text{F}$ -FDG and  $^{68}\text{Ga}$ -chloride was increased in osteomyelitic tibias, and no statistical difference was found for the intensity between the tracers. In the tibias with uncomplicated bone healing,  $^{18}\text{F}$ -FDG exhibited an elevated uptake, but  $^{68}\text{Ga}$ -chloride resulted in a significantly lower uptake. In addition, the intensity of  $^{68}\text{Ga}$ -chloride uptake reflected pathological cortical bone changes in osteomyelitic animals, as measured by pQCT.  $^{68}\text{Ga}$ -chloride is applicable as a PET tracer in the evaluation of infectious lesions in bone. It may even prove to be more specific than  $^{18}\text{F}$ -FDG in the early post-operative or post-traumatic phase.

Gallium-68 was used in the form of  $^{68}\text{Ga}$ -chloride. As different isotopes differ only by their physical properties and their chemical and physiological behaviour is comparable, it can be assumed that  $^{68}\text{Ga}$ -citrate and  $^{67}\text{Ga}$ -citrate function comparably. However, there may be some differences between  $^{68}\text{Ga}$ -chloride and  $^{68}\text{Ga}$ -citrate. When administered as  $^{68}\text{Ga}$ -citrate into the physiological pH of blood,  $^{68}\text{Ga}$  and citrate rapidly separate, and binding to transferrin follows, as does the formation of only a soluble anion (Green and Welch 1989). In acidic conditions,  $^{68}\text{Ga}$ -chloride is stable and soluble, but it needs to be neutralized prior to intravenous administration. In physiological pH,  $^{68}\text{Ga}$ -chloride may form insoluble colloids that may affect its accumulation profile (Mäcke and André 2007, Fani et al. 2008).  $^{68}\text{Ga}$ -chloride was initially chosen for further study, as a promising accumulation was seen in dynamic PET imaging when it was used as a control in a  $^{68}\text{Ga}$ -labelled oligonucleotide study (Roivainen et al. 2004). Secondly,  $^{68}\text{Ga}$ -chloride was readily available through a relatively simple cyclotron

independent manufacturing process at the Turku PET centre.

Previously, Koort et al. (2004) compared the use of  $^{18}\text{F}$ -FDG PET in experimental rabbit models of *S. aureus* osteomyelitis and uncomplicated bone healing. In tibias with healing bone defects, an increased  $^{18}\text{F}$ -FDG uptake was seen at 3 weeks, but by 6 weeks the uptake had decreased almost to normal. In comparison, the osteomyelitic animals showed an increased  $^{18}\text{F}$ -FDG uptake at both 3 and 6 weeks. Jones-Jackson et al. (2005) performed PET scans weekly for the evaluation of post-surgical inflammation and *S. aureus* bone infection in a rabbit model. They concluded that differentiating between infection and post-surgical infection was possible as early as 8 days after surgery, but significant differences in the SUV were noted at 15 days post-surgery. A comparison of the present results and results obtained by Koort et al. (2004) and Jones-Jackson et al. (2005) is difficult because of differences in the animal species and the imaging schedule. The present results are in concordance with the preliminary clinical results of Nanni et al. (2010) and therefore confirm the role of  $^{68}\text{Ga}$  PET/CT in the diagnosis of osteomyelitis.

### 6.1.2. $^{68}\text{Ga}$ -DOTA-VAP-P1 imaging of osteomyelitis and bone healing

Chemotactic peptides and endothelial adhesion molecules form a group of promising radiopharmaceuticals, as they are able to accumulate rapidly at the site of an inflammatory reaction (Corstens and van der Meer 1999, Signore et al. 2003). A linear peptide binding to a groove of a VAP-1 molecule was introduced and radiolabelled with  $\text{Ga}^{68}$  (Yegutkin et al. 2004, Ujula et al. 2009). VAP-1 is absent from normal unaffected tissues, but, upon inflammatory reaction, it is rapidly expressed in the endothelium, both as membrane-associated and as soluble-circulating (Jaakkola et al. 2000). It plays a critical role in cellular trafficking, and it recruits lymphocytes into inflamed tissues, regulates lymphocyte rolling and stimulates glucose transport, is critically involved in the process of leukocyte adhesion, and mediates leukocyte entry into affected tissues (Smith et al. 1998, Jaakkola et al. 2000, Zorzano et al. 2003, Merinen



et al. 2005, Stolen et al 2005). These results indicate that VAP-1 is as a highly promising target molecule for depicting the progress of inflammatory reaction in vivo by PET.

Study II was designed to evaluate  $^{68}\text{Ga}$ -DOTA-VAP-P1 for the assessment of early inflammatory and infectious processes in healing bones. In the initial time-series analysis, an increased tracer uptake occurred in both the osteomyelitic tibias and in the tibias with healing bone defects during the first 36 hours, but thereafter only the osteomyelitic tibias showed an increased uptake. In the pivotal series, the healing tibias showed a transient uptake at 24 hours after surgery, which tended to normalize by 7 days. In comparison, the osteomyelitis tibias resulted in increasing, locally intense tracer uptake that reflected the progress of the infection. Already at 7 days after surgery,

the tested tracer allowed differentiation between these two inflammatory conditions. According to the results,  $^{68}\text{Ga}$ -DOTA-VAP-P1 accurately detects the phase of inflammation in healing bones and the progress of *S. aureus* osteomyelitis. In clinical settings, this novel radiopharmaceutical may be valuable in the detection of osteomyelitis in its early phase. However, as the tracer accumulation is not specific for infectious processes, but instead describes the rate of inflammatory reaction, it is anticipated that this novel tracer is not able to differentiate between prosthesis aseptic loosening and periprosthetic infection.

Recently, studies on VAP-1-targeting tracers in PET imaging have been published in turpentine oil-induced acute sterile inflammation, tumour xenografts and in biodistribution studies (Autio et al. 2010 and 2011, Aalto et al. 2011).

## 6.2. Significance of causative bone pathogens and the presence of positive bacterial cultures in PET

Osteomyelitic patients form a highly heterogeneous population, because of diverse routes of infection, multiple potential causative pathogens, and differences in patient-related factors.  $^{18}\text{F}$ -FDG PET seems to be reliable in clinical circumstances, but its accuracy in detecting bone infections may vary under different infectious conditions. As an example of this situation, the American Academy of Orthopaedic Surgeons gave only a weak recommendation for the use of nuclear medicine methods in the diagnosis of periprosthetic infections (Della Valle et al. 2011). The inaccuracy of  $^{18}\text{F}$ -FDG PET in the detection of implant infections may be associated with the predominance of low-virulent microbes, mainly *S. epidermidis* strains. In addition, 15% to 47% of osteomyelitis cases are reported to remain culture negative (Dich et al. 1975, Craigen et al. 1992, Floyd and Steele 2003). For paediatric patients, the existence of non-bacterial osteomyelitis has also been introduced (Floyd and Steele 2003, Khanna et al. 2009, Borzutzky et al. 2012).

More information is needed on the applicability of  $^{18}\text{F}$ -FDG PET in different infectious conditions before the possible limitations and factors contributing to its accuracy can be identified. The

second phase of the current research project focused on evaluating the significance of causative bone pathogens in standardized animal models, as well as on determining whether  $^{18}\text{F}$ -FDG uptake differs in culture-positive and culture-negative osteomyelitis cases in clinical  $^{18}\text{F}$ -FDG PET imaging.

### 6.2.1. $^{18}\text{F}$ -FDG uptake in *S. aureus* osteomyelitis and *S. epidermidis* foreign-body bone infection

The most frequent causative microbes of any type of osteomyelitis are staphylococci, but virtually any organism has the potential to cause osteomyelitis. The clinical manifestations of classical suppurative *S. aureus* osteomyelitis and indolent *S. epidermidis* foreign-body infections markedly differ. In clinical studies, specific microbiological results have not constantly been properly reported, but rather presented only as culture positive or negative (Table 6). It is expected that a less severe or more chronic state may result in less dense tracer uptake.

van der Laken et al. (1997) studied a novel radiopharmaceutical when evaluating a soft-tissue infection due to *E. coli* and *S. aureus*. They found no difference in the uptake of  $^{99\text{m}}\text{Tc}$ -labelled

chemotactic peptides to *E. coli* or *S. aureus* soft-tissue abscesses. In contrast, Akhtar et al. (2004) reported a significantly increased uptake of <sup>99m</sup>Tc-labelled antimicrobial peptide in *S. aureus*, thigh-muscle abscesses when compared with the uptake in *E. coli* abscesses. For the use of PET in osteomyelitic cases, no such comparative studies have been performed. It is not known whether the virulence of the causative pathogen and the severity of the subsequent infection contribute to the intensity of <sup>18</sup>F-FDG uptake in PET imaging.

The purpose of study III was to determine the impact of the causative staphylococcal bone pathogen on the level of <sup>18</sup>F-FDG uptake in the PET imaging of experimental *S. aureus* osteomyelitis and foreign-body-associated *S. epidermidis* infection. Classical suppurative osteomyelitis caused by *S. aureus* resulted in a higher local <sup>18</sup>F-FDG accumulation (mean SUV) than did the implant infection due to *S. epidermidis*.

Interestingly, there was also a statistical difference in the comparison of non-operated contralateral tibias in animals with *S. aureus* and *S. epidermidis* (54580) inoculum. Therefore, a statistical comparison of SUV ratios, presenting the radioactivity ratio between the operated and control tibias, showed only a trend (P=0.053, ANOVA). The difference in the uptake of non-operated tibias can be speculated to be due to the differences in the impact of the surgery and the severity of the infection on the mobility of the animal. In addition, acute suppurative *S. aureus* osteomyelitis may induce a systemic effect by increasing the proliferation of WBCs in the bone marrow of intact contralateral tibias.

In animals with positive bacterial cultures, a significant correlation was found between intramedullary leukocyte infiltration and the <sup>18</sup>F-FDG mean SUV. The animals with the standard strain of *S. epidermidis* (ATCC 35983) inoculation did

not show active infection in a histological evaluation. Their mean SUV ratios were at the same level at 6 weeks as the SUV ratios of non-infected healing bones at 3 weeks, as reported previously by Koort et al. (2004) (Table 15).

When extrapolated to clinical settings, our results provide initial answers to the reported problems associated with <sup>18</sup>F-FDG PET imaging in the diagnosis of periprosthetic, often indolent, low-grade infections. But simultaneously, the presented results are in concordance with the positive results of previous experimental and clinical studies on <sup>18</sup>F-FDG PET imaging in the evaluation of osteomyelitis commonly due to *S. aureus*.

### 6.2.2. <sup>18</sup>F-FDG uptake in culture-positive and culture-negative patients with histologically confirmed chronic osteomyelitis

Identification of the causative pathogen is of crucial importance in the diagnosis and treatment of orthopaedic infections, but despite careful preoperative investigations the causative microbe may remain unidentified. One aspect of osteomyelitis that has received little attention is the <sup>18</sup>F-FDG PET imaging findings of cases in which no bacterial pathogen was identified. This presents as a major issue, as the rate of positive cultures in histologically proven cases of osteomyelitis obtained with imaging-guided biopsy is reported to be as low as 30%–34% (Wu et al. 2007, Heyer et al. 2012, Sehn and Gilula 2012). The factors that predict positive or negative culture results are not clearly known (Wu et al. 2007, Calhoun et al. 2009), as there seems to be cases in which even repeated open biopsies fail to reveal the underlying pathogen. Technical biopsy errors and antibiotic exposure before biopsy may affect culture results. One reason is inappropriate culture conditions. It has been suggested that false-negative infections

**Table 15.** Comparison of <sup>18</sup>F-FDG SUV ratio in *S. epidermidis* foreign-body infection and uncomplicated bone healing (mean ± SD)

<sup>18</sup> F-FDG SUV ratio (Study III)		<sup>18</sup> F-FDG SUV ratio (Koort et al. 2004)	
<i>S. aureus</i> (52/52A/80)	3.75 ± 0.80	Pre-operative	1.02 ± 0.04
<i>S. epidermidis</i> ATCC 35983	2.50 ± 0.88	Healing bone at 3 weeks	2.35 ± 0.26
<i>S. epidermidis</i> T-54580	2.96 ± 0.98	Healing bone at 6 weeks	1.32 ± 0.54

may be due to viable, but non-culturable bacteria localized in biofilm (Calhoun et al. 2009). Certain cases of culture-negative, low-grade osteomyelitis may represent clinical conditions with an inherent difference in metabolic activity as compared with culture-positive cases. It was assumed that  $^{18}\text{F}$ -FDG PET could potentially detect such a difference because intracellular accumulation of the glucose analogue tracer reflects the metabolic rate of cells at sites of infection and inflammation. The significance of the existence of low-uptake lesions during  $^{18}\text{F}$ -FDG PET has not been fully elucidated, and, if no anatomical disturbances are evident, these lesions have been categorized as false-positive findings (Meller et al. 2007).

The purpose of study IV was to determine whether the level of  $^{18}\text{F}$ -FDG uptake differs in culture-negative and culture-positive cases of histologically or microbiologically proven osteomyelitis. Bone specimens from 7 patients out of 16 remained culture negative. The rate of positive cultures was similar to the previously reported rates in studies of imaging-guided biopsies with combined histological and microbiological evaluation (White et al. 1995, Wu et al. 2007, Heyer et al. 2012, Sehn and Gilula 2012). In opposition to the hypothesis of study IV, the  $^{18}\text{F}$ -FDG uptake in cases of culture-negative osteomyelitis was not lower than in the culture-positive cases. The result favours the concept that culture-negative cases are true infections due to non-culturable microbes. Thus  $^{18}\text{F}$ -FDG PET may be able to con-

firm the presence of metabolically active infection in patients with culture-negative, histologically confirmed, chronic low-grade osteomyelitis.

Initially, the aim was also to evaluate the impact of causative bone pathogen on  $^{18}\text{F}$ -FDG uptake also in clinical series. Due to the small number of each cultured pathogen, statistical evaluation was not possible. Dehdashti et al. (1996) have suggested an SUV of 2.0 as a cut-off value for discrimination between benign and malignant osseous lesions, in addition to visual analysis alone. When applied to the patients with osteomyelitis, the mean SUV was lower than 2.0 for nine patients, and the maximum SUV value was below the limit only for two patients. However, for all of the patients, a significant increase occurred in the SUV ratio. In two of the nine patients bone infection was caused by coagulase-negative staphylococci, for one patient it was bacillus, and surprisingly, in two cases *S. aureus* was identified as the causative pathogen, while the rest of the cultures remained negative.

The current results support the concept that a negative  $^{18}\text{F}$ -FDG scan can virtually rule out active, even low-grade, chronic osteomyelitis (Prandini et al. 2006, Termaat et al. 2005). When compared with other conventional imaging modalities,  $^{18}\text{F}$ -FDG PET may have brought a significant diagnostic addition to cases of this retrospective analysis when the findings of the MRI or labelled leukocyte scintigraphy were false negative.

### 6.3. Animal models

In studies I and II, a rat model of diffuse tibial osteomyelitis was adopted, which represents Stage IVA in the Cierny-Mader classification and osteomyelitis secondary to a contiguous focus of infection in the Waldvogel classification. *S. aureus* was used as the pathogen in both studies. Consistently, in the osteomyelitic animals, culture-positive infection with a typical histological picture of osteomyelitis was confirmed. Previously, this model has been used with equally good results for research on bone infections and also in the evaluation of novel radiopharmaceuticals (Mader 1985, O'Reilly and Mader 1999, Gratz et al. 2001). For

rats, the model of a cortical bone defect in the tibia was applied to mimic uncomplicated bone healing following fracture or surgical osteotomy.

In study III, a rabbit model of diffuse tibial osteomyelitis due to *S. aureus* simulating human intra-medullary Stage IIIA osteomyelitis of a long-bone (Cierny-Mader classification) and biomaterial-related bone infection due to *S. epidermidis* were adopted. All of the bone cultures and the retrieved cement block specimens were positive for the inoculated clinical strain of *S. aureus*. The applied rabbit model of *S. aureus* tibial osteomyelitis has been widely accepted as an experimental model for

research on bone infections and also for the evaluation of PET imaging (Koort et al. 2004 and 2005).

The *S. epidermidis* foreign-body-associated infection model was modified from that of Mayberry-Carson et al. (1992). Whereas, Mayberry-Carson et al. used a silastic tube as the foreign-body material, in comparison, in study III, a block of bone cement was used to mimic cement remnants with *S. epidermidis* biofilms in patients with infected cemented hip arthroplasties. In addition, polymethylmethacrylate has been shown to be a potent foreign body (Petty et al. 1985). Lambe et al. (1991) published results of a similar foreign-body-associated *S. epidermidis* osteomyelitis model that used rabbit tibia. *S. epidermidis* could be cultured from all of the silastic foreign bodies and from all of the samples of bone marrow, but only two out of five bone samples were positive for the inoculated pathogen (Lambe et al. 1991). In study III, the bone specimen was cultured as one block, includ-

ing the bone marrow, which may have increased the ratio of the positive bone culture rate. The cases reported as negative by Lambe et al. (1991) in their histological evaluation occurred more frequently in time points furthest from the induction of the infection. This phenomenon was also seen in the current series, and it is probable that a longer follow-up would have resulted in the healing of some of the low-grade *S. epidermidis* infections.

The applied experimental models have important benefits. Standardized tibial osteomyelitis or foreign-body-associated infection is relatively easy to produce, and both are reproducible. The induced infection is primarily localized in the medullary cavity and its adjacent bone; it thus minimizes the effect on the general well-being of the animal. From the clinical point of view, the utilized experimental osteomyelitis models are comparable to post-traumatic osteomyelitis that arises from grossly contaminated long-bone fractures.

## 6.4. Limitations of the study

The most significant limitation of the applied experimental osteomyelitis models is that a large bacterial inoculum administered directly to the medullary cavity is needed for successful induction of bone infection (Mader 1985). In most experimental osteomyelitis models, sodium morrhuate, a sclerosing agent, has been applied (Rissing et al. 1985a). Sodium morrhuate was used in rats in studies I and II, as well as in study III in conjunction with *S. epidermidis* inoculum. It causes aseptic bone necrosis, promotes the progression of osteomyelitis, and decreases the required amount of bacterial inoculum. As a disadvantage, sodium morrhuate may result in changes mimicking diffuse osteomyelitis (Mader 1985). In studies I and II, *S. aureus* was used as the only pathogen in the induction of infection. Indeed, *S. aureus* is the most frequent pathogen in all types of osteomyelitis. But because of marked differences in the manifestations of different pathogens, the results cannot be directly applied to describe the outcome with different causative microbes, as demonstrated in study III.

The main technological shortcoming of the experimental studies was that, at the time of the studies, no access was available to a suitable

dedicated small-animal PET scanner. All of the imaging studies were performed with a clinical PET scanner. The imaging focus with experimental animals is small (1 cm or less in diameter) when compared with that of clinical settings, and, therefore, there was a risk of a partial-volume effect (PVE) occurring. PVE means that the apparent pixel values in PET images are influenced by the surrounding high pixel values and, therefore, possibly invalidate the quantitative PET data (Hoffman et al. 1979). To minimize the influence of PVE, the animals were placed in the centre of the gantry to gain the highest possible spatial resolution and the average radioactivity concentration within the ROI as well as SUV ratios were used to quantify the tracer uptake.

The experimental studies could have benefited from the application of high-resolution MRI in the further characterization of the infection process. It would have been especially valuable in the evaluation of the extent of the infection into the soft tissues.

In studies I and III only a single time point was used for the PET evaluations. Additional PET scans might have provided more-detailed information. The potential risks associated with

repeated general anaesthesia were considered to outweigh the possible additional information.

In preclinical studies, none of the analyses could be done in a blind manner because the study groups had clearly identifiable differences. This situation may have influenced the results. The study results were analysed by two persons in mutual agreement or were presented as an average of their interpretation to minimize single-observer bias.

As a retrospective analysis, the clinical study had limitations. The inclusion of the patients at

the university hospital was based on highly selected referral for  $^{18}\text{F}$ -FDG PET imaging; they therefore represented a group of patients with complex disease conditions. The order and time in which the imaging studies were performed varied. A major shortcoming was the imaging with a plain PET scanner without an inline CT apparatus, as, currently, most scanners are combined PET/CT devices that provide the means to acquire more precise anatomic and metabolic information, resulting in higher specificity and sensitivity.

## 6.5. Future prospects

PET has emerged as a powerful tool in the clinical diagnosis of osteomyelitis. It is well anticipated that, as the use of combined PET/CT devices becomes more widespread, the impact on imaging of orthopaedic infections will increase. As a research modality with possibilities to visualize and quantitate cellular and molecular processes in vivo with high-resolution PET, molecular imaging is a revolutionizing method for basic research as well (Mayer-Kuckuk and Boskey 2006).

The use of  $^{18}\text{F}$ -FDG has become a standard for PET. So far, none of the published novel radiopharmaceuticals have been accepted for wide clinical use or have proven superior to  $^{18}\text{F}$ -FDG (Gemmel et al. 2009, Goldsmith and Vallabhajosula 2009, Roivainen et al. 2012). In the current research the use of two novel tracers was evaluated,  $^{68}\text{Ga}$ -chloride and  $^{68}\text{Ga}$ -DOTA-VAP-P1 in standardized animal models of *S. aureus* osteomyelitis and uncomplicated bone healing. Naturally, these promising experimental results warrant further studies. It would be of special interest to evaluate the tested radiopharmaceuticals in the most challenging cases, such as in low-grade *S. epidermidis* periprosthetic infections.

Different isotopes vary only according to their physical properties, and their chemical and physiological behaviour is comparable, but there may be some differences between  $^{68}\text{Ga}$ -chloride and  $^{68}\text{Ga}$ -citrate. The possible difference between the uptake profiles of these two  $^{68}\text{Ga}$ -tracers needs to be studied in standardized experimental models to determine which of the two shows

the more-promising results for the evaluation of post-traumatic and post-operative osteomyelitis. Gallium-68, in form of  $^{68}\text{Ga}$ -citrate, has already shown promising initial results in evaluations of patients with bone infections (Nanni et al. 2010). Further clinical studies are needed to confirm the role of  $^{68}\text{Ga}$  as a PET tracer.

Typically, high expectations have been set for novel PET tracers, and it has been hypothesized that they would be able to differentiate between infectious processes and sterile inflammation (Lupetti et al. 2003). VAP-1 is an endothelial protein that co-ordinates the extravasation of WBCs to inflammatory areas, whose expression is induced only under inflammatory conditions (Salmi and Jalkanen 1992, Koskinen et al. 2004). After the initial results in study II, the VAP-1 binding radiopharmaceutical has been further developed (Silvola et al. 2010, Autio et al. 2010 and 2011). The unique properties of VAP-1 binding tracers may offer a means with which to also detect low-grade infections, as it already demonstrates the initial phase of WBC accumulation in the site of an inflammatory area.

Aseptic inflammation plays a significant role in explaining the difficulties reported for the  $^{18}\text{F}$ -FDG PET imaging of periprosthetic infections and for discriminating between aseptic and septic loosening of joint prostheses (Kwee et al. 2008, Della Valle et al. 2011). Neither of the presented novel tracers are infection specific, but it remains to be seen whether they are able to help orthopaedic surgeons determine the cause of pain after arthroplasty.

## 7. CONCLUSIONS

On the basis of these experimental studies and the clinical retrospective study, the following conclusions can be drawn:

1.  $^{68}\text{Ga}$ -chloride seems to be better than  $^{18}\text{F}$ -FDG in discriminating between bacterial infections from the non-specific uptake caused by the physiological inflammatory processes of normal bone healing. The intensity of  $^{68}\text{Ga}$ -chloride uptake was related to pathological structural changes in infected cortical bone.
2.  $^{68}\text{Ga}$ -DOTAVAP-P1 was capable of demonstrating the phase of inflammation in healing bones and the progress of bacterial infection in osteomyelitic bones. The tracer allowed a differentiation between *S. aureus* osteomyelitis and normal bone healing as soon as 7 days after their onset.
3. *S. epidermidis* foreign-body infections were characterized by low  $^{18}\text{F}$ -FDG uptake, whereas classical *S. aureus* osteomyelitis resulted in high uptake values. The degree of leukocyte infiltration, reflecting the virulence of the causative staphylococcal strain, contributed to the level of local  $^{18}\text{F}$ -FDG uptake.
4. In the PET imaging of patients with confirmed osteomyelitis, the  $^{18}\text{F}$ -FDG uptake in cases of culture-negative osteomyelitis did not differ from that of in culture-positive cases. Thus  $^{18}\text{F}$ -FDG PET may help to confirm the presence of a metabolically active infection process in patients with culture-negative, histologically proven, low-grade osteomyelitis.

## ACKNOWLEDGEMENTS

This study was carried out in 2004–2013 in the Orthopaedic Research Unit of the Department of Orthopaedic Surgery and Traumatology and in the Turku PET Centre, Institute of Clinical Medicine, Department of Clinical Physiology and Nuclear Medicine, both of which are a part of the Faculty of Medicine of the University of Turku. Professor Hannu Aro, Director of the Orthopaedic Research Unit, and Professor Juhani Knuuti, Director of the Turku PET Centre, are warmly acknowledged for allowing me to use their facilities during this study.

I am deeply indebted to my supervisor Professor Hannu Aro, whose vast knowledge in orthopaedic research, skills in scientific writing, and passion for science are continuously producing high-quality research. It has been a privilege to follow him and to learn from his enthusiasm. I owe my deepest gratitude to Professor Anne Roivainen for her invaluable support during this study. She always had the time to guide me, always with a positive attitude.

Docent Petri Virolainen, Chairman of Orthopaedic Surgery and Traumatology at the Turku University Hospital, and Professor Pertti Aarnio, Chairman of Surgery at the Satakunta Central Hospital, are thanked for their support of this work.

My gratitude also goes to the official reviewers of this dissertation, Professor Matti Lehto and Professor Aapo Ahonen, for their scientific expertise, thorough evaluation, and valuable constructive criticism.

Furthermore, my steering group members, Professor Juhani Knuuti, Professor Pertti Törmälä, and Professor Mikko Hupa, are gratefully acknowledged for their interest in my thesis.


I wish to express my thanks to all of my co-authors for their valuable contribution. Docent Jari Jalava, Docent Antti Hakanen and Professor Pentti Huovinen are acknowledged for their contribution to this thesis in the field of microbiology. I thank Docent Marko Seppänen for his guidance and contribution in analysing clinical <sup>18</sup>F-FDG PET scans. Professor Sirpa Jalkanen is acknowledged for her expertise in immunology.

My gratitude also goes to all of the personnel in the PET Centre and to all of the personnel of the Central Animal Laboratory, particularly Ulla-Marjut Jaakkola and Rafael Frias, as well as to all of my colleagues in the Department of Orthopaedic Surgery and Traumatology.

In addition, I warmly thank all of the members of the Orthopaedic Research Unit and extend my special gratitude to Tatu Mäkinen and Kaisa Lehtimäki for the countless hours spent in doing the experimental studies. I thank Satu Timlin for her continuous help. My warm thanks also goes to Janek Frantzén for his support and optimism and for him being a mentor also during my clinical work. I thank Jessica Alm for the many fruitful talks about our research projects. Docent Niko Moritz is warmly acknowledged for his extensive knowledge of orthopaedic research and his important contribution to this thesis.

I owe my deepest gratitude to my family and friends for their tremendous support. My parents, Annukka and Sakari Lankinen, are thanked for their love and patience. My most sincere gratitude goes to my fiancée, Roosa Kirstilä, for her patience, never ending optimism, for believing in me and for being there for me. Without your support this thesis would not have been possible. This work was financially supported by the National Technology Agency (TEKES), the Sigrid Juselius Foundation, the National Doctoral Programme of Musculoskeletal Disorders and Biomaterials (TBDP), the Turku University Hospital (EVO-grant), the Finnish Medical Foundation, The Finnish Cultural Foundation, the Instrumentarium Foundation, the Finnish Research Foundation for Orthopaedics and Traumatology, the Emil Aaltonen Foundation, the Hilda Kauhanen Memorial Foundation, and the Turku University Foundation.

Turku, May 2013

  
Petteri Lankinen

## REFERENCES

- Aalto K, Autio A, Kiss EA, Elima K, Nymalm Y, Veres TZ, Marttila-Ichihara F, Elovaara H, Saanijoki T, Crocker PR, Maksimow M, Blight E, Salminen TA, Salmi M, Roivainen A, Jalkanen S. Siglec-9 is a novel leukocyte ligand for vascular adhesion protein-1 and can be used in PET imaging of inflammation and cancer. *Blood*. 2011;118:3725–3733.
- Abella A, Marti L, Camps M, Claret M, Fernández-Alvarez J, Gomis R, Gumà A, Viguier N, Carpené C, Palacin M, Testar X, Zorzano A. Semicarbazide-sensitive amine oxidase/vascular adhesion protein-1 activity exerts an antidiabetic action in goto-kakizaki rats. *Diabetes*. 2003;52:1004–1013.
- Ak I, Stokkel MPM, Pauwels EKJ. Positron emission tomography with 2-[18F] fluoro-2-deoxy-D-glucose in oncology. *J Cancer Res Clin Oncol*. 2000;126:560–574.
- Akhtar MS, Iqbal J, Khan MA, Irfanullah J, Jehangir M, Khan B, Ul-Haq I, Muhammad G, Nadeem MA, Afzal MS, Imran MB. 99mTc-labeled antimicrobial peptide ubiqaicidin (29-41) accumulates less in escherichia coli infection than in staphylococcus aureus infection. *J Nucl Med*. 2004;45:849–856.
- Al-Sheikh W, Sfakianakis GN, Mnaymneh W, Hourani M, Heal A, Duncan RC, Burnett A, Ashkar FS, Serafini AN. Subacute and chronic bone infections: Diagnosis using In-111, Ga-67 and Tc-99m MDP bone scintigraphy, and radiography. *Radiology*. 1985;155:501–506.
- Andriole VT, Nagel DA, Southwick WO. A paradigm for human chronic osteomyelitis. *J Bone Joint Surg Am*. 1973;55:1511–1515.
- Andriole VT, Nagel DA, Southwick WO. Chronic staphylococcal osteomyelitis: an experimental model. *Yale J Biol Med*. 1974;47:33–39.
- Aro HT, Chao EYS. Bone-healing patterns affected by loading, fracture fragment stability, fracture type, and fracture site compression. *Clin Orthop*. 1993;293:8–17.
- Arvilommi AM, Salmi M, Kalimo K, Jalkanen S. Lymphocyte binding to vascular endothelium in inflamed skin revisited: a central role for vascular adhesion protein-1 (VAP-1). *Eur J Immunol*. 1996;26:825–833.
- Autio A, Henttinen T, Sipilä HJ, Jalkanen S, Roivainen A. Mini-PEG spacing of VAP-1-targeting (68)Ga-DOTA-VAP-P1 peptide improves PET imaging of inflammation. *EJNMMI Res*. 2011;1:1–7.
- Autio A, Ujula T, Luoto P, Salomäki S, Jalkanen S, Roivainen A. PET imaging of inflammation and adenocarcinoma xenografts using vascular adhesion protein 1 targeting peptide 68Ga-DOTAVAP-P1: comparison with 18F-FDG. *Eur J Nucl Med Mol Imaging*. 2010;37:1918–1925.
- Barnes GL, Kostenuik PJ, Gerstenfeld LC, Einhorn TA. Growth factor regulation of fracture repair. *J Bone Miner Res*. 1999;14:1805–1815.
- Becker W, Goldenberg DM, Wolf F. The use of monoclonal antibodies and antibody fragments in the imaging of infectious lesions. *Semin Nucl Med*. 1994;24:142–153.
- Beckers C, Ribbens C, André B, Marcelis S, Kaye O, Mathy L, Kaiser MJ, Hustinx R, Foidart J, Malaise MG. Assessment of disease activity in rheumatoid arthritis with 18F-FDG PET. *J Nucl Med*. 2004;45:956–964.
- Berbari E, Mabry T, Tsaras G, Spangehl M, Erwin PJ, Murad MH, Steckelberg J, Osmon D. Inflammatory blood laboratory levels as markers of prosthetic joint infection: a systematic review and meta-analysis. *J Bone Joint Surg Am*. 2010;92:2102–2109.
- Bernstein LR. Mechanisms of therapeutic activity for gallium. *Pharmacol Rev*. 1998;50:665–682.
- Betgeowda C, Foss CA, Cheong I, Wang Y, Diaz L, Agrawal N, Fox J, Dick J, Dang LH, Zhou S, Kinzler KW, Vogelstein B, Pomper MG. Imaging bacterial infections with radiolabeled 1-(2'-deoxy-2'-fluoro-β-D-arabinofuranosyl)-5-iodouracil. *Proc Natl Acad Sci USA*. 2005;102:1145–1150.
- Bielby R, Jones E, McGonagle D. The role of mesenchymal stem cells in maintenance and repair of bone. *Injury*. 2007;38:S26–32.
- Blyth MJ, Kincaid R, Craigen MA, Bennett GC. The changing epidemiology of acute and subacute haematogenous osteomyelitis in children. *J Bone Joint Surg Br*. 2001;83:99–102.
- Bolander ME. Regulation of fracture repair by growth factors. *Proc Soc Exp Biol Med*. 1992;200:165–170.
- Borzutzky A, Stern S, Reiff A, Zurakowski D, Steinberg EA, Dedeoglu F, Sundel RP. Pediatric chronic non-bacterial osteomyelitis. *Pediatrics*. 2012;130:e1190–1197.
- Brady R, Leid J, Costerton J, Shirliff M. Osteomyelitis: clinical overview and mechanisms of infection persistence. *Clin Microbiol News*. 2006;28:65–72.
- Brenner W. 18F-FDG PET in rheumatoid arthritis: there still is a long way to go. *J Nucl Med*. 2004;45:927–929.
- Brodie BC. An Account of some Cases of Chronic Abscess of the Tibia. *Med Chir Trans*. 1832;17:239–249.
- Broekhuizen CA, de Boer L, Schipper K, Jones CD, Quadir S, Feldman RG, Dankert J, Vandenbroucke-Grauls CM, Weening JJ, Zaat SA. Peri-implant tissue is an important niche for staphylococcus epidermidis in experimental biomaterial-associated infection in mice. *Infect Immun*. 2007;75:1129–1136.
- Broekhuizen CA, de Boer L, Schipper K, Jones CD, Quadir S, Vandenbroucke-Grauls CM, Zaat SA. Staphylococcus epidermidis is cleared from biomaterial implants but persists in peri-implant tissue in mice despite rifampicin/vancomycin treatment. *J Biomed Mater Res A*. 2008;85:498–505.
- Brown TL, Spencer HJ, Beenken KE, Alpe TL, Bartel TB, Bellamy W, Gruenwald JM, Skinner RA, McLaren SG, Smeltzer MS. Evaluation of dynamic [18F]-FDG-PET imaging for the detection of acute post-surgical bone infection. *PLoS One*. 2012;7:e41863.
- Bruijnen ST, van der Weijden MA, Klein JP, Hoekstra OS, Boellaard R, van Denderen JC, Dijkmans BA, Voskuyl AE, van der Horst-Bruinsma IE, van



- der Laken CJ. Bone formation rather than inflammation reflects ankylosing spondylitis activity on PET-CT: a pilot study. *Arthritis Res Ther*. 2012;14:R71.
- Brunner M, Langer O, Dobrozemsky G, Müller U, Zeitlinger M, Mitterhauser M, Wadsak W, Dudczak R, Kletter K, Müller M. [18F] ciprofloxacin, a new positron emission tomography tracer for noninvasive assessment of the tissue distribution and pharmacokinetics of ciprofloxacin in humans. *Antimicrob Agents Chemother*. 2004;48:3850–3857.
- Buckwalter JA. Effects of early motion on healing of musculoskeletal tissues. *Hand Clin*. 1996;12:13–24.
- Buckwalter J, Glimcher M, Cooper R, Recker R. Bone biology. *J Bone Joint Surg*. 1995;77:1276–1289.
- Butalia S, Palda VA, Sargeant RJ, Detsky AS, Mourad O. Does this patient with diabetes have osteomyelitis of the lower extremity? *JAMA*. 2008;299:806–813.
- Butcher EC, Picker LJ. Lymphocyte homing and homeostasis. *Science*. 1996;272:60–66.
- Butt WP. The radiology of infection. *Clin Orthop Relat Res*. 1973;96:20–30.
- Calhoun JH, Manring MM, Shirliff M. Osteomyelitis of the long bones. *Semin Plast Surg*. 2009;23:59–72.
- Carey K, Saboury B, Basu S, Brothers A, Ogdie A, Werner T, Torigian DA, Alavi A. Evolving role of FDG PET imaging in assessing joint disorders: a systematic review. *Eur J Nucl Med Mol Imaging*. 2011;38:1939–1955.
- Chacko TK, Zhuang H, Nakhoda KZ, Moussavian B, Alavi A. Applications of fluorodeoxyglucose positron emission tomography in the diagnosis of infection. *Nucl Med Commun*. 2003;24:615–624.
- Chacko TK, Zhuang H, Stevenson K, Moussavian B, Alavi A. The importance of the location of fluorodeoxyglucose uptake in periprosthetic infection in painful hip prostheses. *Nucl Med Commun*. 2002;23:851–855.
- Chadha HS, Fitzgerald RH, Jr, Wiater P, Sud S, Nasser S, Wooley PH. Experimental acute hematogenous osteomyelitis in mice. I. Histopathological and immunological findings. *J Orthop Res*. 1999;17:376–381.
- Cheng D, Wang Y, Liu X, Pretorius PH, Liang M, Rusckowski M, Hnatoiwch DJ. Comparison of 18F PET and 99mTc SPECT imaging in phantoms and in tumored mice. *Bioconjug Chem*. 2010;21:1565–1570.
- Chianelli M, Mather SJ, Martin-Comin J, Signore A. Radiopharmaceuticals for the study of inflammatory processes: a review. *Nucl Med Commun*. 1997;18:437–455.
- Cho TJ, Gerstenfeld LC, Einhorn TA. Differential temporal expression of members of the transforming growth factor  $\beta$  superfamily during murine fracture healing. *J Bone Miner Res*. 2002;17:513–520.
- Chryssikos T, Parvizi J, Ghanem E, Newberg A, Zhuang H, Alavi A. FDG-PET imaging can diagnose periprosthetic infection of the hip. *Clin Orthop Relat Res*. 2008;466:1338–1342.
- Ciorny G, Mader JT, Penninck JJ. A clinical staging system for adult osteomyelitis. *Contemp Orthop*. 1985;10:17–37.
- Claes L, Recknagel S, Ignatius A. Fracture healing under healthy and inflammatory conditions. *Nat Rev Rheumatol*. 2012;8:133–143.
- Copenhaver WM, Kelly DE, Wood RL. The connective tissues: cartilage and bone. In: Copenhaver WM, Kelly DE, Wood RL, eds. *Bailey's Textbook of Histology*, 17th ed. Baltimore: Williams & Wilkins. 1978:170–205.
- Corstens FH, van der Meer JW. Nuclear medicine's role in infection and inflammation. *Lancet*. 1999;354:765–770.
- Craig MA, Watters J, Hackett JS. The changing epidemiology of osteomyelitis in children. *J Bone Joint Surg Br*. 1992;74:541–545.
- Cunningham R, Cockayne A, Humphreys H. Clinical and molecular aspects of the pathogenesis of staphylococcus aureus bone and joint infections. *J Med Microbiol*. 1996;44:157–164.
- Davis MA, Jones AG. Comparison of 99m-Tc-labeled phosphate and phosphonate agents for skeletal imaging. *Semin Nucl Med*. 1976;6:19–31.
- De Winter F, Gemmel F, Van De Wiele C, Poffijn B, Uytendaele D, Dierckx R. 18-Fluorine fluorodeoxyglucose positron emission tomography for the diagnosis of infection in the postoperative spine. *Spine*. 2003;28:1314–1319.
- De Winter F, van de Wiele C, Vogelaers D, de Smet K, Verdonk R, Dierckx RA. Fluorine-18 fluorodeoxyglucose-position emission tomography: a highly accurate imaging modality for the diagnosis of chronic musculoskeletal infections. *J Bone Joint Surg Am*. 2001;83:651–660.
- De Winter F, Vogelaers D, Gemmel F, Dierckx R. Promising role of 18-F-fluoro-D-deoxyglucose positron emission tomography in clinical infectious diseases. *Eur J Clin Microbiol Infect Dis*. 2002;21:247–257.
- DeGrado TR, Turkington TG, Williams JJ, Stearns CW, Hoffman JM, Coleman RE. Performance characteristics of a whole-body PET scanner. *J Nucl Med*. 1994;35:1398–1406.
- Dehdashti F, Siegel BA, Griffith LK, Fuseselman MJ, Trask DD, McGuire AH, McGuire DJ. Benign versus malignant intraosseous lesions: discrimination by means of PET with 2-[F-18] fluoro-2-deoxy-D-glucose. *Radiology*. 1996;200:243–247.
- Delank KS, Schmidt M, Michael JW, Dietlein M, Schicha H, Eysel P. The implications of 18F-FDG PET for the diagnosis of endoprosthetic loosening and infection in hip and knee arthroplasty: results from a prospective, blinded study. *BMC Musculoskelet Disord*. 2006;7:20.
- Della Valle C, Parvizi J, Bauer TW, DiCesare PE, Evans RP, Segreti J, Spangehl M, Watters WC, 3rd, Keith M, Turkelson CM, Wies JL, Sluka P, Hitchcock K. American academy of orthopaedic surgeons clinical practice guideline on: the diagnosis of periprosthetic joint infections of the hip and knee. *J Bone Joint Surg Am*. 2011;93:1355–1357.
- Diaz LA, Jr, Foss CA, Thornton K, Nimmagadda S, Endres CJ, Uzuner O, Seyler TM, Ulrich SD, Conway J, Bettogoda C, Agrawal N, Cheong I, Zhang X, Ladenson PW, Vogelstein BN, Mont MA, Zhou S, Kinzler KW, Vogelstein B, Pomper MG. Imaging of musculoskeletal bacterial infections by [124I]FIAU-PET/CT. *PLoS One*. 2007;2:e1007.
- Dich VQ, Nelson JD, Haltalin KC. Osteomyelitis in infants and children. A

- review of 163 cases. *Am J Dis Child*. 1975;129:1273–1278.
- Diederichs CG, Staib L, Glatting G, Berger HG, Reske SN. FDG PET: elevated plasma glucose reduces both uptake and detection rate of pancreatic malignancies. *J Nucl Med*. 1998;39:1030–1033.
- Dimitriou R, Tsiridis E, Giannoudis PV. Current concepts of molecular aspects of bone healing. *Injury*. 2005;36:1392–1404.
- Dinh MT, Abad CL, Safdar N. Diagnostic accuracy of the physical examination and imaging tests for osteomyelitis underlying diabetic foot ulcers: meta-analysis. *Clin Infect Dis*. 2008;47:519–527.
- Dumarey N, Egrise D, Blocklet D, Stallenberg B, Remmelink M, del Marmol V, Van Simaey G, Jacobs F, Goldman S. Imaging infection with 18F-FDG-labeled leukocyte PET/CT: initial experience in 21 patients. *J Nucl Med*. 2006;47:625–632.
- Ehrhardt GJ, Welch MJ. A new germanium-63/gallium-68 generator. *J Nucl Med*. 1978;19:925–929.
- Einhorn TA. The cell and molecular biology of fracture healing. *Clin Orthop*. 1998;355:S7–21.
- Einhorn TA. The science of fracture healing. *J Orthop Trauma*. 2005;19:S4–6.
- Einhorn TA, Majeska RJ, Rush EB, Levine PM, Horowitz MC. The expression of cytokine activity by fracture callus. *J Bone Miner Res*. 1995;10:1272–1281.
- El-Maghraby T, Moustafa H, Pauwels E. Nuclear medicine methods for evaluation of skeletal infection among other diagnostic modalities. *Q J Nucl Med Mol Imaging*. 2006;50:167–192.
- Elzinga E, Van Der Laken C, Comans EFI, Lammertsma A, Dijkman BAC, Voskuyl A. 2-deoxy-2-[F-18] fluoro-D-glucose joint uptake on positron emission tomography images: rheumatoid arthritis versus osteoarthritis. *Mol Imaging Biol*. 2007;9:357–360.
- Familiari D, Glaudemans AW, Vitale V, Prosperi D, Bagni O, Lenza A, Cavallini M, Scopinaro F, Signore A. Can sequential 18F-FDG PET/CT replace WBC imaging in the diabetic foot? *J Nucl Med*. 2011;52:1012–1019.
- Fani M, André JP, Mäcke HR. 68Ga-PET: a powerful generator-based alternative to cyclotronbased PET radiopharmaceuticals. *Contrast Media Mol Imaging*. 2008;3:67–77.
- Fathinul F, Nordin AJ. 18F-FDG PET/CT as a potential valuable adjunct to MRI in characterising the Brodie's abscess. *Biomed Imaging Interv J*. 2010;6:e26.
- Fayad LM, Cohade C, Wahl RL, Fishman EK. Sacral fractures: a potential pitfall of FDG positron emission tomography. *Am J Roentgenol*. 2003;181:1239–1243.
- Fenollar F, Roux V, Stein A, Drancourt M, Raoult D. Analysis of 525 samples to determine the usefulness of PCR amplification and sequencing of the 16S rRNA gene for diagnosis of bone and joint infections. *J Clin Microbiol*. 2006;44:1018–1028.
- Fernandes JC, Martel-Pelletier J, Pelletier JP. The role of cytokines in osteoarthritis pathophysiology. *Biorheology*. 2002;39:237–246.
- Fihman V, Hannouche D, Bousson V, Bardin T, Lioté F, Raskine L, Riahi J, Sanson-Le Pors MJ, Berçot B. Improved diagnosis specificity in bone and joint infections using molecular techniques. *J Infect*. 2007;55:510–517.
- Fischman AJ, Alpert NM, Livni E, Ray S, Sinclair I, Elmaleh DR, Weiss S, Correia JA, Webb D, Liss R. Pharmacokinetics of 18F-labeled fluconazole in rabbits with candidal infections studied with positron emission tomography. *J Pharmacol Exp Ther*. 1991;259:1351–1359.
- Fitzgerald RH, Jr. Experimental osteomyelitis: description of a canine model and the role of depot administration of antibiotics in the prevention and treatment of sepsis. *J Bone Joint Surg Am*. 1983;65:371–380.
- Floyd RL, Steele RW. Culture-negative osteomyelitis. *Pediatr Infect Dis J*. 2003;22:731–736.
- García-Barrecheguren E, Rodríguez Fraile M, Toledo Santana G, Valentí Nin J, Richter Echevarría J. 18FDG-PET: a new diagnostic approach in hip prosthesis infection. *Rev Esp Med Nucl*. 2007;26:208–220.
- Gemmel F, Dumarey N, Palestro CJ. Radionuclide imaging of spinal infections. *Eur J Nucl Med Mol Imaging*. 2006;33:1226–1237.
- Gemmel F, Dumarey N, Welling M. Future diagnostic agents. *Semin Nucl Med*. 2009;39:11–26.
- Gemmel F, Rijk PC, Collins JMP, Parlevliet T, Stumpe KD, Palestro CJ. Expanding role of 18F-fluoro-D-deoxyglucose PET and PET/CT in spinal infections. *Eur Spine J*. 2010;19:540–551.
- Genat HK, Bautovich GJ, Singh M, Lathrop KA, Harper PV. Bone-seeking radionuclides: an in vivo study of factors affecting skeletal uptake. *Radiology*. 1974;113:373–382.
- Glithero PR, Grigoris P, Harding LK, Hesselwood SR, McMinn DJ. White cell scans and infected joint replacements. failure to detect chronic infection. *J Bone Joint Surg Br*. 1993;75:371–374.
- Gold RH, Hawkins RA, Katz RD. Bacterial osteomyelitis: findings on plain radiography, CT, MR, and scintigraphy. *AJR Am J Roentgenol*. 1991;157:365–370.
- Goldsmith SJ, Vallabhajosula S. Clinically proven radiopharmaceuticals for infection imaging: mechanisms and applications. *Semin Nucl Med*. 2009;39:2–10.
- Golla A, Jansson A, Ramser J, Hellebrand H, Zahn R, Meitinger T, Belohradsky BH, Meindl A. Chronic recurrent multifocal osteomyelitis (CRMO): evidence for a susceptibility gene located on chromosome 18q21.3–18q22. *Eur J Hum Genet*. 2002;10:217–221.
- Gratz S, Dörner J, Fischer U, Behr TM, Béhé M, Altenuoerde G, Meller J, Grabbe E, Becker W. 18F-FDG hybrid PET in patients with suspected spondylitis. *Eur J Nucl Med*. 2002;29:516–524.
- Gratz S, Rennen HJMM, Boerman OC, Oyen WJG, Burma P, Corstens FHM. 99mTc-interleukin-8 for imaging acute osteomyelitis. *J Nucl Med*. 2001;42:1257–1264.
- Green MA, Welch MJ. Gallium radiopharmaceutical chemistry. *Nucl Med Biol*. 1989;16:435–448.
- Greenbaum M, Kanat I. Current concepts in bone healing. Review of the literature. *J Am Podiatr Med Assoc*. 1993;83:123–129.
- Grey AC, Davies AM, Mangham DC, Grimer RJ, Ritchie DA. The 'pneumonia sign' on T1-weighted MR imaging in subacute osteomyelitis: frequency,

- cause and significance. *Clin Radiol*. 1998;53:587–592.
- Gristina AG, Naylor PT, Myrvik QN. Musculoskeletal infection, microbial adhesion, and antibiotic resistance. *Infect Dis Clin North Am*. 1990;4:391–408.
- Gristina AG, Oga M, Webb LX, Hobgood CD. Adherent bacterial colonization in the pathogenesis of osteomyelitis. *Science*. 1985;228:990–993.
- Guhlmann A, Brecht-Krauss D, Suger G, Glatting G, Kotzerke J, Kinzl L, Reske SN. Chronic osteomyelitis: detection with FDG PET and correlation with histopathologic findings. *Radiology*. 1998a;206:749–754.
- Guhlmann A, Brecht-Krauss D, Suger G, Glatting G, Kotzerke J, Kinzl L, Reske SN. Fluorine-18-FDG PET and technetium-99m antigranulocyte antibody scintigraphy in chronic osteomyelitis. *J Nucl Med*. 1998b;39:2145–2152.
- Gustilo R, Anderson J. Prevention of infection in the treatment of one thousand and twenty-five open fractures of long bones: retrospective and prospective analyses. *J Bone Joint Surg Am*. 1976;58:453–458.
- Hamacher K, Coenen HH, Stocklin G. Efficient stereospecific synthesis of no-carrier-added 2-[<sup>18</sup>F]-fluoro-2-deoxy-D-glucose using aminopolyether supported nucleophilic substitution. *J Nucl Med*. 1986;27:235–238.
- Hartmann A, Eid K, Dora C, Trentz O, von Schulthess GK, Stumpe KD. Diagnostic value of 18F-FDG PET/CT in trauma patients with suspected chronic osteomyelitis. *Eur J Nucl Med Mol Imaging*. 2007;34:704–714.
- Heelan BT, Osman S, Blyth A, Schnorr L, Jones T, George AJT. Use of 2-[<sup>18</sup>F]fluoro-2-deoxyglucose as a potential agent in the prediction of graft rejection by positron emission Tomography. *Transplantation*. 1998;66:1101–1103.
- Henderson MS, Simon HE. Brodie's abscess. *Arch Surg*. 1924;9:504–515.
- Heyer CM, Brus LJ, Peters SA, Lemburg SP. Efficacy of CT-guided biopsies of the spine in patients with spondylitis - an analysis of 164 procedures. *Eur J Radiol*. 2012;81:e244–249.
- Hoffer P. Gallium: Mechanisms. *J Nucl Med*. 1980;21:282–285.
- Hoffman EJ, Huang SC, Phelps ME. Quantitation in positron emission computed tomography: 1. effect of object size. *J Comput Assist Tomogr*. 1979;3:299–308.
- Hsu W, Feeley B, Krenke L, Stout D, Chatziioannou A, Lieberman J. The use of 18 F-fluoride and 18F-FDG PET scans to assess fracture healing in a rat femur model. *Eur J Nucl Med Mol Imaging*. 2007;34:1291–1301.
- Hudson MC, Ramp WK, Nicholson NC, Williams AS, Nousiainen MT. Internalization of staphylococcus aureus by cultured osteoblasts. *Microb Pathog*. 1995;19:409–419.
- Hulth A. Current concepts of fracture healing. *Clin Orthop*. 1989;249:265–284.
- Jaakkola K, Nikula T, Holopainen R, Vähäsilta T, Matikainen MT, Laukkanen ML, Huupponen R, Halkola L, Nieminen L, Hiltunen J, Parviainen S, Clark MR, Knuuti J, Savunen T, Kääpä P, Voipio-Pulkki LM, Jalkanen S. In vivo detection of vascular adhesion protein-1 in experimental inflammation. *Am J Pathol*. 2000;157:463–471.
- Jevtic V. Vertebral infection. *Eur Radiol*. 2004;14:43–52.
- Johansson A, Svensson O, Blomgren G, Eliasson G, Nord CE. Anaerobic osteomyelitis. A new experimental rabbit model. *Clin Orthop Relat Res*. 1991;265:297–301.
- Johnson JA, Christie MJ, Sandler MP, Parks PF Jr, Homra L, Kaye JJ. Detection of occult infection following total joint arthroplasty using sequential technetium-99m HDP bone scintigraphy and indium-111 WBC imaging. *J Nucl Med*. 1988;29:1347–1353.
- Jones-Jackson L, Walker R, Purnell G, McLaren SG, Skinner RA, Thomas JR, Suva LJ, Anaissie E, Miceli M, Nelson CL, Ferris EJ, Smeltzer MS. Early detection of bone infection and differentiation from post-surgical inflammation using 2-deoxy-2-[<sup>18</sup>F]-fluoro-D-glucose positron emission tomography (FDG-PET) in an animal model. *J Orthop Res*. 2005;23:1484–1489.
- Joseph TN, Mujtaba M, Chen AL, Maurer SL, Zuckerman JD, Maldjian C, Di Cesare PE. Efficacy combined technetium-99m sulphur-colloid/indium-111 leukocyte scans to detect infected total hip and knee arthroplasties. *J Arthroplasty*. 2001;16:753–758.
- Jurik AG. Chronic recurrent multifocal osteomyelitis. *Semin Musculoskelet Radiol*. 2004;8:243–253.
- Kahn MF, Chamot AM. SAPHO syndrome. *Rheum Dis Clin North Am*. 1992;18:225–246.
- Kaim AH, Gross T, von Schulthess GK. Imaging of chronic posttraumatic osteomyelitis. *Eur Radiol*. 2002;12:1193–1202.
- Kaim A, Ledermann HP, Bongartz G, Messmer P, Muller-Brand J, Steinbrich W. Chronic post-traumatic osteomyelitis of the lower extremity: comparison of magnetic resonance imaging and combined bone scintigraphy/immunoscintigraphy with radiolabelled monoclonal antigranulocyte antibodies. *Skeletal Radiol*. 2000;29:378–386.
- Kalfas IH. Principles of bone healing. *Neurosurg Focus*. 2001;10:1–4.
- Källicke T, Schmitz A, Risse JH, Arens S, Keller E, Hansis M, Schmitt O, Biersack HJ, Grünwald F. Fluorine-18 fluorodeoxyglucose positron emission tomography in infectious bone diseases: Results of histologically confirmed cases. *Eur J Nucl Med Mol Imaging*. 2000;27:524–528.
- Kaplan SL. Osteomyelitis in children. *Infect Dis Clin North Am*. 2005;19:787–798.
- Kapoor A, Page S, LaValley M, Gale DR, Felson DT. Magnetic resonance imaging for diagnosing foot osteomyelitis: A meta-analysis. *Arch Intern Med*. 2007;167:125–132.
- Keidar Z, Militianu D, Melamed E, Bar-Shalom R, Israel O. The diabetic foot: initial experience with 18F-FDG PET/CT. *J Nucl Med*. 2005;46:444–449.
- Khalil H, Williams RJ, Stenbeck G, Henderson B, Meghji S, Nair SP. Invasion of bone cells by staphylococcus epidermidis. *Microbes Infect*. 2007;9:460–465.
- Khanna G, Sato TS, Ferguson P. Imaging of chronic recurrent multifocal osteomyelitis. *Radiographics*. 2009;29:1159–1177.

- Klein P, Schell H, Streitparth F, Heller M, Kassi JP, Kandziara F, Bragulla H, Haas NP, Duda GN. The initial phase of fracture healing is specifically sensitive to mechanical conditions. *J Orthop Res*. 2003;21:662–669.
- Klosterhalfen B, Peters K, Tons C, Hauptmann S, Klein C, Kirkpatrick C. Local and systemic inflammatory mediator release in patients with acute and chronic posttraumatic osteomyelitis. *J Trauma*. 1996;40:372–378.
- Kon T, Cho TJ, Aizawa T, Yamazaki M, Nooh N, Graves D, Gerstenfeld LC, Einhorn TA. Expression of osteoprotegerin, receptor activator of NF- $\kappa$ B ligand (osteoprotegerin ligand) and related proinflammatory cytokines during fracture healing. *J Bone Miner Res*. 2001;16:1004–1014.
- Koort JK, Mäkinen TJ, Knuuti J, Jalava J, Aro HT. Comparative 18F-FDG PET of experimental staphylococcus aureus osteomyelitis and normal bone healing. *J Nucl Med*. 2004;45:1406–1411.
- Koort JK, Mäkinen TJ, Suokas E, Veiranto M, Jalava J, Knuuti J, Törmälä P, Aro HT. Efficacy of ciprofloxacin-releasing bioabsorbable osteoconductive bone defect filler for treatment of experimental osteomyelitis due to staphylococcus aureus. *Antimicrob Agents Chemother*. 2005;49:1502–1508.
- Koskinen K, Vainio PJ, Smith DJ, Pihlavisto M, Yla-Herttua S, Jalkanen S, and Salmi M. Granulocyte transmigration through the endothelium is regulated by the oxidase activity of vascular adhesion protein-1 (VAP-1). *Blood*. 2004;103:3388–3395.
- Kostakoglu L, Hardoff R, Mirtcheva R, Goldsmith SJ. PET-CT fusion imaging in differentiating physiologic from pathologic FDG uptake. *Radiographics*. 2004;24:1411–1431.
- Kubota R, Yamada S, Kubota K, Ishiwata K, Tamahashi N, Ido T. Intratumoral distribution of fluorine-18-fluorodeoxyglucose in vivo: high accumulation in macrophages and granulation tissues studied by microautoradiography. *J Nucl Med*. 1992;33:1972–1980.
- Kumar R, Basu S, Torigian D, Anand V, Zhuang H, Alavi A. Role of modern imaging techniques for diagnosis of infection in the era of 18F-fluorodeoxyglucose positron emission tomography. *Clin Microbiol Rev*. 2008;21:209–224.
- Kumar V, Boddeti DK. (68)Ga-radiopharmaceuticals for PET imaging of infection and inflammation. *Recent Results Cancer Res*. 2013;194:189–219.
- Kumar V, Boddeti DK, Evans SG, Roesch F, Howman-Giles R. Potential use of 68Ga-apo-transferrin as a PET imaging agent for detecting *Staphylococcus aureus* infection. *Nucl Med Biol*. 2011;38:393–398.
- Kwee TC, Kwee RM, Alavi A. FDG-PET for diagnosing prosthetic joint infection: Systematic review and metaanalysis. *Eur J Nucl Med Mol Imaging*. 2008;35:2122–2132.
- Lambe DW, Jr, Ferguson KP, Mayberry-Carson KJ, Tober-Meyer B, Costerton JW. Foreign-body-associated experimental osteomyelitis induced with bacteroides fragilis and staphylococcus epidermidis in rabbits. *Clin Orthop Relat Res*. 1991;266:285–294.
- Langer O, Brunner M, Zeitlinger M, Ziegler S, Müller U, Dobrozemsky G, Lackner E, Joukhadar C, Mitterhauser M, Wadsak W, Minar E, Dudczak R, Kletter K, Müller M. In vitro and in vivo evaluation of [18F] ciprofloxacin for the imaging of bacterial infections with PET. *Eur J Nucl Med Mol Imaging*. 2005;32:143–150.
- Larikka MJ, Ahonen AK, Junila JA, Niemelä O, Hämäläinen MM, Syrjälä HP. Extended combined 99mTc-white blood cell and bone imaging improves the diagnostic accuracy in the detection of hip replacement infections. *Eur J Nucl Med*. 2001a;28:288–293.
- Larikka MJ, Ahonen AK, Junila JA, Niemelä O, Hämäläinen MM, Syrjälä HP. Improved method for detecting knee replacement infections based on extended combined 99mTc-white blood cell/bone imaging. *Nucl Med Commun*. 2001b;22:1145–1150.
- Larikka MJ, Ahonen AK, Niemelä O, Junila JA, Hämäläinen MM, Britton K, Syrjälä HP. Comparison of 99mTc ciprofloxacin, 99mTc white blood cell and three-phase bone imaging in the diagnosis of hip prosthesis infections: improved diagnostic accuracy with extended imaging time. *Nucl Med Commun*. 2002a;23:655–661.
- Larikka MJ, Ahonen AK, Niemelä O, Puronto O, Junila JA, Hämäläinen MM, Britton K, Syrjälä HP. 99m Tc-ciprofloxacin (Infecton) imaging in the diagnosis of knee prosthesis infections. *Nucl Med Commun*. 2002b;23:167–170.
- Lavery LA, Armstrong DG, Wunderlich RP, Mohler MJ, Wendel CS, Lipsky BA. Risk factors for foot infections in individuals with diabetes. *Diabetes Care*. 2006;29:1288–1293.
- Lavery LA, Armstrong DG, Wunderlich RP, Tredwell J, Boulton AJM. Diabetic foot syndrome evaluating the prevalence and incidence of foot pathology in Mexican Americans and non-Hispanic whites from a diabetes disease management cohort. *Diabetes Care*. 2003;26:1435–1438.
- Lazzarini L, Mader JT, Calhoun JH. Osteomyelitis in long bones. *J Bone Joint Surg Am*. 2004;86:2305–2318.
- Ledermann HP, Kaim A, Bongartz G, Steinbrich W. Pitfalls and limitations of magnetic resonance imaging in chronic posttraumatic osteomyelitis. *Eur Radiol*. 2000;10:1815–1823.
- Lee JA, Huh SJ, Oh D, Bae DS. Osteoradionecrosis after three-dimensional conformal radiotherapy for recurrent cervical cancer presenting as a progressive osteolytic lesion. *Ann Nucl Med*. 2008;22:139–141.
- Lehmann K, Angerstein C, Meller J, Behr M, Becker W. The basis of 18F-FDG scintigraphy for imaging infection. *Nucl Med Commun*. 2001;22:1157–1158.
- Lew DP, Waldvogel FA. Osteomyelitis. *N Engl J Med*. 1997;336:999–1007.
- Lew DP, Waldvogel FA. Osteomyelitis. *Lancet*. 2004;364:369–379.
- Lexer E. Zur experimentellen erzeugung osteomyelitischer herde. *Arch Klin Chir*. 1894;48:181–200.
- Lieberman JR, Daluiski A, Einhorn TA. The role of growth factors in the repair of bone. Biology and clinical applications. *J Bone Joint Surg Am*. 2002;84:1032–1044.
- Lin PW, Liu RS, Liou TH, Pan LC, Chen CH. Correlation between joint [F-18] FDG PET uptake and synovial TNF- $\alpha$  concentration: A study with two rabbit models of acute inflammatory arthritis. *Appl Radiat Isot*. 2007;65:1221–1226.

- Lipsky BA. Osteomyelitis of the foot in diabetic patients. *Clin Infect Dis*. 1997;25:1318–1326.
- Lipsky BA, Berendt AR, Cornia PB, Pile JC, Peters EJ, Armstrong DG, Deery HG, Embil JM, Joseph WS, Karchmer AW, Pinzur MS, Senneville E. 2012 Infectious Diseases Society of America clinical practice guideline for the diagnosis and treatment of diabetic foot infections. *Clin Infect Dis*. 2012;54:e132–173.
- Liu S, Chang J, Ng S, Chan S, Yen T. False positive fluorine-18 fluorodeoxy-D-glucose positron emission tomography finding caused by osteoradionecrosis in a nasopharyngeal carcinoma patient. *Br J Radiol*. 2004;77:257–260.
- Lopes TD, Reinus WR, Wilson AJ. Quantitative analysis of the plain radiographic appearance of Brodie's abscess. *Invest Radiol*. 1997;32:51–58.
- Love C, Marwin SE, Palestro CJ. Nuclear medicine and the infected joint replacement. *Semin Nucl Med*. 2009;39:66–78.
- Love C, Marwin SE, Tomas MB, Krauss ES, Tronco GG, Bhargava KK, Nichols KJ, Palestro CJ. Diagnosing infection in the failed joint replacement: A Comparison of Coincidence Detection <sup>18</sup>F-FDG and <sup>111</sup>In-Labeled Leukocyte/<sup>99m</sup>Tc-Sulfur Colloid Marrow Imaging. *J Nucl Med*. 2004;45:1864–1871.
- Love C, Palestro CJ. Radionuclide Imaging of Infection. *J Nucl Med Technol*. 2004;32:47–57.
- Lucke M, Schmidmaier G, Sadoni S, Wildemann B, Schiller R, Stemberger A, Haas NP, Raschke M. A new model of implant-related osteomyelitis in rats. *J Biomed Mater Res B Appl Biomater*. 2003;67:593–602.
- Lupetti A, Welling MM, Pauwels EKJ, Nibbering PH. Radiolabelled antimicrobial peptides for infection detection. *Lancet Infect Dis*. 2003;3:223–229.
- Ma LD, Frasca FJ, Bluemke DA, Fishman EK. CT and MRI evaluation of musculoskeletal infection. *Crit Rev Diagn Imaging*. 1997;38:535–568.
- Mäcke HR, André JP. 68Ga-PET radiopharmacy: a generator-based alternative to 18F radiopharmacy. In: Schubiger PA, Lehmann M, Friebe M, eds. *PET Chemistry, the driving force in molecular imaging*. New York: Springer. 2007:215–241.
- Mackowiak PA, Jones SR, Smith JW. Diagnostic value of sinus-tract cultures in chronic osteomyelitis. *JAMA*. 1978;239:2772–2775.
- Mader JT. Animal models of osteomyelitis. *Am J Med*. 1985;78:213–217.
- Mader JT, Cripps MW, Calhoun JH. Adult posttraumatic osteomyelitis of the tibia. *Clin Orthop Relat Res*. 1999;360:14–21.
- Mader J, Shirliff M. The rabbit model of bacterial osteomyelitis of the tibia. In: Zak O, Sande MA, eds. *Handbook of Animal Models of Infection Experimental Models in Antimicrobial Chemotherapy*. London: Academic Press, Ltd. 1999:581–591.
- Mader JT, Wilson KJ. Comparative evaluation of cefamandole and cephalothin in the treatment of experimental staphylococcus aureus osteomyelitis in rabbits. *J Bone Joint Surg Am*. 1983;65:507–513.
- Mahfouz T, Miceli MH, Saghafifar F, Stroud S, Jones-Jackson L, Walker R, Graziutti ML, Purnell G, Fassas A, Tricot G, Barlogie B, Anaissie E. 18F-fluorodeoxyglucose positron emission tomography contributes to the diagnosis and management of infections in patients with multiple myeloma: a study of 165 infectious episodes. *J Clin Oncol*. 2005;23:7857–7863.
- Mäkinen TJ, Veiranto M, Knuuti J, Jalava J, Törmälä P, Aro HT. Efficacy of bioabsorbable antibiotic containing bone screw in the prevention of biomaterial-related infection due to staphylococcus aureus. *Bone*. 2005;36:292–299.
- Mandell GL, Douglas RG, Bennett JE, Dolin R. Osteomyelitis. In: *Mandell, Douglas, and Bennett's Principles and Practice of Infectious Diseases*. Philadelphia: Churchill Livingstone. 2009;103:1457–1467.
- Manolagas SC. Birth and death of bone cells: basic regulatory mechanisms and implications for the pathogenesis and treatment of osteoporosis. *Endocr Rev*. 2000;21:115–137.
- Manthey N, Reinhard P, Moog F, Knesevitsch P, Hahn K, Tatsch K. The use of [18F]fluorodeoxyglucose positron emission tomography to differentiate between synovitis, loosening and infection of hip and knee prostheses. *Nucl Med Commun*. 2002;23:645–653.
- Manthey P, Reinhard P, Tatsch K, Hahn K. FDG PET to differentiate between loosening and infection of hip and knee prostheses. *J Nucl Med*. 1999;40:S96–97.
- Maor G, Karnieli E. The insulin-sensitive glucose transporter (GLUT4) is involved in early bone growth in control and diabetic mice, but is regulated through the insulin-like growth factor I receptor. *Endocrinology*. 1999;140:1841–1851.
- Marcus CD, Ladam-Marcus VJ, Leone J, Malgrange D, Bonnet-Gausserand FM, Menanteau BP. MR imaging of osteomyelitis and neuropathic osteoarthropathy in the feet of diabetics. *Radiographics*. 1996;16:1337–1348.
- Martínez MJ, Ziegler S, Beyer T. PET and PET/CT: basic principles and instrumentation. *Recent Results Cancer Res*. 2008;170:1–23.
- Matthews PC, Berendt AR, McNally MA, Byren I. Diagnosis and management of prosthetic joint infection. *BMJ*. 2009;338:1378–1383.
- Matsui T, Nakata N, Nagai S, Nakatani A, Takahashi M, Momose T, Ohtomo K, Koyasu S. Inflammatory cytokines and hypoxia contribute to 18F-FDG uptake by cells involved in pannus formation in rheumatoid arthritis. *J Nucl Med*. 2009;50:920–926.
- Mayberry-Carson KJ, Tober-Meyer B, Gill LR, Lambe DW, Jr, Hossler FE. Effect of ciprofloxacin on experimental osteomyelitis in the rabbit tibia, induced with a mixed infection of staphylococcus epidermidis and bacteroides thetaiotaomicron. *Microbios*. 1990;64:49–66.
- Mayberry-Carson KJ, Tober-Meyer B, Lambe DW, Jr, Costerton JW. Osteomyelitis experimentally induced with Bacteroides thetaiotaomicron and Staphylococcus epidermidis. Influence of a foreign-body implant. *Clin Orthop Relat Res*. 1992;280:289–299.
- Mayer-Kuckuk P, Boskey AL. Molecular imaging promotes progress in orthopedic research. *Bone*. 2006;39:965–977.
- Meller J, Sahlmann CO, Liersch T, Hao Tang P, Alavi A. Nonprosthesis orthopedic applications of 18F fluoro-2-de-

- oxy-D-glucose PET in the detection of osteomyelitis. *Radiol Clin North Am.* 2007;45:719–733.
- Menon S, Wagner HN, Jr, Tsan MF. Studies on gallium accumulation in inflammatory lesions: II. uptake by staphylococcus aureus: Concise communication. *J Nucl Med.* 1978;19:44–47.
- Merinen M, Irjala H, Salmi M, Jaakkola I, Hänninen A, Jalkanen S. Vascular adhesion protein-1 is involved in both acute and chronic inflammation in the mouse. *Am J Pathol.* 2005;166:793–800.
- Merkel KD, Brown ML, Dewanjee MK, Fitzgerald RH. Comparison of indium-labeled-leukocyte imaging with sequential technetium-gallium scanning in the diagnosis of low-grade musculoskeletal sepsis. *J Bone Joint Surg Am.* 1985;67:465–476.
- Metser U, Even-Sapir E. Increased 18F-fluorodeoxyglucose uptake in benign, nonphysiologic lesions found on whole-body positron emission tomography/computed tomography (PET/CT): Accumulated data from four years of experience. *Semin Nucl Med.* 2007;37:206–222.
- Meyer M, Gast T, Raja S, Hubner K. Increased F-18 FDG accumulation in an acute fracture. *Clin Nucl Med.* 1994;19:13–14.
- Morrison WB, Schweitzer ME, Batte W, Radack DP, Russel KM. Osteomyelitis of the foot: relative importance of primary and secondary MR imaging signs. *Radiology.* 1998;207:625–632.
- Mulamba L, Ferrant A, Leners N, de Nayer P, Rombouts JJ, Vincent A. Indium-111 leukocyte scanning in the evaluation of painful hip arthroplasty. *Acta Orthop Scand.* 1983;54:695–697.
- Mumme T, Reinartz P, Alfer J, Muller-Rath R, Buell U, Wirtz DC. Diagnostic values of positron emission tomography versus triple-phase bone scan in hip arthroplasty loosening. *Arch Orthop Trauma Surg.* 2005;125:322–329.
- Myers ER, Wilson SE. Biomechanics of osteoporosis and vertebral fracture. *Spine.* 1997;22:S25–31.
- Nair SP, Meghji S, Wilson M, Reddi K, White P, Henderson B. Bacterially induced bone destruction: Mechanisms and misconceptions. *Infect Immun.* 1996;64:2371–2380.
- Nanni C, Errani C, Boriani L, Fantini L, Ambrosini V, Boschi S, Rubello D, Pettinato C, Mercuri M, Gasbarrini A, Fanti S. 68Ga-citrate PET/CT for evaluating patients with infections of the bone: Preliminary results. *J Nucl Med.* 2010;51:1932–1936.
- Nawaz A, Torigian DA, Siegelman ES, Basu S, Chryssikos T, Alavi A. Diagnostic performance of FDG-PET, MRI, and plain film radiography (PFR) for the diagnosis of osteomyelitis in the diabetic foot. *Mol Imaging Biol.* 2010;12:335–342.
- NNIS (National Nosocomial Infections Surveillance System). National nosocomial infections surveillance (NNIS) system report, data summary from January 1992 through June 2004, issued October 2004. *Am J Infect Control.* 2004;32:470–485.
- Nelson DR, Buxton TB, Luu QN, Rissing JP. The promotional effect of bone wax on experimental staphylococcus aureus osteomyelitis. *J Thorac Cardiovasc Surg.* 1990;99:977–980.
- Norden CW. Experimental osteomyelitis. I. A description of the model. *J Infect Dis.* 1970;122:410–418.
- Norden CW, Kennedy E. Experimental Osteomyelitis. II. Therapeutic trials and measurement of antibiotic levels in bone. *J Infect Dis.* 1971;124:565–571.
- Norden CW, Myerowitz RL, Keleti E. Experimental osteomyelitis due to Staphylococcus aureus or Pseudomonas aeruginosa: a radiographic-pathological correlative analysis. *Br J Exp Pathol.* 1980;61:451–460.
- O'Reilly T, Mader JT. Rat model of bacterial osteomyelitis of the tibia. In: Zak O, Sande MA, eds. *Handbook of Animal Models of Infection Experimental Models in Antimicrobial Chemotherapy.* London: Academic Press, Ltd. 1999:561–575.
- Otto M. Staphylococcal biofilms. *Curr Top Microbiol Immunol.* 2008;322:207–228.
- Pääkkönen M, Kallio MJT, Kallio PE, Pelto H. Sensitivity of erythrocyte sedimentation rate and C-reactive protein in childhood bone and joint infections. *Clin Orthop Relat Res.* 2010;468:861–866.
- Pakos EE, Trikalinos TA, Fotopoulos AD, Ioannidis JP. Prosthesis infection. Diagnosis after total joint arthroplasty with antigranulocyte scintigraphy with 99mTc-labeled monoclonal antibodies - a meta-analysis. *Radiology.* 2007;242:101–108.
- Palestro CJ, Kim CK, Swyer AJ, Capozzi JD, Solomon RW, Goldsmith SJ. Total hip arthroplasty: Periprosthetic indium-111-labeled leukocyte activity and complementary technetium-sulfur-colloid imaging in suspected infection. *J Nucl Med.* 1990;31:1950–1955.
- Palestro CJ, Love C, Miller TT. Diagnostic imaging tests and microbial infections. *Cell Microbiol.* 2007;9:2323–2333.
- Palestro CJ, Swyer AJ, Kim CK, Goldsmith SJ. Infected knee prosthesis: diagnosis with In-111 leukocyte, Tc-99m sulphur colloid, and Tc-99m MDP imaging. *Radiology.* 1991;179:645–648.
- Patel M, Rojavin Y, Jamali AA, Wasielewski SJ, Salgado CJ. Animal Models for the Study of Osteomyelitis. *Semin Plast Surg.* 2009;23:148–154.
- Pauwels E, Blom J, Camps J, Hermans J, Rijke A. A comparison between the diagnostic efficacy of 99m tc-MDP, 99m tc-DPD and 99m tc-HDP for the detection of bone metastases. *Eur J Nucl Med Mol Imaging.* 1983;8:118–122.
- Pauwels E, Sturm E, Bombardieri E, Cleton F, Stokkel M. Positron-emission tomography with [18F] fluorodeoxyglucose. *J Cancer Res Clin Oncol.* 2000;126:549–559.
- Pellegrino D, Bonab AA, Dragotakes SC, Pitman JT, Mariani G, Carter EA. Inflammation and infection: imaging properties of 18F-FDG-labeled white blood cells versus 18F-FDG. *J Nucl Med.* 2005;46:1522–1530.
- Pelletier JP, Martel-Pelletier J, Abramson SB. Osteoarthritis, an inflammatory disease: potential implication for the selection of new therapeutic targets. *Arthritis Rheum.* 2001;44:1237–1247.
- Perry M. Erythrocyte sedimentation rate and C reactive protein in the assessment of suspected bone infection - are they reliable indices? *J R Coll Surg Ed-inb.* 1996;41:116–118.
- Petri WH, 3rd. Evaluation of antibiotic-supplemented bone allograft in a rabbit model. *J Oral Maxillofac Surg.* 1991;49:392–396.

- Petty W, Spanier S, Shuster JJ, Silverthorne C. The influence of skeletal implants on incidence of infection. Experiments in a canine model. *J Bone Joint Surg Am.* 1985;67:1236–1244.
- Pichler R, Weiglein K, Schmekal B, Sfetos K, Maschek W. Bone scintigraphy using Tc-99m DPD and F18-FDG in a patient with SAPHO syndrome. *Scand J Rheumatol.* 2003;32:58–60.
- Pill SG, Parvizi J, Tang PH, Garino JP, Nelson C, Zhuang H, Alavi. Comparison of fluorodeoxyglucose positron emission tomography and (111)indium-white blood cell imaging in the diagnosis of periprosthetic infection of the hip. *J Arthroplasty.* 2006;21:91–97.
- Pineda C, Espinosa R, Pena A. Radiographic imaging in osteomyelitis: the role of plain radiography, computed tomography, ultrasonography, magnetic resonance imaging, and scintigraphy. *Semin Plast Surg.* 2009;23:80–89.
- Prandini N, Lazzeri E, Rossi B, Erba P, Parisella MG, Signore A. Nuclear medicine imaging of bone infections. *Nucl Med Commun.* 2006;27:633–644.
- Prokesch RC, Hand WL. Antibiotic entry into human polymorphonuclear leukocytes. *Antimicrob Agents Chemother.* 1982;21:373–380.
- Queck SY, Otto M. Staphylococcus epidermidis and other coagulase-negative staphylococci. In: Lindsay JA, ed. *Staphylococcus: Molecular Genetics.* Norfolk: Caister Academic Press. 2008:227–254.
- Ramsey SD, Newton K, Blough D, McCulloch DK, Sandhu N, Reiber GE, Wagner EH. Incidence, outcomes, and cost of foot ulcers in patients with diabetes. *Diabetes Care.* 1999;22:382–387.
- Recker RR. Embryology, anatomy, and microstructure of bone. In: Coe FL, Favus MJ, eds. *Disorders of Bone and Mineral Metabolism.* New York: Raven. 1992:219–240.
- Reiber GE. The epidemiology of diabetic foot problems. *Diabet Med.* 1996;13:S6–11.
- Reinartz P, Mumme T, Hermanns B, Cremerius U, Wirtz DC, Schaefer WM, Niethard F-U, Buell U. Radionuclide imaging of the painful hip arthroplasty: positron-emission tomography versus triple-phase bone scanning. *J Bone Joint Surg Br.* 2005;87:465–470.
- Ren W, Muzik O, Jackson N, Khoury B, Shi T, Flynn JC, Chakraborty P, Markel DC. Differentiation of septic and aseptic loosening by PET with both 11C-PK11195 and 18F-FDG in rat models. *Nucl Med Commun.* 2012;33:747–756.
- Resch A, Rosenstein R, Nerz C, Gotz F. Differential gene expression profiling of staphylococcus aureus cultivated under biofilm and planktonic conditions. *Appl Environ Microbiol.* 2005;71:2663–2676.
- Rini JN, Bhargava KK, Tronco GG, Singer C, Caprioli R, Marwin SE, Richardson HL, Nichols KJ, Pugliese PV, Palestro CJ. PET with FDG-labeled leukocytes versus scintigraphy with 111In-Oxine-labeled leukocytes for detection of infection. *Radiology.* 2006;238:978–987.
- Rissing JP. Animal models of osteomyelitis. knowledge, hypothesis, and speculation. *Infect Dis Clin North Am.* 1990;4:377–390.
- Rissing JP, Buxton TB, Fisher J, Harris R, Shockley RK. Arachidonic acid facilitates experimental chronic osteomyelitis in rats. *Infect Immun.* 1985a;49:141–144.
- Rissing JP, Buxton TB, Weinstein RS, Shockley RK. Model of experimental chronic osteomyelitis in rats. *Infect Immun.* 1985b;47:581–586.
- Rodet A. The classic: An experimental study on infectious osteomyelitis. 1884. *Clin Orthop Relat Res.* 2005;439:11–12.
- Rohde H, Burandt EC, Siemssen N, Frommelt L, Burdelski C, Wurster S, Scherpe S, Davies AP, Harris LG, Horstkotte MA, Knobloch JK, Ragunath C, Kaplan JB, Mack D. Polysaccharide intercellular adhesion or protein factors in biofilm accumulation of staphylococcus epidermidis and staphylococcus aureus isolated from prosthetic hip and knee joint infections. *Biomaterials.* 2007;28:1711–1720.
- Roivainen A, Jalkanen S, Nanni C. Gallium-labelled peptides for imaging of inflammation. *Eur J Nucl Med Mol Imaging.* 2012;39:S68–77.
- Roivainen A, Parkkola R, Yli-Kerttula T, Lelikoinen P, Viljanen T, Mötönen T, Nuutila P, Minn H. Use of positron emission tomography with methyl-11C-choline and 2-18F-fluoro-2-deoxy-D-glucose in comparison with magnetic resonance imaging for the assessment of inflammatory proliferation of synovium. *Arthritis Rheum.* 2003;48:3077–3084.
- Roivainen A, Tolvanen T, Salomäki S, Lendvai G, Velikyán I, Numminen P, Väilä M, Sipilä H, Bergström M, Härkönen P, Lönnberg H, Långström B. 68Ga-labeled oligonucleotides for in vivo imaging with PET. *J Nucl Med.* 2004;45:347–355.
- Rosen RS, Fayad L, Wahl RL. Increased 18F-FDG uptake in degenerative disease of the spine: Characterization with 18F-FDG PET/CT. *J Nucl Med.* 2006;47:1274–1280.
- Rosenbaum SJ, Lind T, Antoch G, Bockisch A. False-positive FDG PET uptake – the role of PET/CT. *Eur Radiol.* 2006;16:1054–1065.
- Rosenthal VD, Bijie H, Maki DG, Mehta Y, Apisarnthanarak A, Medeiros EA, Leblebicioglu H, Fisher D, Álvarez-Moreno C, Khader IA, Del Rocio González Martínez M, Cuellar LE, Navoa-Ng JA, Abouqal R, Guanche Garcell H, Mitrev Z, Pirez García MC, Hamdi A, Dueñas L, Cancel E, Gurskis V, Rasslan O, Ahmed A, Kanj SS, Ugalde OC, Mapp T, Raka L, Yuet Meng C, Thu le TA, Ghazal S, Gikas A, Narváez LP, Mejia N, Hadjieva N, Gamar Elanbya MO, Guzmán Siritt ME, Jayatilleke K. International nosocomial infection control consortium (INICC) report, data summary of 36 countries, for 2004–2009. *Am J Infect Control.* 2012;40:396–407.
- Russell TA. General Principles of Fracture Treatment. In: Crenshaw AH, ed. *Campbell's Operative Orthopedics*, 8th ed. St. Louis: Mosby-Year Book Inc. 1992:725–784.
- Ruotsalainen E, Valttonen V. Osteomyelitis - what old, what new? *Duodecim.* 2001;117:2217–2224.
- Sahlmann CO, Siefker U, Lehmann K, Meller J. Dual time point 2-[18F]fluoro-2'-deoxyglucose positron emission tomography in chronic bacterial osteomyelitis. *Nucl Med Commun.* 2004;25:819–823.
- Salber D, Gunawan J, Langen KJ, Fricke E, Klauth P, Burchert W, Zijlstra S. Comparison of 99mTc- and 18F-ubiquitin autoradiography to anti-Staphylo-

- coccus aureus immunofluorescence in rat muscle abscesses. *J Nucl Med.* 2008;49:995–999.
- Salmi M, Jalkanen S. A 90-kilodalton endothelial cell molecule mediating lymphocyte binding in humans. *Science.* 1992;257:1407–1409.
- Salmi M, Jalkanen S. VAP-1: an adhesion and an enzyme. *Trends Immunol.* 2001;22:211–216.
- Salmi M, Jalkanen S. Cell-surface enzymes in control of leukocyte trafficking. *Nat Rev Immunol.* 2005;5:760–771.
- Salmi M, Kalimo K, Jalkanen S. Induction and function of vascular adhesion protein-1 at sites of inflammation. *J Exp Med.* 1993;178:2255–2260.
- Salmi M, Tohka S, Jalkanen S. Human vascular adhesion protein-1 (VAP-1) plays a critical role in lymphocyte-endothelial cell adhesion cascade under shear. *Circ Res.* 2000;86:1245–1251.
- Sammak B, Abd El Bagi M, Al Shahed M, Hamilton D, Al Nabulsi J, Youssef B, Al Thagafi M. Osteomyelitis: a review of currently used imaging techniques. *Eur Radiol.* 1999;9:894–900.
- Sanchez-Crespo A, Andreo P, Larsson SA. Positron flight in human tissues and its influence on PET image spatial resolution. *Eur J Nucl Med Mol Imaging.* 2004;31:44–51.
- Sapico FL, Montgomerie JZ. Vertebral osteomyelitis in intravenous drug abusers: report of three cases and review of the literature. *Rev Infect Dis.* 1980;2:196–206.
- Schauwecker DS. The scintigraphic diagnosis of osteomyelitis. *AJR Am J Roentgenol.* 1992;158:9–18.
- Schauwecker DS, Park HM, Mock BH, Burt RW, Kernick CB, Ruoff AC, 3rd, Sinn HJ, Wellman HN. Evaluation of complicating osteomyelitis with Tc-99m MDP, In-111 granulocytes, and Ga-67 citrate. *J Nucl Med.* 1984;25:849–853.
- Scheman L, Janota M, Lewin P. The production of experimental osteomyelitis: preliminary report. *JAMA.* 1941;177:1525–1529.
- Schiesser M, Stumpe KD, Trentz O, Kossmann T, Von Schulthess GK. Detection of metallic implant-associated infections with FDG PET in patients with trauma: correlation with microbiologic results. *Radiology.* 2003;226:391–398.
- Schmitz A, Risse J, Grünwald F, Gassel F, Biersack H, Schmitt O. Fluorine-18 fluorodeoxyglucose positron emission tomography findings in spondylodiscitis: preliminary results. *Eur Spine J.* 2001;10:534–539.
- Schmitz A, Risse JH, Textor J, Zander D, Biersack HJ, Schmitt O, Palmedo H. FDG-PET findings of vertebral compression fractures in osteoporosis: preliminary results. *Osteoporos Int.* 2002;13:755–761.
- Schulak DJ, Rayhack JM, Lippert FG, 3rd, Convery FR. The erythrocyte sedimentation rate in orthopaedic patients. *Clin Orthop Relat Res.* 1982;167:197–202.
- Schwegler B, Stumpe KD, Weishaupt D, Strobel K, Spinaz GA, von Schulthess GK, Hodler J, Böni T, Donath MY. Unsuspected osteomyelitis is frequent in persistent diabetic foot ulcer and better diagnosed by MRI than by 18F-FDG PET or 99mTc-MOAB. *J Intern Med.* 2008;263:99–106.
- Sehn JK, Gilula LA. Percutaneous needle biopsy in diagnosis and identification of causative organisms in cases of suspected vertebral osteomyelitis. *Eur J Radiol.* 2012;81:940–946.
- Seltzer SE. Value of computed tomography in planning medical and surgical treatment of chronic osteomyelitis. *J Comput Assist Tomogr.* 1984;8:482–487.
- Senneville E, Melliez H, Beltrand E, Legout L, Valette M, Cazaubiel M, Cordonnier M, Caillaux M, Yazdanpanah Y, Mouton Y. Culture of percutaneous bone biopsy specimens for diagnosis of diabetic foot osteomyelitis: concordance with ulcer swab cultures. *Clin Infect Dis.* 2006;42:57–62.
- Siaens R, Eijssink VGH, Dierckx R, Slegers G. 123I-labeled chitinase as specific radioligand for in vivo detection of fungal infections in mice. *J Nucl Med.* 2004;45:1209–1216.
- Signore A, Chianelli M, Bei R, Oyen W, Modesti A. Targeting cytokine/chemokine receptors: a challenge for molecular nuclear medicine. *Eur J Nucl Med Mol Imaging.* 2003;30:149–156.
- Sivola J, Autio A, Luoto P, Jalkanen S, Roivainen A. Preliminary evaluation of novel 68Ga-DOTAVAP-PEG-P2 peptide targeting vascular adhesion protein-1. *Clin Physiol Funct Imaging.* 2010;30:75–78.
- Smith DJ, Salmi M, Bono P, Hellman J, Leu T, Jalkanen S. Cloning of vascular adhesion protein 1 reveals a novel multifunctional adhesion molecule. *J Exp Med.* 1998;188:17–27.
- Sousa C, Henriques M, Azeredo J, Teixeira P, Oliveira R. *Staphylococcus epidermidis* glucose uptake in biofilm versus planktonic cells. *World J Microbiol Biotechnol.* 2008;24:423–426.
- Stanford CM, Keller JC. The concept of osseointegration and bone matrix expression. *Crit Rev Oral Biol Med.* 1991;2:83–101.
- Stolen CM, Marttila-Ichihara F, Koskinen K, Yegutkin GG, Turja R, Bono P, Skurnik M, Hänninen A, Jalkanen S, Salmi M. Absence of the endothelial oxidase AOC3 leads to abnormal leukocyte traffic in vivo. *Immunity.* 2005;22:105–115.
- Strobel K, Hany TF, Exner GU. PET/CT of a Brodie abscess. *Clin Nucl Med.* 2006;31:210.
- Strobel K, Stumpe KD. PET/CT in musculoskeletal infection. *Semin Musculoskelet Radiol.* 2007;11:353–364.
- Stumpe KDM, Dazzi H, Schaffner A, von Schulthess GK. Infection imaging using whole-body FDG-PET. *Eur J Nucl Med Mol Imaging.* 2000;27:822–832.
- Stumpe KD, Nötzli HP, Zanetti M, Kamel EM, Hany TF, Görres GW, von Schulthess GK, Hodler J. FDG PET for differentiation of infection and aseptic loosening in total hip replacements: Comparison with conventional radiography and three-phase bone scintigraphy. *Radiology.* 2004;231:333–341.
- Stumpe KD, Romero J, Ziegler O, Kamel EM, von Schulthess GK, Strobel K, Hodler J. The value of FDG-PET in patients with painful total knee arthroplasty. *Eur J Nucl Med Mol Imaging.* 2006;33:1218–1225.
- Sugawara Y, Gutowski TD, Fisher SJ, Brown RS, Wahl RL. Uptake of positron emission tomography tracers in experimental bacterial infections: a comparative biodistribution study of radiolabeled FDG, thymidine, L-me-



- thionine, 67Ga-citrate, and 125I-HSA. *Eur J Nucl Med.* 1999;26:333-341.
- Swartzendruber DC, Nelson B, Hayes RL. Gallium-67 localization in lysosomal-like granules of leukemic and nonleukemic murine tissues. *J Natl Cancer Inst.* 1971;46:941-952.
- Takeuchi K, Matsusita M, Takagishi K. A case of SAPHO (synovitis-acne-pustulosis-hyperostosis-osteomyelitis) syndrome in which [18F]fluorodeoxyglucose positron emission tomography was useful for differentiating from multiple metastatic bone tumors. *Mod Rheumatol.* 2007;17:67-71.
- Termaat MF, Raijmakers PG, Scholten HJ, Bakker FC, Patka P, Haarman HJ. The accuracy of diagnostic imaging for the assessment of chronic osteomyelitis: a systematic review and meta-analysis. *J Bone Joint Surg Am.* 2005;87:2464-2471.
- This JA. Understanding the standardized uptake value, its methods, and implications for usage. *J Nucl Med.* 2004;45:1431-1434.
- Tice AD, Hoaglund PA, Shoultz DA. Risk factors and treatment outcomes in osteomyelitis. *J Antimicrob Chemother.* 2003;51:1261-1268.
- Tohka S, Laukkanen M, Jalkanen S, Salmi M. Vascular adhesion protein 1 (VAP-1) functions as a molecular brake during granulocyte rolling and mediates recruitment in vivo. *FASEB J.* 2001;15:373-382.
- Tunney MM, Patrick S, Gorman SP, Nixon JR, Anderson N, Davis RI, Hanna D, Ramage G. Improved detection of infection in hip replacements. A currently underestimated problem. *J Bone Joint Surg Br.* 1998;80:568-572.
- Ujula T, Salomäki S, Virsu P, Lankinen P, Mäkinen TJ, Autio A, Yegutkin GG, Knuuti J, Jalkanen S, Roivainen A. Synthesis, 68Ga labeling and preliminary evaluation of DOTA peptide binding vascular adhesion protein-1: a potential PET imaging agent for diagnosing osteomyelitis. *Nucl Med Biol.* 2009;36:631-641.
- Unkila-Kallio L, Kallio MJ, Eskola J, Pelto H. Serum C-reactive protein, erythrocyte sedimentation rate, and white blood cell count in acute hematogenous osteomyelitis of children. *Pediatrics.* 1994;93:59-62.
- Van Acker F, Nuyts J, Maes A, Vanquickenborne B, Stuyck J, Bellemans J, Vleugels S, Bormans G, Mortelmans L. FDG-PET, 99mTc-HMPAO white blood cell SPET and bone scintigraphy in the evaluation of painful total knee arthroplasties. *Eur J Nucl Med.* 2001;28:1496-1504.
- van der Bruggen W, Bleeker-Rovers CP, Boerman OC, Gotthardt M, Oyen WJG. PET and SPECT in osteomyelitis and prosthetic bone and joint infections: a systematic review. *Semin Nucl Med.* 2010;40:3-15.
- van der Laken CJ, Boerman OC, Oyen WJ, van de Ven MT, Edwards DS, Barrett JA, van der Meer JW, Corstens FH. Technetium-99m-labeled chemotactic peptides in acute infection and sterile inflammation. *J Nucl Med.* 1997;38:1310-1315.
- van Griethuysen A, Bes M, Etienne J, Zbinden R, Kluytmans J. International multicenter evaluation of latex agglutination tests for identification of *Staphylococcus aureus*. *J Clin Microbiol.* 2001;39:86-89.
- Vanquickenborne B, Maes A, Nuyts J, Van Acker F, Stuyck J, Mulier M, Verbruggen A, Mortelmans L. The value of (18)F-FDG-PET for the detection of infected hip prosthesis. *Eur J Nucl Med Mol Imaging.* 2003;30:705-715.
- von Eiff C, Peters G, Heilmann C. Pathogenesis of infections due to coagulase-negative staphylococci. *Lancet Infect Dis.* 2002;2:677-685.
- von Schulthess G, Meier N, Stumpe K. Joint accumulations of FDG in whole body PET scans. *Nuklearmedizin.* 2001;40:193-197.
- von Schulthess GK, Steinert HC, Hany TF. Integrated PET/CT: current applications and future directions. *Radiology.* 2006;238:405-422.
- Wald ER. Risk factors for osteomyelitis. *Am J Med.* 1985;78:206-212.
- Waldvogel FA, Medoff G, Swartz MN. Osteomyelitis: a review of clinical features, therapeutic considerations and unusual aspects. *N Engl J Med.* 1970a;282:198-206.
- Waldvogel FA, Medoff G, Swartz MN. Osteomyelitis: a review of clinical features, therapeutic considerations and unusual aspects. *N Engl J Med.* 1970b;282:260-266.
- Waldvogel FA, Medoff G, Swartz MN. Osteomyelitis: a review of clinical features, therapeutic considerations and unusual aspects. *N Engl J Med.* 1970c;282:316-322.
- Wandler E, Kramer EL, Sherman O, Babb J, Scarola J, Rafii M. Diffuse FDG shoulder uptake on PET is associated with clinical findings of osteoarthritis. *Am J Roentgenol.* 2005;185:797-803.
- Wang GL, Zhao K, Liu ZF, Dong MJ, Yang SY. A meta-analysis of fluorodeoxyglucose-positron emission tomography versus scintigraphy in the evaluation of suspected osteomyelitis. *Nucl Med Commun.* 2011;12:1134-1142.
- Weitz-Marshall AD, Bosse MJ. Timing of closure of open fractures. *J Am Acad Orthop Surg.* 2002;10:379-384.
- Whalen JL, Brown ML, McLeod R, Fitzgerald RH, Jr. Limitations of indium leukocyte imaging for the diagnosis of spine infections. *Spine (Phila Pa 1976).* 1991;16:193-197.
- White LM, Schweitzer ME, Deely DM, Gannon F. Study of osteomyelitis: utility of combined histologic and microbiologic evaluation of percutaneous biopsy samples. *Radiology.* 1995;197:840-842.
- Wing V, Jeffrey R, Federle M, Helms C, Trafton P. Chronic osteomyelitis examined by CT. *Radiology.* 1985;154:171-174.
- Worlock P, Slack R, Harvey L, Mawhinney R. An experimental model of post-traumatic osteomyelitis in rabbits. *Br J Exp Pathol.* 1988;69:235-244.
- Wu JS, Gorbachova T, Morrison WB, Haims AH. Imaging-guided bone biopsy for osteomyelitis: are there factors associated with positive or negative cultures? *AJR Am J Roentgenol.* 2007;188:1529-1534.
- Wukich DK, Abreu SH, Callaghan JJ, Van Nostrand D, Savory CG, Eggli DF, Garcia JE, Berrey BH. Diagnosis of infection by preoperative scintigraphy with indium-labeled white blood cells. *J Bone Joint Surg Am.* 1987;69:1353-1360.

- Yegutkin GG, Salminen T, Koskinen K, Kurtis C, McPherson MJ, Jalkanen S, Salmi M. A peptide inhibitor of vascular adhesion protein-1 (VAP-1) blocks leukocyte-endothelium interactions under shear stress. *Eur J Immunol.* 2004;34:2276–2285.
- Zak O, Zak F, Rich R, Tosch W, Kradolfer F, Sheld W. Experimental staphylococcal osteomyelitis in rats: therapy with rifampin and cloxacillin, alone or in combination. In: *Current Chemotherapy and Immunotherapy, Proceedings of the 12th International Congress of Chemotherapy.* Florence, Italy: American Society for Microbiology, Washington, DC. 1981;2:973–974.
- Zalavras CG, Rigopoulos N, Lee J, Leach T, Patzakis MJ. Magnetic resonance imaging findings in hematogenous osteomyelitis of the hip in adults. *Clin Orthop Relat Res.* 2009;467:1688–1692.
- Zhuang H, Alavi A. 18-Fluorodeoxyglucose positron emission tomographic imaging in the detection and monitoring of infection and inflammation. *Semin Nucl Med.* 2002;32:47–59.
- Zhuang H, Chacko TK, Hickeson M, Stevenson K, Feng Q, Ponzo F, Garino JP, Alavi A. Persistent non-specific FDG uptake on PET imaging following hip arthroplasty. *Eur J Nucl Med Mol Imaging.* 2002;29:1328–1333.
- Zhuang H, Duarte PS, Pourdehnad M, Maes A, Van Acker F, Shnier D, Garino JP, Fitzgerald RH, Alavi A. The promising role of 18F-FDG PET in detecting infected lower limb prosthesis implants. *J Nucl Med.* 2001;42:44–48.
- Zhuang H, Duarte PS, Pourdehand M, Shnier D, Alavi A. Exclusion of chronic osteomyelitis with F-18 fluorodeoxyglucose positron emission tomographic imaging. *Clin Nucl Med.* 2000;25:281–284.
- Zhuang H, Sam JW, Chacko TK, Duarte PS, Hickeson M, Feng Q, Nakhoda KZ, Guan L, Reich P, Altamari SM, Alavi A. Rapid normalization of osseous FDG uptake following traumatic or surgical fractures. *Eur J Nucl Med Mol Imaging.* 2003;30:1096–1103.
- Zijlstra S, Gunawan J, Freytag C, Burchert W. Synthesis and evaluation of fluorine-18 labelled compounds for imaging of bacterial infections with PET. *Appl Radiat Isot.* 2006;64:802–807.
- Zimmerli W. Clinical practice. Vertebral osteomyelitis. *N Engl J Med.* 2010;362:1022–1029.
- Zimmerli W, Trampuz A, Ochsner PE. Prosthetic-joint infections. *N Engl J Med.* 2004;351:1645–1654.
- Zorzano A, Abella A, Marti L, Carpena C, Palacin M, Testar X. Semicarbazide-sensitive amine oxidase activity exerts insulin-like effects on glucose metabolism and insulin-signaling pathways in adipose cells. *Biochim Biophys Acta.* 2003;1647:3–9.